ELECTRICAL SIGNATURE ANALYSIS OF SYNCHRONOUS MOTORS UNDER SOME MECHANICAL ANOMALIES

A Dissertation

by

YONG LI

Submitted to the Office of Graduate Studies of
Texas A&M University
in partial fulfillment of the requirements for the degree of

DOCTOR OF PHILOSOPHY

Approved by:

Chair of Committee,	Alexander G. Parlos
Committee Members,	Bryan Rasmussen
	Reza Langari
	Jose Silva-Martinez
Head of Department,	Jerald Caton

December 2012

Major Subject: Mechanical Engineering

ABSTRACT

Electrical Signature Analysis (ESA) has been introduced for some time to investigate the electrical anomalies of electric machines, especially for induction motors. More recently hints of using such an approach to analyze mechanical anomalies have appeared in the literature. Among them, some articles cover synchronous motors usually being employed to improve the power factor, drive green vehicles and reciprocating compressors or pumps with higher efficiency. Similarly with induction motors, the common mechanical anomalies of synchronous motor being analyzed using the ESA are air-gap eccentricity and single point bearing defects. However torsional effects, which are usually induced by torsional vibration of rotors and by generalized roughness bearing defects, have seldom been investigated using the ESA.

This work presents an analytical method for ESA of rotor torsional vibration and an experimentally demonstrated approach for ESA of generalized roughness bearing defects. The torsional vibration of a shaft assembly usually induces rotor speed fluctuations resulting from the excitations in the electromagnetic (EM) or load torque. Actually, there is strong coupling within the system which is dynamically dependent on the interactions between the electromagnetic air-gap torque of the synchronous machine and the rotordynamics of the rotor shaft assembly. Typically this problem is solved as a one-way coupling by the unidirectional load transfer method, which is based on predetermined or assumed EM or load profile. It ignores the two-way interactions, especially during a start-up transient. In this work, a coupled equivalent circuit method is

applied to reflect this coupling, and the simulation results show the significance of the proposed method by the practical case study of Electric Submersible Pump (ESP) system.

The generalized roughness bearing anomaly is linked to load torque ripples which can cause speed oscillations, while being related to current signature by phase modulation. Considering that the induced characteristic signature is usually subtle broadband changes in the current spectrum, this signature is easily affected by input power quality variations, machine manufacturing imperfections and the interaction of both. A signal segmentation technique is introduced to isolate the influence of these disturbances and improve the effectiveness of applying the ESA for this kind of bearing defects. Furthermore, an improved experimental procedure is employed to closely resemble naturally occurring degradation of bearing, while isolating the influence of shaft currents on the signature of bearing defects during the experiments. The results show that the proposed method is effective in analyzing the generalized roughness bearing anomaly in synchronous motors.

ACKNOWLEDGEMENTS

I would like to first express my appreciation to my committee chair and advisor, Dr. Alexander G. Parlos, for his patience, continuous guidance, technical support and advice through the course of my research work. I would also like to express my appreciation to other members of my committee: Dr. Reza Langari, Dr. Bryan Rasmussen and Dr. Jose Silva-Martinez for their comments and advice.

Thanks also go to the Veros Systems Inc., which provided the experimental facilities, and to Mr. Jianxi Fu who discussed the programming with me. I also want to extend my gratitude to my friends Mr. Pang-Chun Chu, Mr. Gang Li, Mr. Tengxi Wang and at Texas A&M University for their insightful discussions on related and unrelated topics.

Special thanks should be dedicated to my beloved wife and parents for her encouragement, patience and love during the life of my Phd study.

NOMENCLATURE

AM	Amplitude Modulation
CART	Classification and Regression Tree
CT	Current Transformer
DAQ	Data Acquisition
ESA	Electrical Signature Analysis
EM	Electromagnetic Torque
EDM	Electric Discharge Machining
ESP	Electric Submersible Pump
FM	Frequency Modulation
IPM	Interior Permanent Magnet
MCSA	Motor Current Signature Analysis
MMF	Magnetomotive Force
PM	Phase Modulation
PMSM	Permanent Magnet Synchronous Machine
PQ	Power Quality
PT	Potential Transformer
RMS	Root Mean Square
TASS	Tree-based Adaptive Segmented Spectrogram
UMP	Unbalanced Magnetic PULL
VFD	Variable Frequency Drive

TABLE OF CONTENTS

Page

ABSTRACT ii

ACKNOWLEDGEMENTS iv

NOMENCLATURE v

TABLE OF CONTENTS vi

LIST OF FIGURES ix

LIST OF TABLES xiii

CHAPTER

I INTRODUCTION 1

A. Background and Motivation 1
B. Review of Previous Arts 4
1. ESA based Condition Monitoring 4
2. Torsional Vibration Monitoring 6
3. Bearing Anomaly Detection based on ESA 10
C. Research Objective 15
D. Proposed Approach 16
E. Anticipated Contributions 18

II FUNDAMENTALS OF ANALYSIS OF MECHANICAL ANOMALIES BASED ON ESA 20

A. Dynamic Model of Synchronous Motor and Load 20
1. Lateral Vibration Model of Synchronous Motor 22
2. Torsional Vibration Model of Rotor Shaft Assembly 30
B. Measurement of Lateral and Torsional Vibration 35
1. Lateral Vibration Measurement by Accelerometer 35
2. Torsional Vibration Measurement 36
C. Transmission of Mechanical Anomalies to Electric Signal 38
D. Modulation Mechanism of Mechanical Anomalies 40
1. Torsional Effects and Phase Modulation 41
2. Air-gap Eccentricity and Amplitude Modulation 46

E. Mechanical Anomalies Studied 49
1. Torsional Vibration of Rotor Shaft Assembly 49
2. Generalized Roughness Bearing Defect 50
F. Diagram of Electrical Signature Analysis..... 51

III ESA OF TORSIONAL VIBRATION OF SYNCHRONOUS MOTOR SHAFT ASSEMBLY 53

A. Natural Frequencies and Modal Shapes of Torsional Dynamics 54
1. Mode Shape Analysis of a Simplified System 55
2. Generalized Lumped Torsional Model 59
B. Sources of Torsional Excitation 63
1. Load Torque Excitations 63
2. Electromagnetic Torque Excitations..... 66
3. Modulation of Torsional Excitation to Current Signature 70
C. Coupling Between Electromagnetic Torque and Rotor Dynamics.. 72
1. Torque Amplification during Resonance 75
2. Self-excited Torsional Vibration during Start-up..... 82
3. Torsional Analysis Procedure..... 88

IV CASE STUDY--- ESP DRIVEN CENTRIFUGAL PUMP 91

A. Overview of ESP System..... 91
B. Modal Shape and Steady State Analysis…… 93
C. Electromagnetic-Rotordyanmic Coupling…… 97

V ESA OF GENERALIZED ROUGHNESS BEARING ANOMALY UNDER NONSTATIONARY POWER INPUT..... 105

A. Nature of Generalized Roughness Bearing Anomaly 105
B. PQ Variation and Nonstationarity of Power Input 108
1. Power Quality Variation of Input Voltage 109
2. Representation of Non-stationary Signals..... 114
3. Locally and Piecewise Stationary Process 116
C. Signal Segmentation Procedure..... 118
1. Parametric Method..... 118
2. Nonparametric Method 119
D. Processing of Approximately Stationary Segments 124

VI EXPERIMENTAL PROCEDURE AND RESULTS 125

A. Experimental Setup..... 125
1. Vibration Signal Acquisition for Benchmark 128
2. Electrical Data Acquisition for ESA..... 129

B. Explanation of In-situ Bearing Deterioration Experiment 130
C. Influence of Shaft Current on the Rotordynamics of Machine 132
1. Unbalanced Magnetic Pull (UMP) Induced by Shaft Current 133
2. Thermal Effect of Shaft Current on Rotordynamic Coefficients ... 135
3. Thermal Induced Rotor Shaft Bow 141
D. An Improved Experimental Procedure 143
E. Experimental Results 144
1. Vibration and Electrical Signature of Bearing Defect 145
2. Vibration Indicator Trend Analysis 146
3. Electrical Indicator Trend Analysis 149

VII SUMMARY AND CONCLUSIONS 152

A. Summary of Research 152
B. Conclusions 153
C. Suggestions for Future Works 154

REFERENCES 156

APPENDIX 164

LIST OF FIGURES

FIGURE		Page
1	Forward and backward interaction & interface for torque oscillation	6
2	Rolling element bearing geometry	12
3	Overview of proposed approach	17
4	Diagram of ESA and vibration monitoring.....	21
5	A simplified model for rotor-bearing system.....	22
6	Schematics of static unbalance	26
7	Schematics of dynamic unbalance	26
8	Schematic representation of static, dynamic and mixed eccentricity.....	28
9	Two mass torsional system	30
10	Torsional dynamics of motor rotor under unbalance	34
11	Equivalent diagram of coupled magnetic circuits	39
12	The stator and rotor reference frame	43
13	The sample of generalized roughness defect of ball bearing	50
14	Diagram of machine anomaly detection based on ESA	50
15	Simplified model of a motor driven compressor system	54
16	Mode shape related to natural frequency f1.....	57
17	Mode shape related to natural frequency f2.....	57
18	Mode shape related to natural frequency f3.....	58
19	Interference diagram for the simplified system	59
20	Representation of generalized torsional dynamics model	61

21	Electromechanical similarities for a flexible shaft system	74
22	Equivalent circuit diagram of the motor driven compressor system.....	74
23	Shaft torque T12 without damping.....	76
24	Shaft torque T23 without damping.....	77
25	Shaft torque T34 without damping.....	77
26	Shaft torque T12 with damping	78
27	Shaft torque T23 with damping	78
28	Shaft torque T34 with damping	79
29	Relation between the EM torque and current spectrum	80
30	Torque modulation under fixed oscillating frequency and different load levels.....	81
31	Torque modulation under fixed oscillating load level and different frequencies	81
32	Equivalent circuit network of generalized torsional dynamics.....	82
33	Interference diagram for transient 2x –slip frequency	83
34	Motor speed during transient	83
35	Motor current during transient	85
36	Field current during transient.....	85
37	Electromagnetic torque during transient.....	86
38	Shaft torque T12 during transient.....	86
39	Shaft torque T23 during transient.....	87
40	Shaft torque T34 during transient.....	87
41	Electric submersible motor pump system.....	92

42 ESP model---motor with multiply rotors 93
43 The first natural frequency of ESP v.s number of rotor in tandem 96
44 Natural mode for ESP with 15 rotors in tandem 96
45 Electromagnetic torque Tem 99
46 Spectrogram of electromagnetic torque 99
47 ESP motor stator current 100
48 Spectrogram of ESP motor stator current 100
49 Torque on shaft between motor and coupling 111
50 Spectrogram of shaft torque between motor and coupling 111
51 Rotor speed in time domain 102
52 Spectrogram of rotor speed 102
53 Torque on shaft between coupling and pump Tcp, K=1000 lbf· ft/rad 103
54 Torque on shaft between coupling and pump, K=1500 lbf· ft/rad 104
55 Torque on shaft between coupling and pump, K=500 lbf· ft/rad 104
56 Current signature of generalized roughness under torque oscillation 106
57 Normalized voltage RMS variations v.s. Time 111
58 Percentage of voltage imbalance variations v.s. Time 112
59 Voltage THD variations v.s. Time 113
60 Diagram of tree-based signal segmentation procedure 121
61 Diagram of experimental setup 126
62 Experimental setup snapshot 126
63 In-suite bearing deterioration setup by shaft current 127

64 Vibration signal data acquisition system 129

65 Electric signal data acquisition system 130

66 Influence of shaft current on vibration trend 132

67 Capacitive coupling model of induction motor under shaft current 134

68 Capacitive coupling mechanisms for shaft voltages 134

69 Schemes of asperity contact and lubrication regimes between rough surfaces 136

70 Simplified model for ball bearing of rotating machine 138

71 Vibration transmissibility v.s. frequency ratio 140

72 Galling between bearing and shaft under shaft current injection 143

73 Vibration spectrum for bearing at health and failed condition 145

74 Current spectrum for bearing at health and failed condition 146

75 Trend of vibration indicator under full load 147

76 Zoom in view of vibration indicator during current injection 148

77 Trend of electrical indicator under full load 149

78 Trend of electrical indicator under half load 150

79 Trend of electrical indicator under no load 150

LIST OF TABLES

TABLE Page

1	Inertia and stiffness for system components of simplified model.....	56
2	Natural Frequency for of simplified model	56
3	Steady state load torsional excitation or transmission.....	66
4	Electric submersible motor parameters (Series 456).....	94
5	Electric submersible pump impeller parameters (Series 540)	94
6	Vibration Increment as health condition change.....	148
7	Increment of electrical indicator as health condition change	151

CHAPTER I

INTRODUCTION

A. Background and Motivation

Synchronous motors usually find applications in many industrial areas. One of the most important one is to be operated at leading power factor and used for power factor correction [1] in factories which have large number of induction motors or transformers operating at lagging power factor, so that extra charge from utilities can be avoided. In some application such as rubber mills, textile mills, cement factories, air compressors, centrifugal pumps where constant speed is required under possible fluctuating load or high efficiency is needed, synchronous machine could be a reasonable alternative to induction motors. On the other hand, synchronous machines are also widely used in the drive system of green vehicles because of its high power density, compact size and high efficiency [2]. The hybrid vehicle can employs synchronous machine for motoring during startup or low speed driving and generating driven by gasoline or micro-turbine engine during battery charging.

The reliable operation of these systems and preventive maintenance is critical for owner or users. The condition monitoring can provides knowledge about the health condition of machines and the rate of changes so that any deterioration in machine condition can be detected and preventive measures can be taken at appropriate time to avoid catastrophic failures and unscheduled downtime and maintenance.

Generally synchronous machine are well manufactured and robust, but the possibility of incipient faults are inherent due to wear of mechanical parts and stresses involved in the electromechanical energy conversion. The most common causes of system failure consist of electrical and mechanical anomalies which will eventually induce vibration, acoustic and electrical signature. A practical and effective way to detect the electrical fault in stator or field winding is the partial discharge [3] test which is a non-intrusive indicator of the presence of insulation defects, but it is expensive and usually reliable for the machinery of 4KV voltage or higher.

Lateral vibration could be analytically related to mechanical anomaly and be widely accepted as a most sensitive method to detect the mechanical anomalies in machinery [4]. But at some conditions such as synchronous machine in electrical or hybrid vehicle where accelerometer is susceptive to environmental noise and road condition, vibration monitoring is not a wise choice. Other situation such as submersible pump, compressor and their drives, the vibration monitoring will be very hard or even infeasible to implement. Furthermore the comparatively high cost of implementing this approach limits its application to the expensive machinery. Notice the fact that mechanical anomalies cause vibration signatures also induce corresponding electrical signatures, so a cost effective method, Electrical Signal Analysis (ESA), has been developed initially at the Oak Ridge National Laboratory in the mid 1980s [5]. It is also a non-intrusive approach which is easier and cheaper to retrofit the existing systems.

In most majority of literature on anomaly detection of electric machine, the vibration considered is only confined as lateral or translational vibration. Actually either

mechanical or electrical anomalies could eventually induce both translational vibration and torsional effects or vibration, which is usually ignored in the condition monitoring of electric machine. The influence of torsional effects usually induced by oscillating load torque or air-gap torque and may cause the torsional vibration resonance or shaft fatigue and coupling snap [6]. The damage caused by the torsional vibration is cumulative and may go unnoticed until catastrophic failure of shaft assembly occurs. So there is a strong need to apply the cost-effective ESA to condition monitoring of torsional vibration.

On the other hand, the generalized roughness [7] is the most practical bearing defect in the field because of contamination of the lubricant, lack or loss of lubricant, shaft current. Unlike the single-point or localized defect which is Amplitude Modulated (AM) [8] into current signal, it is more reasonable to be linked to torque ripple which can cause speed ripple and related current signature by Phase Modulation (PM) [9]. Considering that the induced characteristic signature is usually subtle broadband change in current spectrum [7], it is easy to be affected by the input Power Quality (PQ) variation, machine manufacturing imperfections, and the interaction of both. An approach is strongly encouraged to isolate the influence of these disturbances and improve the effectiveness of ESA for this kind of bearing defect.

This dissertation will investigate a nonintrusive ESA approach to monitor the torsional vibration of the synchronous motor-load assembly induced by oscillating torque, and analyze the subtle torsional effect produced by generalized-roughness bearing deterioration with isolation of the influence of PQ variation and machine manufacturing imperfections.

B. Review of Previous Arts

The anomalies of electric machine, electrical or mechanical, will induce both translational and torsional vibration signature, and related signature in the electrical signal. In the following section, first the basic ideal underlying ESA of electrical and mechanical anomalies will be presented. Then the monitoring of torsional vibration of rotor shaft assembly will be addressed. Finally two different types of bearing defects will be analyzed and ESA for both will be covered.

1. ESA based Condition Monitoring

The electric machine can be modeled as equivalent coupled magnetic circuits based on winding function approach [10], and an equation of motion by Newton's law. They are coupled by rotating speed and torque as shown in the following equations.

$$V_s = R_s I_s + L_s(pI_s) + (pL_{sf}(\theta_m(t)))i_f + L_{sf}(\theta_m(t))(pi_f) \tag{1.1}$$

$$V_f = R_f i_f + (pL_{sf}^T(\theta_m(t)))I_s + L_{sf}^T(\theta_m(t))(pI_s) + L_f(pi_f) \tag{1.2}$$

$$T_e = I_s^T \frac{dL_{sf}}{dt} i_f \qquad T_e - T_L = T_R = J_t\ddot{\theta}_m + b_p\dot{\theta}_m \tag{1.3}$$

where $L_s = \begin{bmatrix} L_{aas} & L_{ab} & L_{ac} \\ L_{ba} & L_{bbs} & L_{bc} \\ L_{ca} & L_{cb} & L_{ccs} \end{bmatrix}$, $L_{sf} = \begin{bmatrix} L_{af} & L_{bf} & L_{cf} \end{bmatrix}^T$, $L = \begin{bmatrix} L_s & L_{sf} \\ L_{sf}^T & L_f \end{bmatrix}$

$R_s = diag\begin{bmatrix} R_{as} & R_{bs} & R_{cs} \end{bmatrix}$, $V_s = [v_{as} \quad v_{bs} \quad v_{cs}]$, $I_s = [i_{as} \quad i_{bs} \quad i_{cs}]^T$

p is the derivative operator, i_f is the field current, T_e is the electromagnetic (EM) torque and θ_m is the relative displacement of rotor with respect to stator reference.

From the above equations, the electrical anomalies such as stator and rotor winding short circuit can induce asymmetrical resistance R_s or R_f and self-inductance matrix L_s or L_f in equivalent circuit, and then the electrical signal will involve corresponding changes. Mechanical anomalies such as misalignment, shaft bow and localized bearing defect or wear could cause mechanical, geometrical asymmetry and lead to the air-gap eccentricity, which will change mutual inductance matrix L_{sf} and eventually relate to characteristic electrical signatures by circuit analysis.

There are many literatures involve the detection of faults such as stator or rotor winding deterioration, air-gap eccentricity, rotor unbalance and misalignment of synchronous machine based on ESA. Stator or rotor winding fault can be monitored by the stator or field current [11]. For the synchronous machine either stator or field current or both if available can be used to detect the static or dynamic air-gap eccentricity [12-14]. The air-gap eccentricity is a major source of mechanical fault of synchronous machine. Because mechanical faults such as misalignment and localized or single point bearing defect will eventually result in static or dynamic air-gap eccentricity. In [15], the ESA are employed to the ship brushless synchronous machine shaft misalignment detection. The single-point bearing defect was analyzed by detecting some characteristic frequencies in stator current spectrum [8]. The approach of ESA can also be applied to monitor another kind of mechanical anomaly – torsional effect or vibration.

2. Torsional Vibration Monitoring

From the equation (1.3), the factors affect resulting torque T_R will excite the torsional vibration. There are many factors which can impact resulting torque and cause shaft torsional vibration in AC machine systems. These include start up, sudden changes of mechanical load, power system condition, current harmonics and inter-harmonics from the electrical machine during various transient operations and anomalies [16].

The primary sources of excitation which produce torsional vibrations can be divided into four categories, depending upon where in the system they originate. Fig.1 shows the major components of a drive system consisting of the electrical supply, motor, mechanical system and load. These major components interface and interact with each other through the interface variables defined in the figure. The first two types impact the electromagnetic torque, and the last two affect the load torque and speed.

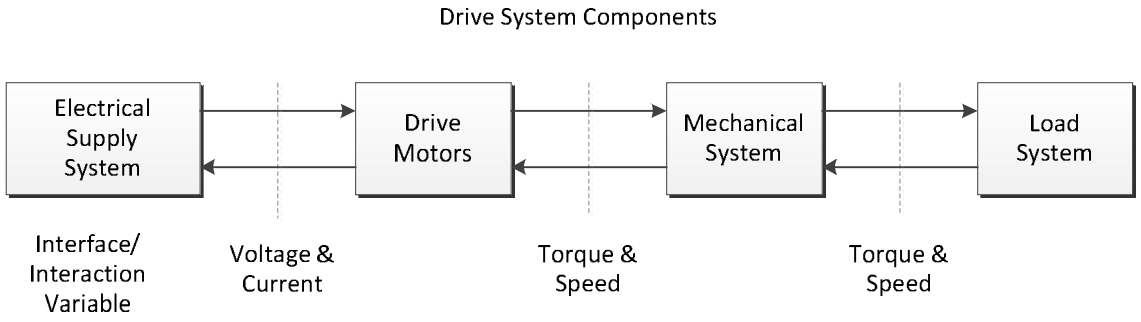

Fig.1 Forward and backward interaction & interface for torque oscillation

Electrical Supply System Excitation

AC electric motors are generally designed to operate from pure single frequency sinusoidal supply voltages and will produce smooth continuous torque with no pulsations under steady state conditions. In reality, however, the power systems used for

AC machines will be non-sinusoidal or contains harmonics, such as distorted utility power line and Variable Frequency Drive (VFD). This will induces significant torque pulsation in the electromagnetic torque of the motor. These pulsations will change frequency with operating speed and must be considered in the torsional design when employed such drives [17]. On the other hand, transient conditions such as line voltage fault and power quality fluctuation will produce torsional vibration in the mechanical system. For ac machines, this will generally consist of an abrupt change in the average torque, plus a transient pulsating torque of large magnitude at one and twice line frequency. Mechanical torsional resonance at either of these frequencies can result in damaging torques in the system and should be avoided as a general rule.

Motor Excitation

The AC motor itself is also considered as a major source of pulsating torque. A synchronous machine, for example, will produce a large line-frequency torque pulsation at start-up [18]. This pulsation decays quite rapidly (typically less than one second) but mechanical resonances at or near this frequency can produce damaging torque amplification during this brief period. Synchronous motor started “across-the–line” also produce oscillatory torque at the twice slip frequency during acceleration (i.e., starting at 120 Hz and decreasing to 0 Hz at full speed). This torque generally requires additional transient torsional analysis because of the potential for damage. A salient pole synchronous machine also will produce very significant saliency torque pulsations [19] during start-up. So the transient response of the torsional system during start-up of large

synchronous machine drives should always be adequately analyzed. Failure to do so can lead to an inadequate design of the drive systems and result in, as experience has shown, rapid damage or component failure to shaft, gear, coupling and other components.

Interior Permanent Magnet (IPM) motor can provide wide speed range ruggedness of the rotor high speed application. High torque pulsation, however, is the major drawback of most IPM configurations [20], can probably excite the torsional dynamic of rotor and load shaft assembly.

Mechanical System Excitation

The frequency of the disturbances coming from the mechanical portion of the drive train are always directly proportional to speed and occur at a frequency of once, twice, three times, etc., per shaft revolution. These disturbances arise from practical imperfections in the mechanical system and are generally of quite small magnitude, at least initially. Experience has shown, however, that operating continuously at speeds where such disturbances coincide with torsional resonance will produce a positive feedback mechanism involving component wear. This can eventually results in serious torsional vibrations and component failure. Because the torsional stress produced by resonant torque amplification of the initially small mechanical imperfection will be in synchronism with the excitation. Small but finite component wear, which results due to the torque oscillation, reinforces the original imperfections, causing it to grow.

The centrifugal force produced by rotor mass unbalance [21] will tend to bend the shaft, and then reinforce this unbalance until the excessive vibration make the system

failed. Due to gear coupling imperfection, the presence of internal exciting forces such as mesh stiffness variation, friction force and transmission error leads to torque oscillations at wheel, pinion and mesh frequencies [23]. This oscillating torque will probably excite the torsional vibration of the shaft assembly.

In a recent article [9], an analytical model based on two effects on the radial rotor movement and on the torque variations caused by bearing fault has been proposed. It is shown that the generalized roughness bearing defect produces torque oscillations affecting on the rotor, and causes mechanical rotation speed fluctuation.

Load Excitation

The final source of excitation is the load. This type of torque disturbances produced by the load system will depend upon the application. Centrifugal fans, compressors driven under normal conditions are unlikely to produce any torque pulsation, except for a small level of disturbance arising from fan blades passing the air system entrance or exit ductwork. While for reciprocating compressors [6], the torque pulsation is induced from the operation of crankshaft. This application is one of two anomalies studied in this dissertation.

Techniques for Torsional Vibration Monitoring

It has been explained that the torsional vibration resonance or shaft fatigue may be experienced under torque oscillation, and lead to destructive effects on certain parts of rotor shaft assembly. To monitor the torsional vibration, therefore, is important for the safety operation of equipment and preventing potential damage.

Accelerometer used for lateral vibration monitoring is not effective for torsional effect monitoring. Currently the popular techniques to measure torsional vibration include mounting strain gauge [24] on the shaft of the assembly or using laser torsional vibrometers [25], which are intrusive or expensive to be implemented. Considering that the torsional effects of shaft assembly could manifest itself in the signature of electrical signal of the driven motor, the ESA can also be applied to monitor the torsional effects. The literature is scarce for ESA based torsional vibration monitoring. Harmonic analysis of stator current for Permanent Magnet Synchronous Machines (PMSM) is presented to develop a robust real-time rotor unbalance estimation scheme for condition monitoring [21]. Forced steady state response of torsional vibration of induction machine is analyzed under different excitation frequencies and magnitudes [22]. Gearbox monitoring using stator current signature of induction machines has been studied in [23].

3. Bearing Anomaly Detection based on ESA

In the above section, we mentioned that torsional vibration induced by oscillating load torque will be Phase Modulated (PM) into the carrier sinusoidal current signal. Actually there is another torsional effect --- torque ripple induced by generalized roughness bearing defect.

Few literatures cover the bearing fault of synchronous machine. Jae-won Choi [26] first applied the stator voltages of alternator to detect the bearing fault, but his analysis is just based on some simple signal processing in time and frequency domain. While there are some researches were conducted on the fault detection of bearing fault in

induction motor by Motor Current Signature Analysis (MCSA). According to [7], bearing faults can be categorized into two classes: single point defect and generalized roughness. Single point defects will produce a radial motion between the rotor and stator of machine and eventually cause dynamic air-gap eccentricity, which could induce harmonics with related characteristic frequency in the air-gap permeance and in the air gap flux density. This, in turns, affects the inductances of the motor and produces stator current harmonics with specific frequencies which are amplitude modulated by the current sine wave.

Depending on which component of bearing, i.e. inner race, outer race, rolling ball or cage contains the defect, the harmonics with characteristic frequencies, f_{bng}, in current signature can be calculated from the rotor speed and the bearing geometry as follow,

$$f_{bng} = | f_e + m \bullet f_v | \tag{1.4}$$

where $m = 1, 2, 3 \cdots$ and f_v is one of the characteristic vibration frequencies, which could stand for inner race, out race, ball and cage defect frequencies:

$$f_i = \frac{n}{2} f_{rm} \left[1 + \frac{BD}{PD} \cos \beta \right] \tag{1.5}$$

$$f_o = \frac{n}{2} f_{rm} \left[1 - \frac{BD}{PD} \cos \beta \right] \tag{1.6}$$

$$f_b = \frac{PD}{BD} f_{rm} \left[1 - \left(\frac{BD}{PD} \cos \beta \right)^2 \right] \tag{1.7}$$

$$f_c = \frac{1}{2} f_{rm} \left[1 - \frac{BD}{PD} \cos \beta \right] \tag{1.8}$$

where f_{rm} is the mechanical speed in Hz, n is the number of ball, PD is the bearing pitch diameter, BD is the ball diameter, β is the contact angle of the balls on the races. All the geometrical parameters used in above formulas are illustrated in the Fig.2.

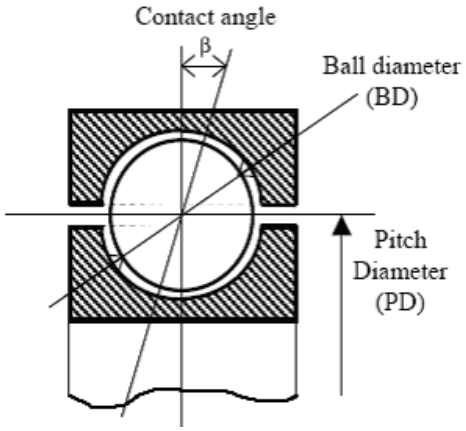

Fig.2 Rolling element bearing geometry

However, the induced characteristic frequency related to single point defect is often not obvious at its early stage, it will be significant detectable when it experiences severe damage just as the artificially fabricated fault conducted in many researches [8,9] by offline drilling a hole in the bearing inner or outer race and carving the rolling balls. This kind of defect is seldom happen in practice and is meaningless for incipient detection of the bearing defect. On the other hand, mechanical bearing often degenerate quickly into generalized roughness, which is a type of defect where the condition of a bearing surface has degraded considerably over a large area and become rough, irregular, or deformed. It is impossible to identify a specific frequency in the electrical signature, while unpredictable broadband changes in stator spectrum could be induced [7]. One of the physical explanations behind is that vibrations cause non uniform subtle

air-gap operation, therefore, the machine inductance oscillates. Because of this oscillation, the line current becomes noisy and the noise floor of current spectrum becomes higher as the severity increases.

For the generalized roughness defect, there is another physical link between bearing defect and current harmonics other than air-gap eccentricity. The vibration caused by generalized roughness defect of bearing will induce the torque ripple that produces a speed ripple which could be observed from torque measurements [27], even though the defect cannot produce detectable air-gap eccentricity and characteristic frequency. The speed variation will induce current harmonics by phase modulation. So the bearing-fault related vibration is seen as a torque or speed component that generates in the current a chain of components. This fault mechanism is best suited for generalized roughness defect, while the air-gap eccentricity fault model is best suited for single point defect. In practice, however, both fault mechanism could manifest for bearing fault more or less depends on how the bearing defect looks like.

Only several articles [28-30] conducted investigation on the analysis of generalized roughness bearing defect based on MCSA for induction motor. The signatures induced from the generalized roughness defect are often subtle and low energy signals, compared with the significant frequency components in the power spectrum such as fundamental and harmonics which could be considered as noise in the bearing anomaly detection. Rather than searching for specific frequency components, a modeling technique called the Mean Spectrum Deviation (MSD) method was proposed by Jason [28]. The signal spectrum was notched out harmonic contents that are not

related to the bearing fault from the current spectrum, and use the residual signal for analysis. The AR spectrum parametric model of the residual signal was estimated by baseline samples and stored as the baseline spectrum, which could be used to track the health change of bearing by monitoring the mean spectral deviation of present spectrum from baseline. Wei [29] employed a noise cancellation technique based on Wiener filter to suppress the significant frequency components that are not related to bearing defect. An adaptive noise-cancellation [30] method was applied to overcome the limitations of the noise cancellation above, which confine the analysis to constant load and frequency.

All above researches including Choi's [26] produced in-situ generalized roughness bearing deterioration by an externally applied shaft current [31], and acquired data during the whole deterioration process. The shaft current, however, could affect the electromagnetic field distribution [32] and then vibration signature of electrical machine, which is observed in our experiment. Actually the shaft current could affect the stray capacitance between stator core and rotor core and induce varying electric field between them, which will affect electromagnetic field distribution. On the other hand, the shaft current will heat the bearing, and increase the stiffness between bearing out ring and bearing housing. The rising temperature will also decrease the viscosity and damping of lubricant. All these change could increase the vibration transmissibility of bearing and amplify the vibration signal. So the bearing deterioration experiment and data acquisition procedure should be improved to closely resemble degradation in the field. Moreover, the above researches did not consider the effect of power quality of non-stationary input on the subtle current signature of generalized-roughness bearing defect.

So it is necessary to isolate the influence of nonstationary power input for improving the ESA of generalized roughness bearing defect.

C. Research Objective

Two major mechanical anomalies, torsional vibration of shaft assembly and generalized roughness bearing defect, will induce torsional effects, which could be reflected, more or less, in the signature of electrical signal. In practice, the non-stationary power input could induce similar signature in the electrical signal and probably mix with the subtle electrical signature induced by generalized roughness bearing defect. So the objectives of this research are as follows:

(1) To model the dynamic inter-coupling between electromagnetic and mechanical parts of the drive-load assembly

(2) To analyze the electrical signature due to shaft assembly torsional vibration, especially at the transient situation.

(3) To improve the experiment of progressive in-suite bearing deterioration in the laboratory to closely resemble degradation in the field.

(4) To analyze generalized roughness bearing anomaly in a synchronous motor using electrical measurements, and isolate the influence of input power variation and machine manufacturing imperfections on ESA of bearing anomaly.

(5) To verify the effect of load level on the bearing anomaly detection based on ESA

D. Proposed Approach

As explained before, the injected current will affect the magnetic field distribution and vibration transmissibility, then eventually the stator current during the bearing deterioration, so the reliability of ESA of bearing anomaly will suffer. To solve this problem, an improved experimental procedure will be introduced. It consists of healthy and several different faulty baseline stages with increasing severity. In-between are the deterioration stages with current injection. Data are acquired for all the stages, but only health and faulty baselines are analyzed for health condition trend analysis.

The main difficulty of ESA based bearing defect detection is that the effects of a bearing anomaly are often subtle and difficult to predict, especially for the generalized roughness, which cannot produce obvious specific characteristic frequencies. Moreover, the fluctuation of power quality of electrical input could induce similar signature and probably mix with the subtle electrical signature of bearing defect. So it is necessary to isolate the influence of non-stationary power input so the reliability of ESA can be achieved. Considering that the spectral characteristics of input voltages are slowly changing, a stationary interval can be defined within which the process is approximately stationary. In this dissertation, a segmentation procedure based on Classification and Regression Tree [33], is described that partitions the data into approximate stationary intervals of possible varying lengths, depending on the “degree of nonstationarity” in each interval. Then concatenate those pieces with the similar “degree of nonstationarity” to a locally piecewise stationary set. So the spectrum analysis can be conducted in the nearly stationary data set.

Usually generalized roughness bearing anomaly induces broadband signature in the current spectrum, the spectrum analysis and selected band pass filter will be applied to measure the broadband signature at specified frequency band, where the indicator can be formulated to track the health condition change of bearing. The flowchart of proposed approach to analyze torsional effect can be illustrated in the Fig.3.

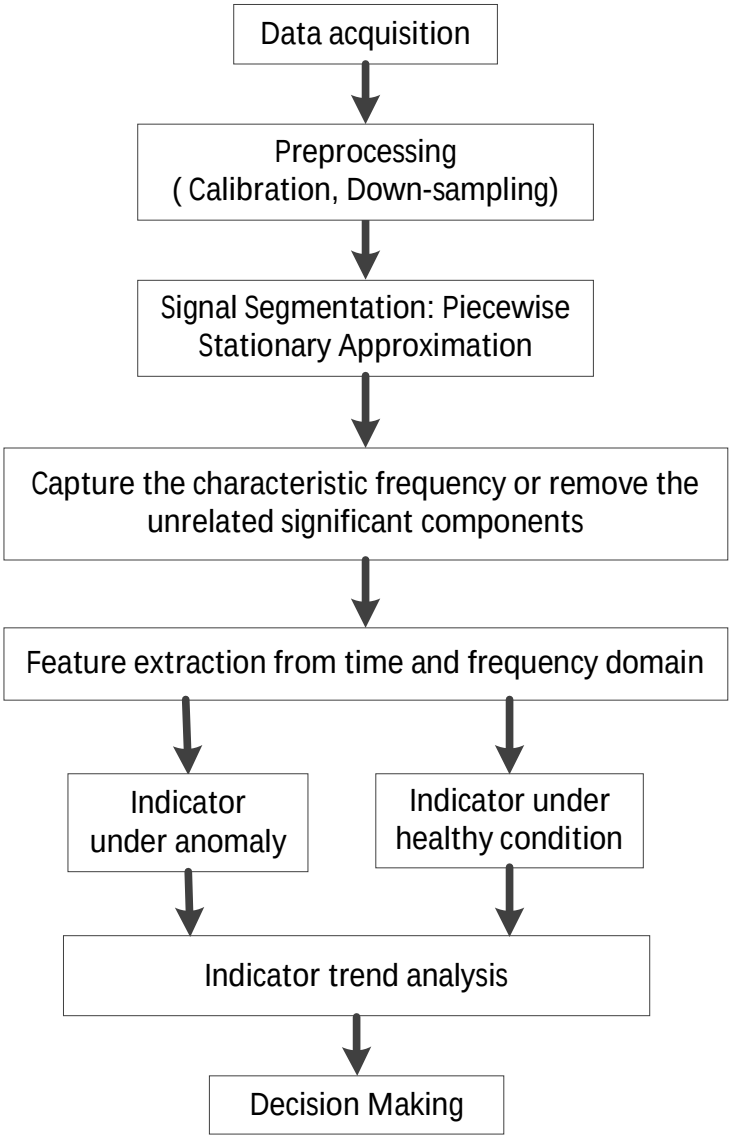

Fig.3 Overview of proposed approach

As for the monitoring of torsional vibration of shaft assembly, several papers [21-23] investigated the forced steady state torsional analysis under oscillating torque, which include critical speed, modal shape analysis and interference or Campbell diagram. While the ESA based transient torsional analysis during start-up is seldom analyzed. The coupling between electromagnetic and mechanical parts of the rotor assembly is dynamically dependent on the air-gap torque v.s. speed relationship of electric machine. This relationship of salient pole synchronous motor is conceptually different from the well-known steady state characteristic or that of induction motor start-up. Moreover, the mechanical torsional vibrations will further change the air-gap torque-speed characteristic during start-up.

In this dissertation, a time domain simulation model of the inter-coupling between electromagnetic and mechanical torsional dynamics will be developed to study the steady state and starting transients of synchronous motors. The electrical signature induced by torsional vibration of shaft assembly under oscillating load or speed can be verified and employed for condition monitoring.

5. Anticipated Contributions

The main contributions of this dissertation is to develop an approach for ESA of torsional effects induced by oscillating torque and generalized roughness bearing defect with improved experimental procedure.

(1) Coupled equivalent circuit method to simulate the dynamic coupling between electromagnetic and torsional dynamics of system, which is employed to estimate the electromagnetic torque

(2) Analyze the electrical signature due to shaft assembly torsional vibration especially at the transient situation.

(3) An improved in-suite experiment procedure to closely emulate the progressive generalized roughness bearing deterioration in the field, and remove the influence of shaft current on the anomaly signature in vibration and current signal.

(4) An approach to analyze generalized roughness bearing anomaly of synchronous motor using electrical measurements, and to isolate the influence of fluctuating input power quality on ESA of bearing anomaly.

CHAPTER II

FUNDAMENTALS OF ANALYSIS OF MECHANICAL ANOMALIES BASED ON ESA

Before we start the ESA of mechanical anomaly of electric machine, it is helpful to introduce the mechanical and electromagnetic dynamics of electrical machine. So we will first cover the lateral and torsional dynamics of synchronous machine and explain the common techniques to measure the lateral and torsional vibration. Then the electromechanical fundamental of synchronous machine will be discussed to explain the transmission of mechanical anomalies to electric signature. Furthermore, the amplitude and phase modulation will be presented to show in detail how these two different mechanisms modulate the mechanical anomaly into electrical signal. Finally two mechanical anomalies to be studied will be briefly covered. A summary diagram for this chapter is shown in the Fig.4.

A. Dynamic Model of Synchronous Motor and Load

The rotating electrical machine can be modeled as a complex system of masses, springs and damping. Some of the parts are considered “stationary” while others are rotating. The relative motions can be lateral vibration or torsional vibration. Usually the amplitude, frequency and other characteristics of these vibrations are measured and used to evaluate the perceived quality of the machine, and for condition monitoring. The mechanical dynamic performance of the system is the result of the interaction between

the various springs, damping and masses involved. The accurate prediction of this performance depends upon how well the characteristics of these masses, damping, springs and damping are determined. The condition monitoring of machine needs to exam how the operation condition, internally grown and externally forced anomaly affect these parameters and lead to machine condition changes.

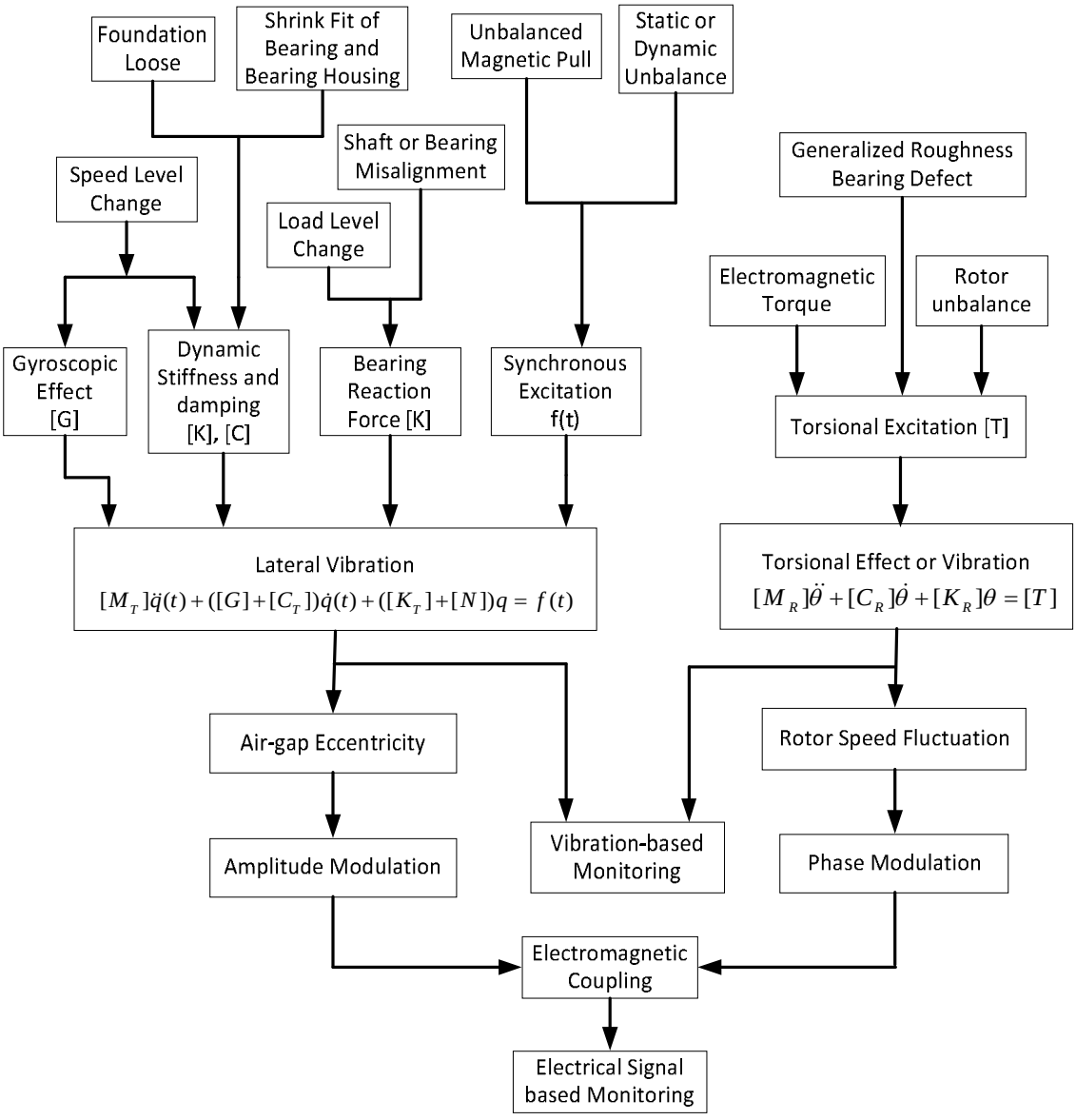

Fig.4 Diagram of ESA and vibration monitoring

1. Lateral Vibration Model of Synchronous Motor

To exam the lateral vibration, we model the synchronous motor as a rigid rotor on flexible bearing and foundation, and assume that the bearing stiffness is linearized at it equilibrium load position. So that the bearing can be modeled as two linear springs in x- and y- axes. The model can be expressed in the Fig.5 below.

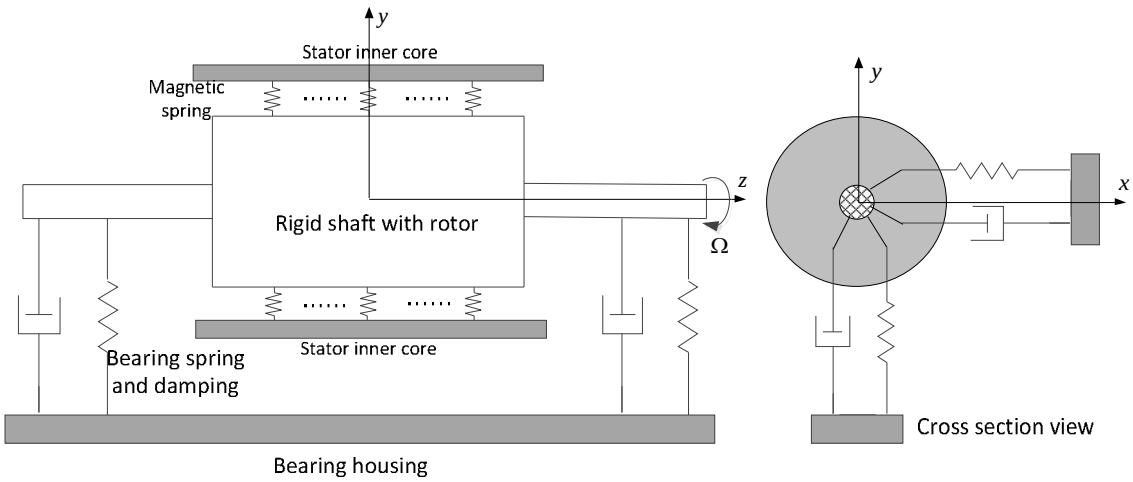

Fig.5 A simplified model for rotor-bearing system

The rotor system is spinning at Ω and with excitations $f(t)$ acting on it. The dynamic model for the vibrational motions of rotor can be expressed as:

$$[M_T]\{\ddot{q}(t)\}+([G]+[C_T])\{\dot{q}(t)\}+([K_T]+[N])\{q\}=\{f(t)\} \qquad (2.1)$$

where $[M_T]$--- Translational mass matrix,

$[G]$--- Represent gyroscopic coupling between x- and y- axes,

$[C_T]$--- Translational dynamic damping matrix,

$[K_T]$--- Linearized bearing translational dynamic stiffness matrix,

$[N]$--- the matrix of the non-conservative bearing forces,

$\{q\}$ --- the generalized displacements of the rotor in inertial coordinates.

$\{f(t)\}$ is the forcing function such as unbalanced mass centrifugal force

The $[K_T]$ and $[C_T]$ are related to dynamic stiffness and damping matrix of system, which will be discussed in detail later. The gyroscopic matrix G is proportional to spin speed Ω. The general solution to the above equation involves complex eigenvectors which are spin speed dependent.

The excitation forces $\{f(t)\}$ acting on the rotor-bearing system can be separated into two broad categories: synchronous and nonsynchronous. Synchronous means that the input force is at the same frequency as the rotor spinning speed. The most common synchronous excitation force in rotating machinery is the residual imbalance in the rotor. As this imbalance rotates, it generates a once-per-turn centrifugal force. Nonsynchronous, as you would expect, refers to any excitation force that is independent of the rotational speed of the machine.

The dynamic stiffness and damping coefficient, radial excitation forces and speed of rotor exert significant influences on the stability and vibration behavior of a rotor-bearing system.

In this section, we will discuss dynamic stiffness and damping, static and dynamic unbalance, static and dynamic air-gap eccentricity, and unbalanced magnetic pull. Each of these cases could affect the coefficients in the rotordynamic equation (2.1) and change the dynamics of spinning rotor and the vibration and electrical signatures used for machine health condition.

Dynamic Stiffness and Damping

As a most popular approach for condition monitoring of machine, vibration is a response to other conditions in a machine. Vibration should be thought of as nothing more than a ratio of the forces $\{f(t)\}$ acting on the machine to its stiffness K_T. In other words, vibration is merely a result of other root causes occurring in a machine. A change in unbalance is an example of a force changing in a machine. In this case, force increases stiffness stays the same, and vibration increases as a result. The other root causes can be changing stiffness. A common case is the so called dynamic stiffness, which is the frequency dependent ratio between a dynamic force and the resulting dynamic displacement.

The synchronous dynamic stiffness [35] can be defined from the Laplace transform of the rotor response equation as shown in eq. (2.1).

$$\vec{R} = \frac{F \angle \varphi}{(K + N - M_T \Omega^2) - j(C_T + G)\Omega} \tag{2.2}$$

The parameters above are defined in the eq.(2.1), which shows the speed dependence of dynamic stiffness. More information about dynamic stiffness can be found in [35]. From the dynamic stiffness, vibration transmissibility can be derived to show the how the stiffness and damping affect the response of excitation as function of rotating speed. It will be covered in detail in chapter IV.

In [36, 37], the bearing stiffness can be analytically derived and experimentally identified as a frequency and load dependent characteristics for rolling element bearing. So the vibration will change as the rotor spinning speed and load change. The radial

clearance between the bearing rolling element and races is also an important factor which affects the bearing stiffness and then the dynamic vibration response transmitted. In [39], S.H. Upadhyay took into account the change in dynamic stiffness due to clearance. The experimental analysis showed that bearing clearance changes the response of a rotor significantly because of the change in dynamic stiffness of the bearing. Furthermore, the increase in clearance will make the region of unstable and chaotic response wider.

The unevenly temperature buildup inside the bearing could cause the clearance change. For example, the shaft current could induce heat across the bearing and the temperature field is built with gradient from the inner ring to outer ring. So the inner ring will expand more than the outer ring does, so that the clearance will be reduced and the vibration measure at the bearing housing will increase due to the stiffness rising between metal contacts. The same logic can be applied to the clearance between the bearing outer ring and bearing housing.

Contamination, inadequate lubrication, misalignment and long term operation could cause the bearing wear and increase the radial clearance. As the clearance rises, the wear is usually accelerated. So the excessive bearing wear could cause rub between stator and rotor, and change the vibration response of system.

Static and Dynamic Unbalance

The technically most important sources for exciting vibrations in a rotor-bearing system are unbalances. If a balanced rotor is mounted on knife-edge or rollers at the

journals, it can be rotated and will come to rest at any position when rotation stops. If unbalanced weights are applied to the surface of the rotor as shown in Fig.6, it will always come to rest with the heavy side down. Weighs of the same size applied diametrically opposite will restore the static balance of the system and it will again stop at random. This is so called static balancing.

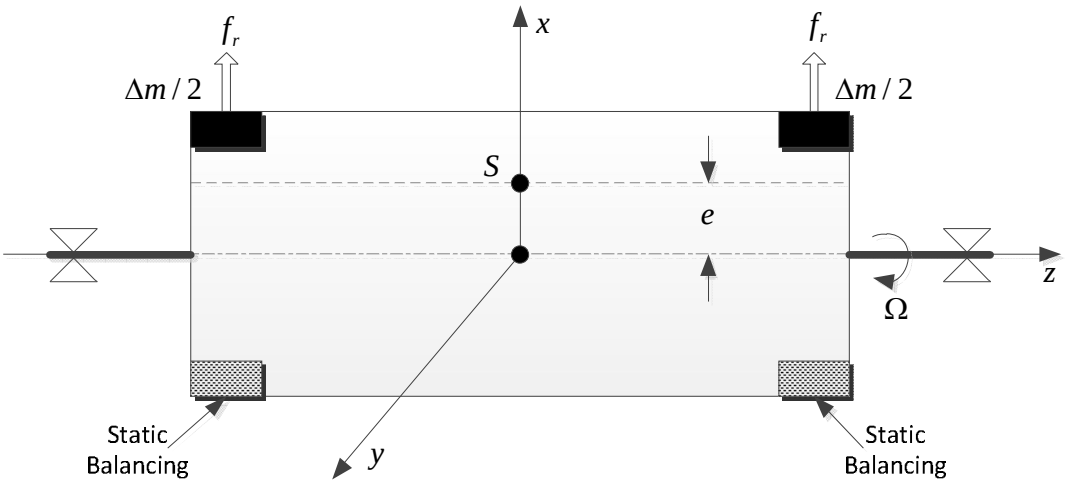

Fig.6 Schematics of static unbalance

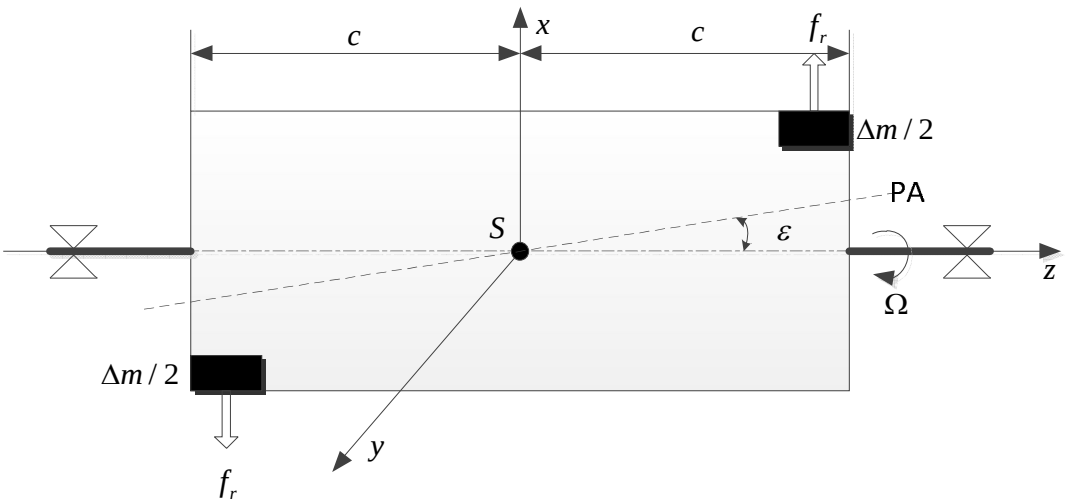

Fig.7 Schematics of dynamic unbalance

For machines under static balanced condition, it could still be in dynamic unbalance. As shown in Fig.7, the rotor could restore to static balance if the weights are equal and located 180 degrees apart. However, it is unbalanced dynamically. The location of the weights form a “couple” which tends to rock the principle axis of rotation as the two ends of the rotor are moving opposite to one another.

A static or dynamic unbalanced rotor, of course, does not exert a constant force or torque but vibrating forces, which finally act through the bearings onto the housing. If the bearings are suspended elastically the rotor has the possibility to move, and it will vibrate. These vibrations in the bearings can be measured, and from the phase angles and the amplitudes of the vibrations with respect to the rotation angle of the rotor, the unbalances can be determined: a static unbalance leads to equally phased vibrations in the left and in the right bearing, a dynamic unbalance to vibrations with opposite phase.

For the spinning rotor, the static unbalance will produce centrifugal force on the rotor and pull the mass center of rotor offset the equilibrium position and induce static air-gap eccentricity. While dynamic unbalance will also induce rotor tilt except the offset of mass center. Different rotor vibration mode shape will produce diverse air-gap eccentricity types, and the air-gap eccentricity also affects the rotor vibration in return [39].

The air-gap eccentricity could induce related current signatures in stator windings by electromagnetic coupling through amplitude modulation, which will be discussed later in this chapter. The rotor unbalance could also produce speed fluctuation and cause torsional vibration, which will be explained in Section A.2.

Static and Dynamic Air-gap Eccentricity

Air-gap eccentricity leads to an air-gap length that is no longer constant with respect to the stator circumference angle and/or time. In general, three types of air-gap eccentricity can be distinguished as shown in Fig.8.

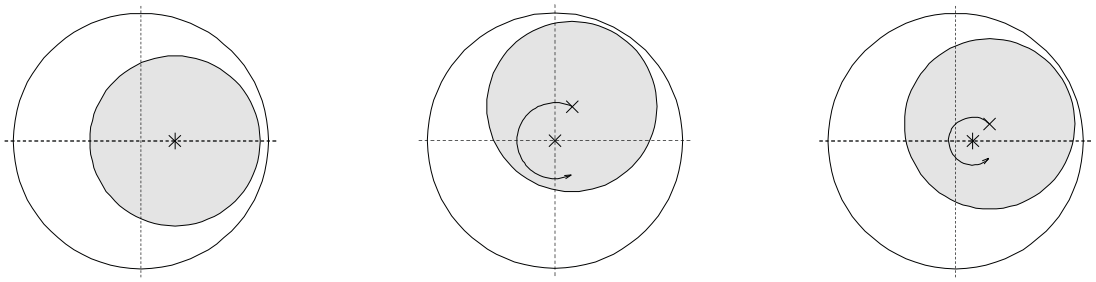

(a) Static eccentricity (b) Dynamic eccentricity (c) Mixed eccentricity

Fig.8 Schematic representation of static, dynamic and mixed eccentricity
× denotes the rotor geometrical center, * denotes the rotor rotational center

Static eccentricity: The rotor geometrical and rotational centers are identical, but different from the stator center. The point of minimal air-gap length is stationary with respect to the stator.

Dynamic eccentricity: The rotor geometrical center differs from the rotational center. The rotational center is identical with the stator geometrical center. The point of minimal air-gap length is moving with respect to the stator.

Mixed eccentricity: The two effects are combined. The rotor geometrical and rotational center as well as the stator geometrical center is different.

Air gap eccentricity may result from the assembly and manufacturing processes. For example, static eccentricity is caused by manufacturing tolerances between the center of the stator bore and bearing centers.

In addition to flaws in the assembly and manufacturing processes, air gap eccentricity is also caused by external mechanical problems in induction motors, such as load unbalance, loose mounting, or shaft misalignment. These mechanical problems cause a radial unbalanced force on the rotor, which pulls the rotor from its normal position and generates a non-uniform air gap.

The air-gap eccentricity could affect the magnetic field distribution, torque production and current signature of the stator winding by the electromechanical coupling, which will be covered in detail in Section C following.

Unbalanced Magnetic Pull and Magnetic Spring

If space, slot and saturation harmonics are neglected, the radial magnetic forces are balanced around the rotor when the rotor is concentric with the stator bore. If the rotor is offset with regard to the stator bore, the radial magnetic forces are unbalanced with the unbalanced force tending to deflect the rotor in the direction of the minimum air-gap. The magnitude of Unbalanced Magnetic Pull (UMP) [40] is directly proportional to the radial displacement of the rotor, and pull the rotor tend to deflect more along the smaller air-gap side. So this magnetic spring constant, k_m, is negative and related to the magnetic loading of the rotor and the air gap geometry as follows:

$$k_m = KB_g^2 DL / g \tag{2.3}$$

where: B_g = Air gap flux density, D = Stator bore diameter,

L = Stator bore length, g = mean air gap length

K is a factor which might depend on a number of variables, such as pole number and the ratio of the air-gap reluctance to that of the whole magnetic circuit.

The negative magnetic spring works directly against the shaft and bearing springs, which tend to return the shaft toward static equilibrium, while the magnetic spring wants to bend the shaft further in the direction of the minimum air gap. The net effect is to reduce the effective spring constant of the shaft and change the lateral response of rotor dynamic system. The weakened shaft spring also further reduces the rotor natural frequency and changes the related mode shapes.

2. Torsional Vibration Model of Motor Shaft Assembly

Torsional vibration involves the transfer of power between two or more connected rotating masses. The applied forces are torsional and tend to twist the connecting shafts, where shear stresses will be developed. Unlike lateral vibration, torsional vibration is not readily recognized nor easily measured or monitored. A simplified two mass torsional dynamic model is shown in Fig.9.

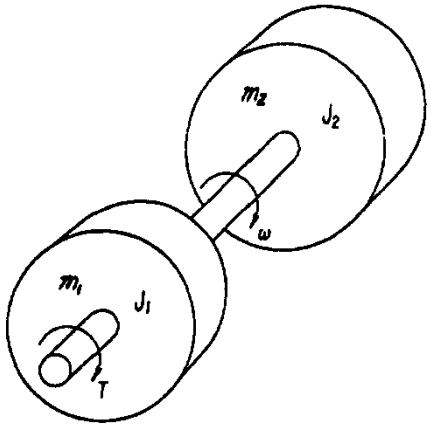

Fig.9 Two mass torsional system

The motor rotor is spinning at Ω under excitations $T_e(t)$ acting on it. The load rotor driven by the motor under resistive torque $T_L(t)$. The dynamic model for the torsional vibrational motions of rotor-assembly can be expressed as:

$$[M_R]\ddot{\theta} + [C_R]\dot{\theta} + [K_R]\theta = [T_R] \tag{2.4}$$

where $[M_R]$ is the inertia matrix of rotors

$[C_R]$ is the torsional damping matrix of rotors

$[K_R]$ is the torsional stiffness matrix of rotors

$[T_R]$ is the torsional excitation matrix of rotors

Usually the torsional damping is comparatively lower unless external damping is introduced intentionally. The torsional stiffness is predetermined by the shaft design. The inertia matrix can be changed by adding flywheel at where the design required.

As discussed in chapter one, the torsional vibration excitations usually come from four major sources depending on where in the system they originate in. Harmonics in the electrical supply voltage and/or current could produce harmonic exciting torque. Excitation from mechanical transmission such as imperfect gear coupling will excite the torsional vibration of shaft assembly. Another important source of torsional excitation is the load, especially for the electric machine driven turbomachinery. For instance, the reciprocating compressors and pumps are sources of complex, harmonic-rich excitation. Harmonics due to electric machine configuration and property, such as slot, non-sinusoidal winding distribution and saturation could also be a very important source of excitation to the rotor system during steady state and especially transient.

Torsional Resonance

The conditions for torsional resonance are the same as for lateral resonance, the exciting frequency approaches the natural frequency of the system. Because torsional resonances are system conditions rather than machine conditions, shafts are designed on the basis of the shear strength as a percentage of the maximum motor torque. The result is that components loaded in shear are less forgiving of stress amplification at resonance. These parts are more susceptible to fatigue failure than those loaded in bending. The natural frequencies and mode shapes can be solved as an eigenvalue problem. Then we can find the critical speed and interference or Campebell map [24] for checking the possibility of torsional resonance.

Torsional Excitation during Startup

All synchronous motors, permanent magnet or external excited, synchronous motors, will generate harmonics between 120Hz~0Hz in the electromagnetic torque profile during start-up [41]. The harmonic electromagnetic torque will interact or couple with the torsional dynamics of the rotor system and load torque.

Most common two and three mass systems, typical of direct-coupled and geared compressor drives, have at least one shaft natural frequency between 10 and 30 Hz. For the downhole applications such as electric submersible pump or compressor [42], the shaft natural frequencies will drop below 120Hz as the length of system increase to fit the power requirement. For these applications, the rotor system will inevitably be excited

during the startup and the electromagnetic torque could also be amplified during a short period of crossing the natural frequency

It has been realized that since the torque oscillation, the torsional vibration resonance or shaft fatigue may be experienced leading to destructive effects on certain parts of motor-load shaft assembly.

The synchronous machines are widely employed as driver where the loads are possibly fluctuating. Furthermore, the synchronous machine itself will produce oscillating electromagnetic torque due to possible harmonic power input and winding pattern etc. Under torsional effects, the oscillating load torque or electromagnetic torque will induce speed fluctuation, which will affect the rotor MMF of the machine and eventually the current signature. This is also the fundamental of the electrical signature analysis of torsional effects.

Unbalanced Induced Torsional Effect

In the last section, we discussed that the rotor unbalance will cause synchronous lateral vibration. Actually it will also induce torque pulsation at the same time. The Fig.10 shows the torsional dynamics of motor rotor under unbalance. This unbalance can be either motor rotor mass unbalance or the load unbalance of a mechanical system. The total moment of inertia J_t consists of J_{mL} -- inertial of motor and load inertia, and J_{um} -- inertial of unbalanced mass. The gravity force produced by the unbalanced mass m could induce a torque to the opposite direction of rotation. The torque is a function of the mechanical rotor position θ_m. The equation of motion can be expressed as eq. (2.5).

$$J_t\ddot{\theta}_m + b_p\dot{\theta}_m = T_e - T_L - mge\sin\theta_m \tag{2.5}$$

This pulsating torque disturbance will cause speed fluctuation. The electromagnetic torque T_e is produced by synchronous motor air-gap. The rotational friction term $b_p\dot{\theta}_m$ is determined by the viscous damping constant and the mechanical rotor speed.

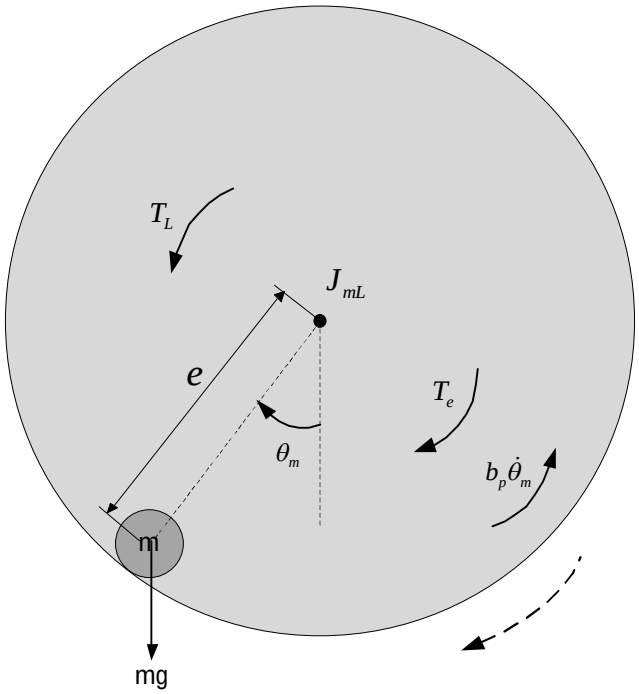

Fig.10 Torsional dynamics of motor rotor under unbalance

If assumed that constant speed is ideally maintained by a speed regulator with an infinite bandwidth, we can neglect the inertia term $J_{mL}\ddot{\theta}_m$. The electromagnetic torque for the motor is represented by (2.6).

$$T_e = b_p\dot{\theta}_m + mge\sin\theta_m + T_L \tag{2.6}$$

The electromagnetic torque oscillation produced by the unbalance makes it possible for one to analyze the intrinsic essence of phase current variation under the unbalance by phase modulation.

B. Measurement of Lateral and Torsional Vibration

To measure machinery or structural vibration, translational or torsional, a transducer or a vibration pickup is used. A transducer is a device that converts one type of energy, such as vibration and strain energy, into a different type of energy, usually an electric current or voltage. Commonly used transducers are velocity pickups, accelerometers and eddy current or proximity probes for translation vibration, Strain gauges and laser torsional vibrometer for torsional vibration. Each type of transducer has distinct advantages for certain applications and limitations as well. Therefore one of the most important considerations for any application is to select the transducer that is best suited for the job. The IEEE standard gave guideline for picking up different transduce to measure corresponding signal [43]. For a more formal treatment of machinery vibration measurement, refers to the books by Bently [35] and Muszynska [44].

1. Translational Vibration Measurement by Accelerometer

Accelerometers are the most popular transducers used for rotating machinery applications. They are rugged, compact, lightweight transducers with a wide frequency response range. Accelerometers are extensively used in many condition-monitoring applications. Components such as rolling element bearings or gear sets generate high vibration frequencies when defective. Machines with these components should be monitored with accelerometers.

Accelerometers are inertial measurement devices that convert mechanical motion into a voltage signal. The signal is proportional to the vibration's acceleration using the

piezoelectric principle. Accelerometers consist of a piezoelectric crystal and a small mass normally enclosed in a protective metal case. When the accelerometer is subjected to vibration, the mass exerts a varying force on the piezoelectric crystal, which is directly proportional to the vibratory acceleration. The charge produced by the piezoelectric crystal is proportional to the varying vibratory force.

2. Torsional Vibration Measurement

Torsional vibration is typically superimposed on the static torque already experienced by power transmission shafts. This may result in extremely high dynamic stresses leading to catastrophic failure. Strain gauges with telemetry data acquisition equipment and laser torsional vibrometer are usually employed to measure the torsional vibration stresses and deflection in rotating equipment.

Strain Gauges with Telemetry Equipment

By installing shear (torsion) strain gauges and lightweight digital telemetry kits on rotating shafts, couplings etc, both the static and dynamic torque, shear strains and shear stresses can be measured during transient and steady state conditions. So that the starting torque assessments (static or dynamic), investigations of coupling or shaft and rotor damage are feasible.

Direct measurement on shaft or coupling spacer provides actual torques, strains and stresses. Both static components and dynamic components exciting torsional vibrations are available. So it is suitable for both transient and steady state analysis.

Laser Torsional Vibrometer

Torsional laser vibrometer takes reading from a ring of reflective tape placed at various locations on a shaft or along a machine train. Then torsional vibrations at each point can be measured as changes in rotational speed (deg/s) or as rotational deflections (deg). With a suitable tacho signal, various locations can be measured while the unit remains at a steady state.

The laser vibrometer can assess torsional vibrations includes analysis of torsional operational deflection shapes (ODS), analysis of torsional critical speed (resonances), investigations of coupling or shaft and rotor damage.

Comparing with strain gauge measurement, laser vibrometer is simple to install with minimum machine downtime and no further downtime required for subsequent installations. It can also be moved to a new location during operation. Both rotation speed changes and deflection amplitudes with phase data can be made available by using a reference tacho. So the torsional operational deflection shapes (ODS) can be constructed from amplitude and phase data. While it cannot measure the dynamic torque and stress on the shaft, the cumulative stress analysis for fatigue life prediction is not feasible. Furthermore, vibrometer is more expensive than strain gauge.

The traditional use of rotating machinery vibration monitoring is to provide warning if vibration levels become sufficiently high to potentially damage the machine. Present diagnostic methods now allow a much broader assessment of a machine's condition from its monitored vibration than just saying "the vibration level is too large." Predictive maintenance is one example of a capability derived from condition

monitoring. While in this dissertation, proposed approach will be shown how electrical signature analysis could replace vibration analysis in condition monitoring with less cost and comparable performance.

C. Transmission of Mechanical Anomalies to Electric Signal

The air-gap torque is the bridge linking the electromagnetic and mechanical phenomena. It can be estimated by (2.7) in which the stator and field current are expressed as summation of dc and harmonic components. On the other hand, the load torque can be decomposed into a deterministic component (DC plus harmonics) and noise, which is shown in (2.8). The mechanical equation of motion is expressed in (2.9)

$$T_e(t) = I_s^T \frac{dL_{sf}}{dt} I_f, where \quad I_k = \sum_h I_{kh} \cos(h\omega_e t + \varphi_h), k = s, f, h = 0,1,2,\cdots \tag{2.7}$$

$$T_L(t) = \sum_h T_h \cos(h\omega_m t + \varphi_h) + T_N, h = 0,1,2,\cdots \tag{2.8}$$

$$T_e - T_L = T_R = J_t \ddot{\theta}_m + b_p \dot{\theta}_m \tag{2.9}$$

In chapter I, the coupled magnetic circuit model is employed to describe the electromagnetic coupling of electric machine by winding function approach [12]. The Fig.11 shows the equivalent circuit diagram (single phase shown) of the coupled stator and field magnetic circuits, which are related by the mutual inductance L_{sf}. The flux linkage in the stator and rotor winding can be expressed as below:

$$\begin{bmatrix} \lambda_{abcs} \\ \lambda_{abcf} \end{bmatrix} = \begin{bmatrix} L_s & L_{sf}(\theta_m(t)) \\ L_{sf}^T(\theta_m(t)) & L_f \end{bmatrix} \begin{bmatrix} i_{abcs} \\ i_{abcf} \end{bmatrix} \tag{2.10}$$

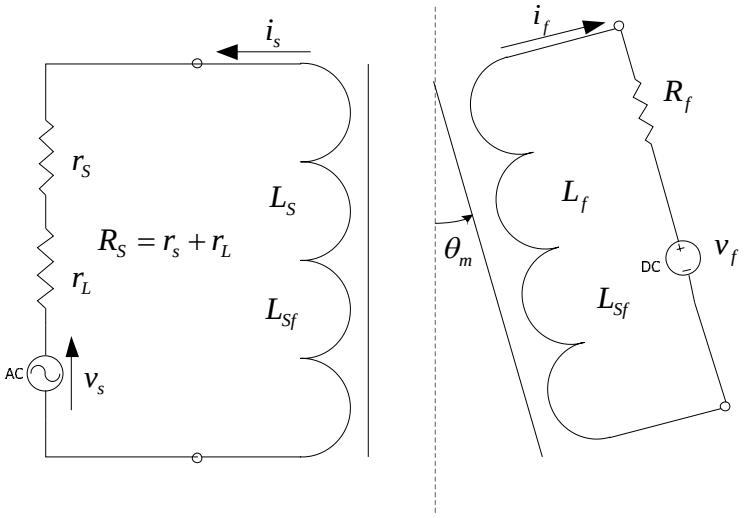

Fig.11 Equivalent diagram of coupled magnetic circuits

Where $\theta_m(t)$ is the mechanical rotating angle of the rotor, the winding inductances L_s, L_r and $L_{sr}(\theta_m(t))$ are functions of angular rotor positions and other machine design parameters. The induced the voltage in the stator and field windings are given by

$$V(t) = R \cdot i(t) + \frac{d\lambda}{dt} \tag{2.11}$$

Substitution of (2.10) into (2.11) will result in the (2.12). The phasor equation [45] can be obtained by replacing the derivative with $j\omega$. For a salient pole synchronous machine, let $V_f = V_0$, it's phasor equation can be expressed as in (2.13). For its phase equation, we expressed the current phasor $\tilde{I}_s$ in terms of voltage phasor $\tilde{V}_{abcs}$ as shown in (2.14).

$$\begin{cases} V_{abcs} = R_s i_{abcs} + L_s(pi_{abcs}) + (pL_{sf}(\theta_m(t)))i_f + L_{sf}(\theta_m(t))(pi_f) \\ V_f = R_f i_f + (pL_{sf}^T(\theta_m(t)))i_{abcs} + L_{sf}^T(\theta_m(t))(pi_{abcs}) + L_f(pi_f) \end{cases} \tag{2.12}$$

$$\begin{cases} \tilde{V}_{abcs} = (R_s + j\omega_s L_s)\tilde{I}_s + (j\omega_s L_{sf}(\theta_m(t)))\tilde{I}_f \\ \tilde{V}_f = j\omega_m L_{sf}^T(\theta_m(t))\tilde{I}_s + (R_f + j\omega_m L_f)\tilde{I}_f \end{cases} \tag{2.13}$$

$$\Rightarrow \tilde{I}_s = M\left(\tilde{V}_{abcs} - \frac{j\omega_s L_{sf}(\theta_m(t))}{R_f + j\omega_m L_f}\tilde{V}_f\right) \tag{2.14}$$

$$\text{where} \quad M = \left[R_s + j\omega_s L_s + \frac{\omega_s \omega_m L_{sf}(\theta_m(t)) L_{sf}^T(\theta_m(t))}{R_f + j\omega_m L_f}\right]^{-1} \tag{2.15}$$

The (2.14) shows the transmission of mechanical or electrical anomalies into current signal. The parameters in (2.14) carry mechanical anomalies are mutual inductance $L_{sf}(\theta_m(t))$ and rotor speed $\omega_m(t)$. The torque oscillation induces mechanical speed oscillation $\Delta\omega_m$, then mutual inductance oscillation and finally current signature, while air-gap eccentricity will affect mutual inductance and finally current signature. Next will show how the mechanical anomalies modulated into current signature in detail.

D. Modulation Mechanism of Mechanical Anomalies

In the previous section, the transmission path of mechanical or electrical anomalies to current signature was derived to show what anomalies could affect the current signal. This section will continue to explain in detail how these anomalies modulated into current signature. Modulation is originally a terminology in communication system in which the information (digital or analog), or the baseband signal to be transmitted is modulated i.e. “encoded” onto a carrier signal. In the case of ESA for synchronous motor, the carrier signal is the sine or cosine signal with supply frequency and usually

together with its low magnitude harmonics. The electrical or mechanical anomaly signature will be "encoded" into the carrier wave. If we assume that the carrier is a Fourier series, there are three parameters of the carrier that can be modulated and used for information transfer. These parameters are the amplitude $a(t)$, frequency $f(t)$ and phase $\phi(t)$. The modulated carrier is

$$s(t) = A(t)\cos\left(2\pi\int_0^t \omega(\tau)d\tau + \phi(t)\right) \tag{2.16}$$

If the anomaly related characteristic signature is encoded to $A(t)$, the corresponding modulation is called Amplitude Modulation (AM). So the Frequency Modulation (FM) and Phase Modulation (PM) are defined as the anomaly signature is encoded to $\omega(t)$ and/or $\phi(t)$. FM and PM are also referred to as angular modulation and are related in that the frequency is the phase changing speed. FM and PM will have the same effect on signal encode, so if without mentioned, only PM will be used in the following of this dissertation. For convenience to illustrate, below torsional effects and phase modulation will be discussed first.

1. Torsional Effects and Phase Modulation

Martin [9] used the MMF and permeance wave approach to study the stator current modulation caused by torque oscillation for induction machines. Here it will be extend it to synchronous machine.

Under a mechanical fault, the load torque as a function of time is modeled by a constant component T_{const} and an additional component varying at the characteristic

frequency f_c, depending on the fault type. For simplicity, the higher order terms are neglected in the following, and only the fundamental term is considered. The load torque can therefore be described by

$$T_L(t) = T_{const} + T_c \cos(\omega_c t) \tag{2.17}$$

where T_c is the amplitude of the load torque oscillation and $\omega_c = 2\pi f_c$. The machine mechanical equation relates the torque oscillation to the motor speed ω_r as follows:

$$\sum T(t) = T_e(t) - T_L(t) = J\frac{d\omega_r}{dt} = J\frac{d^2\theta_r}{dt^2} \tag{2.18}$$

where T_e is the electromagnetic torque produced by the synchronous machine and J is the total inertial of the machine and the load.

After integration twice, θ_r is obtained as

$$\theta_r(t) = \int_{t_0}^{t} \omega_r(\tau)d\tau = \frac{\sum T(t)}{J\omega_c^2}\cos(\omega_c t) + \omega_{r0}t \tag{2.19}$$

In steady state, the motor torque T_e is equal to the constant part T_{const} of the load torque. The mechanical speed is then expressed as

$$\omega_r = \frac{1}{J}\int_{t_0}^{t} T_c \cos(\omega_c \tau)d\tau + C = \frac{T_c}{J\omega_c}\sin(\omega_c t) + \omega_{r_0} \tag{2.20}$$

The mechanical speed consists therefore of synchronous speed ω_s and a sinusoidal oscillation. Finally, the mechanical speed integration provides the mechanical rotor position θ_r. In contrast to the healthy machine where $\theta_r = \omega_s t$, oscillations at the characteristic frequency are present on the mechanical rotor position.

$$\theta_r(t) = \int_{t_0}^{t} \omega_r(\tau) d\tau = \frac{T_c}{J\omega_c^2} \cos(\omega_c t) + \omega_s t \tag{2.21}$$

Effect on Rotor MMF

For the rotor and stator MMF considered here, only the fundamental space and time harmonic is taken into account; higher order space and time harmonics are neglected. The oscillations of mechanical rotor position θ_r act on the rotor MMF, which is excited by a DC current or permanent magnet. In a normal state, the rotor MMF in the stator reference frame is a wave with p pole pairs given by

$$F_r^R(\theta_r, t) = F_r \cos(p\theta') \tag{2.22}$$

where θ is the mechanical angle in the stator reference frame (R), and higher order space and time harmonics are neglected.

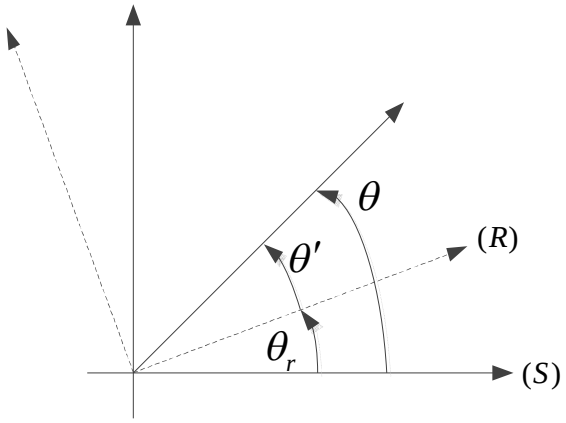

Fig.12 The stator and rotor reference frame

Fig.12 displays the transformation between the rotor and stator reference frame, defined by $\theta = \theta' + \theta_r$. Using (2.21), thus, the rotor MMF given in (2.22) can be

transformed to the stationary stator reference frame using (2.21) and the relation:

$$F_r(\theta,t) = F_r(p\theta - \omega_s t - \beta\cos(\omega_c t)) \tag{2.23}$$

With $$\beta = p\frac{T_c}{J\omega_c^2} \tag{2.24}$$

Equation (2.23) clearly shows that the load torque oscillations at frequency f_c lead to a phase modulation of the rotor MMF in the stator reference frame. This phase modulation is characterized by the introduction of the term $\beta\cos(\omega_c t)$ in the phase of the MMF wave. The parameter β is generally called the modulation index. For physically reasonable values J, T_c and ω_c, the approximation $\beta \ll 1$ holds in most cases.

The torsional effects have no direct effect on the stator MMF and so it is considered to have the following form:

$$F_s(\theta,t) = F_s(p\theta - \omega_s t - \varphi_s) \tag{2.25}$$

Let $\gamma = \varphi_s - \beta\cos(\omega_c t)$, γ is the phase difference between rotor and stator MMF, φ_s is the initial phase difference without torque oscillation. γ is also called load angle, it related to torque production, and match with a specific torque value. The basic idea behind is that the torque oscillation could cause the load angle change correspondingly, which will be phase modulated into resulting MMF and flux density.

Effect on Flux Density and Stator Current

The magnetic field in the air-gap can then be determined by multiplying the permeance by the sum of rotor and stator MMFs. The equivalent magnetic flux in one

phase is obtained by integration of the magnetic field in each turn of the phase winding. The induced phase voltage, related to the current by the stator voltage equation, is then deduced from the magnetic flux.

The air-gap flux density $B(\theta,t)$ is the product of total MMF and air-gap permeance P. The rotor speed is supposed to be constant because no torsional effects are taken into account for the sake of clarity and simplicity.

$$\begin{aligned} B(\theta,t) &= \left[F_s(\theta,t) + F_r(\theta,t)\right]P \\ &= B_s\cos(p\theta - \omega_s t - \varphi_s) + B_r(p\theta - \omega_s t - \beta\cos(\omega_c t)) \end{aligned} \tag{2.26}$$

The phase modulation of the flux density $B(\theta,t)$ exists for the flux $\Phi(t)$ itself, as $\Phi(t)$ is obtained by simple integration of $B(\theta,t)$ with respect to the winding structure. The winding structure has only an influence on the amplitudes of the flux harmonic components, not on their frequencies. Therefore, $\Phi(t)$ in an arbitrary phase can be expressed in a general form:

$$\Phi(t) = \Phi_s\cos(\omega_s t + \varphi_s) + \Phi_r\cos(\omega_s t + \beta\cos(\omega_c t)) \tag{2.27}$$

The relation between the flux and the stator current in a considered phase is given by the stator voltage equation:

$$V(t) = R_s I(t) + \frac{d\Phi(t)}{dt} \tag{2.28}$$

With $V(t)$ imposed by the voltage source, the resulting stator current will be in a linear relation to the time derivative of the phase flux $\Phi(t)$ and will have an equivalent frequency content. Differentiating (2.27) leads to:

$$\frac{d\Phi(t)}{dt} = -\omega_s \Phi_s \sin(\omega_s t + \varphi_s) - \omega_s \Phi_r \cos(\omega_s t + \beta \cos(\omega_c t)) + \omega_c \beta \Phi_r \sin(\omega_s t + \beta \cos(\omega_c t)) \sin(\omega_c t) \tag{2.29}$$

The amplitude of the last term is smaller than that of the other terms due to $\beta \ll 1$. Thus, the last term in (2.29) will be neglected in the following. As a consequence, the stator current in an arbitrary phase can be expressed in a general form:

$$I(t) = i_{st}(t) + i_{rt}(t) = I_{st} \sin(\omega_s t + \varphi_s) + I_{rt} \sin(\omega_s t + \beta \cos(\omega_c t)) \tag{2.30}$$

Therefore the stator current $I(t)$ can be considered as the sum of two components. The term $i_{st}(t)$ results from the stator MMF and it is not modulated. The term $i_{rt}(t)$ which is a direct consequence of the rotor MMF shows the phase modulation due to the considered load torque oscillations. The healthy case is obtained for $\beta = 0$.

2. Air-gap Eccentricity and Amplitude Modulation

The air-gap length $g(\theta, t)$ can be approximated for a small air-gap and low levels of static or dynamic eccentricity by the following expression [9]:

$$\begin{aligned} g_{se}(\theta, t) &\approx g_0 (1 - \delta_s \cos(\theta)) \\ g_{de}(\theta, t) &\approx g_0 (1 - \delta_d \cos(\theta - \omega_r t)) \end{aligned} \tag{2.31}$$

where δ_s, δ_d denote the relative degrees of static or dynamic eccentricity and g_0 the mean air-gap length without eccentricity. Note that static eccentricity can be considered as a special case of dynamic eccentricity since $g_{se}(\theta, t)$ corresponds to $g_{de}(\theta, t)$ with $\omega_r = 0$, i.e. the point of minimum air-gap length is stationary. Since dynamic eccentricity is more general, it will mainly be considered in the following.

The air-gap permeance $P(\theta,t)$ is obtained as the inverse of $g(\theta,t)$ multiplied by the permeability of free space μ_0. Following a classical approach, the permeance is written as a Fourier series:

$$P_{de}(\theta,t) = P_0 + \sum_{i=1}^{\infty} P_i \cos[i(\theta - \omega_r t)] \tag{2.32}$$

where $P_0 = \mu_0 / g_0$ is the permeance without eccentricity. The higher order coefficients of the Fourier series can be written as:

$$P_i(\theta,t) = \frac{2\mu_0(1-\sqrt{1-\delta^2})^i}{g_0\delta_d^i\sqrt{1-\delta^2}} \tag{2.33}$$

Dorrell has shown in [46] that the coefficients with i are rather small for $\delta_d < 40\%$. For the sake of simplicity, they are neglected in the following considerations.

The air-gap flux density is the product of permeance with the magnetomotive force (MMF). The total fundamental MMF wave can be written as:

$$F_{tot}(\theta,t) \approx F_s \cos(\omega_s t) + F_r \cos(\omega_r t + \gamma) = F_1 \cos(p\theta - \omega_s t - \varphi_t) \tag{2.34}$$

with φ_t the initial phase. In this case, constant torque is assumed, so the torque angle is also kept unchanged. So the air-gap eccentricity could not change the MMF on either rotor or stator, but change the permeance.

The flux density in presence of dynamic eccentricity is:

$$B_{de}(\theta,t) \approx B_1\left[1 + 2\frac{P_1}{P_0}\cos(\theta - \omega_r t)\right]\cos(p\theta - \omega_s t - \varphi_t) \tag{2.35}$$

with $B_1 = P_0 F_1$, the fraction $2P_1 / P_0$ equals approximately δ_d for small levels of eccentricity. The air-gap flux density can therefore be written as:

$$B_{de}(\theta,t) \approx B_1\left[1+\delta_d \cos(\theta-\omega_r t)\right]\cos(p\theta-\omega_s t-\varphi_t) \tag{2.36}$$

The equation shows the fundamental effect of dynamic eccentricity on the air-gap magnetic flux density: the modified air-gap permeance causes an amplitude modulation of the fundamental flux density wave with respect to time and space. The AM modulation index is approximately the degree of dynamic eccentricity. In case of static eccentricity, the fundamental flux density expresses as:

$$B_{se}(\theta,t) \approx B_1\left[1+2\delta_s \cos(\theta)\right]\cos(p\theta-\omega_s t-\varphi_t) \tag{2.37}$$

which shows that static eccentricity leads only to flux density AM with respect to space. Follow the same procedure from eq.()~eq.(), the amplitude modulation can also be found on the stator current I(t), that is expressed as follows in case of dynamic eccentricity:

$$I_{de}(t) \approx I_1\left[1+\alpha \cos(\omega_r t)\right]\cos(\omega_s t-\varphi_t) \tag{2.38}$$

In this expression, I_1 denotes the amplitude of the stator current fundamental component, α is the AM index which is proportional to the degree of dynamic eccentricity δ_d. Static eccentricity does not lead to frequencies different from ω_s since the corresponding additional flux density waves are also at the supply pulsation ω_s. It can be concluded that theoretically, pure static eccentricity cannot be detected by stator current analysis.

E. Mechanical Anomalies Studied

Two mechanical anomalies will be investigated in detail in this dissertation, torsional vibration of rotor-shaft assembly and generalized roughness bearing defect. Both of them can be recognized as torsional effects, which are caused by torque ripple

induced speed oscillation. The torque harmonics will be transmitted into the current signature of synchronous machine by phase modulation.

1. Torsional Vibration of Rotor Shaft Assembly

The electric machine driven turbo-machinery in oil and gas applications is usually subject to a broad range of varied and often severe torsional disturbances, especially in the case of machine driven by VFD. These sources of torsional excitations, already discussed in chapter I, could produce torsional resonance during steady state or transient. Unlike the translational vibration will usually accompany with sound and noise, the torsional vibration will goes without notice until shaft fatigue failure.

For electric machines driven turbo-machinery, the torsional vibration related to the direct coupling between electromagnetic dynamics of electric machine and the rotordynamics of shaft assembly, especially during the transient. This coupling can also significantly alter the transient torsional response at resonance when the excitation is coming from the electrical machine, as in the case of synchronous machine during line-frequency starting. Such coupling or interaction may need to be taken into account when an accurate prediction of stress level is required. The research will identify this strong coupling, and conduct electromagnetic-rotordynamic integrated analysis for the system.

2. Generalized Roughness Bearing Defect

Generalized roughness is a type of fault where the condition of a bearing surface has degraded considerably over a large area and become rough, irregular, or deformed as

shown in Fig.13. This damage may or may not be visible to the unaided eye. Nevertheless, there is no localized defect to be identified as the fault; rather, large areas of the bearing surface(s) have deteriorated. The main causes of this defect are overload, misalignment, contamination resulting from rough environment conditions (sand, dust, corrosion), loss of lubricant due or Electric Discharge Machining (EDM), which is due to a destructive electrical current flow through the bearing.

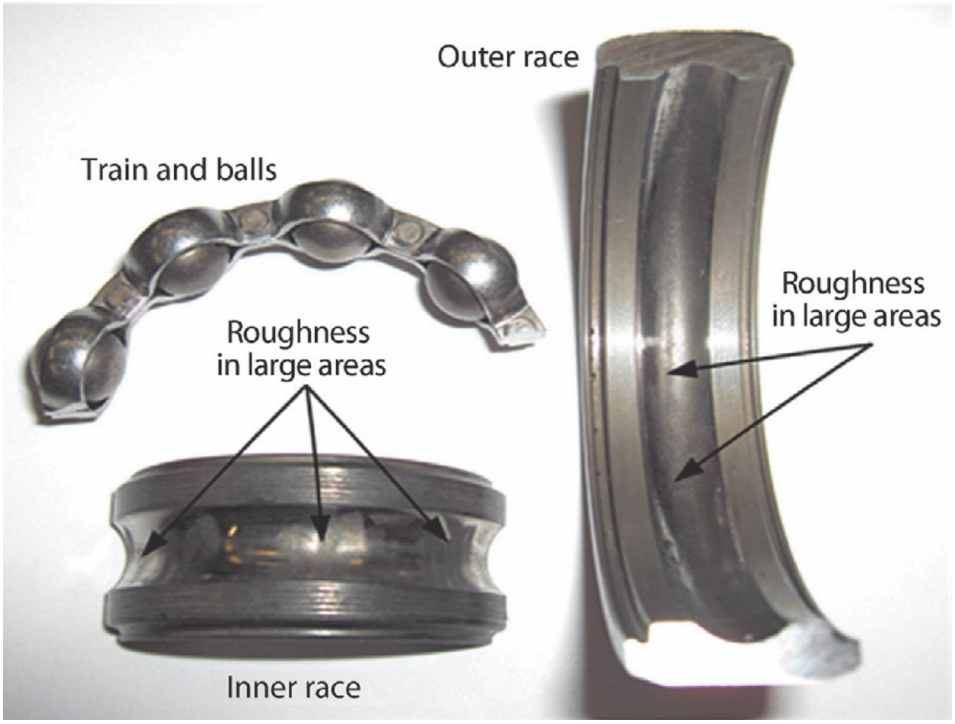

Fig.13 The sample of generalized roughness defect of ball bearing

Generalized roughness faults are common in industry, while they are often neglected in the research literature. It is also recognized as the incipient stage of the bearing deterioration process. When a generalized roughness fault reaches an advanced stage and the bearing is seriously damaged, this defect typically accompanying with

increased machine vibration can be detected via the rudimentary vibration monitoring techniques commonly employed in industry [50]. Unlike single point defects, generalized roughness does not generate a specific characteristic vibration frequency. Hence, bearing frequency identification techniques cannot be used for both vibration and current signature analysis. So there is a strong need for a condition monitoring scheme to analysis the incipient generalized roughness, which will be covered in Chapter III and IV.

F. Diagram of Electrical Signature Analysis

So far we understand that how mechanical anomalies such as air-gap eccentricity, bearing defect and torsional vibration are modulated into current signal by either AM or PM. The characteristics of these mechanical anomalies can be related to harmonics or specific signature in some frequency or frequency bands, depend on which type of anomalies. So the ESA of these anomalies is to detect the related harmonics or signature, if there is no disturbance affects and causes misleading information to the analysis.

However, the Power Quality (PQ) variation, machine manufacturing imperfections and interactions of both could impact the current signature of mechanical anomalies especially during it incipient stage, which presented in the Fig.14. In the Appendix F, the effect of unbalanced voltage on machine space harmonics is explained to show how the PQ variation can affect the analysis the mechanical anomalies. The influence of the interaction between PQ variation and machine manufacturing

imperfections could also be imposed on the ESA of mechanical anomalies, which is illustrated in Appendix G. Moreover, the load and speed level change could also affect the current signature of mechanical anomalies significantly.

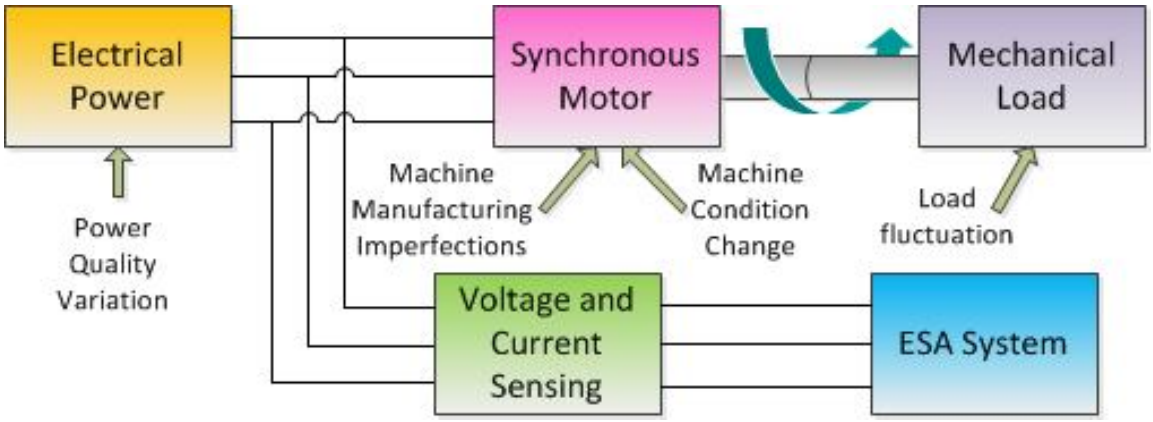

Fig. 14 Diagram of machine anomaly detection based on ESA

To improve the effectiveness of ESA approach, it is necessary to isolate the influence of these disturbances and operation conditions, especially for some mechanical anomalies with subtle electrical signature or at it incipient stage. In chapter V, a signal segmentation technique will be introduced to detect the subtle signature induced by generalized roughness bearing defect.

The reliability of ESA approach also depends on the fidelity of acquired signal and the dynamic range of it. The anomaly creation experiment usually could bring disturbance to the vibration or electrical signal acquired for machine condition monitoring. An improved experiment procedure will be introduced to isolate the influence of shaft current during in-suit bearing deterioration experiment in chapter VI.

CHAPTER III

ESA OF TORSIONAL VIBRATION OF SYNCHRONOUS MOTOR SHAFT ASSEMBLY

The synchronous machines are widely employed to drive loads such as pumps and compressors, which require constant speed under possibly fluctuating load. It has been realized that since the torque oscillation, the torsional vibration resonance or shaft fatigue may be experienced and lead to destructive effects on certain parts of motor-load shaft assembly. This problem is extremely serious for submersible pumps or compressors driven by synchronous motor. For downhole applications, the machines usually built with longer dimension due to the smaller diameter constraint to achieve required power. Currently a popular technique to measure torsional vibration is to mount strain gauge on the shaft, which is intrusive, expensive and hard, maybe infeasible to be implemented such as the downhole applications. Considering that the torsional vibration of shaft assembly could manifest itself in the current signature of the driven motor, this chapter will investigate a nonintrusive and cost effective approach to analyze the torsional vibration of synchronous motor-load assembly, so the torsional vibration of shaft assembly can be avoided at the design stage or be monitored during operation.

The torsional dynamics modeling of the motor-load assembly will be discussed first to show the natural frequencies, model shapes, the torsional resonance and it effect on the shaft assembly. Then sources of torsional excitation such as electromagnetic torque of synchronous machine especially at it transient state, and load torque will be illustrated. A numerical approach is introduced to obtain the forced response of torsional

dynamics and estimate the shaft torques on each shaft segment. Based on the estimated electromagnetic and shaft torques, the shaft torsional shear stresses can be calculated to evaluate the probability of fatigue failure of each shaft segment for steady state operation. Finally a cumulative fatigue life prediction technique will be employed to evaluate the transient torsional vibration damage to shaft assembly.

A. Natural Frequencies and Modal Shapes of Torsional Dynamics

Here we start from a simplified and lumped model including synchronous motor, coupling and a reciprocating compressor to calculate torsional natural frequencies and mode shapes. Then the interference diagram is introduced to check possible coincidence between the expected excitation frequencies and the natural frequencies obtained above within the operating speed ranges. The simplified system is shown in Fig.14 below:

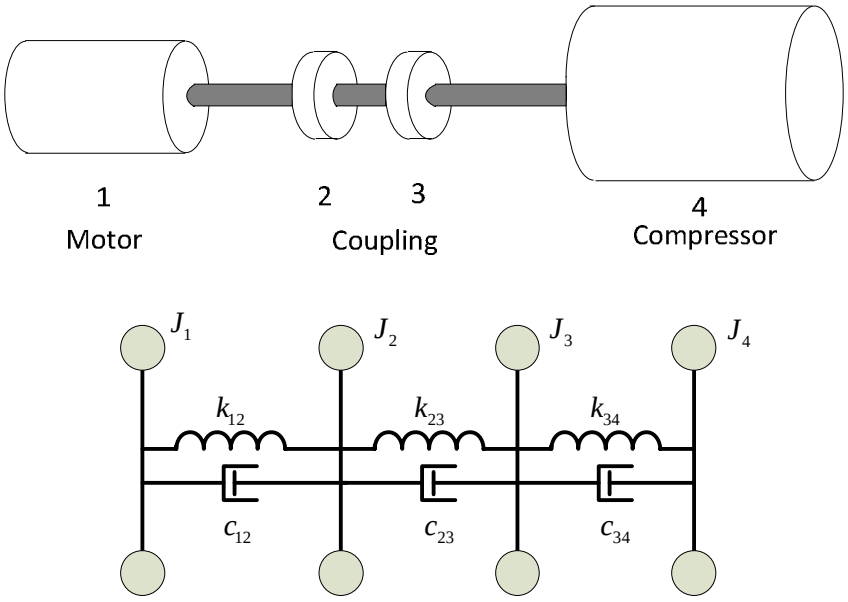

Fig.15 Simplified model of a motor driven compressor system

The torsional model is comprised of diagonal inertias matrix J and triple band diagonal torsional spring and damping matrix K and C. For this simplified system, the inertia elements in the matrix J are calculated for synchronous motor rotor (12 poles machine), each coupling half and driven load --- reciprocating compressor.

The torsional spring and damping elements in the matrix K and C are calculated for motor shaft from the core to coupling, coupling stiffness and driven load shaft. The inertia and stiffness matrix can be built from the Tab.1 and Tab.2.

1. Mode Shape Analysis of a Simplified System

We can have the equation of motion of the torsional vibration:

$$[J]\ddot{\theta} + [C]\dot{\theta} + [K]\theta = [T] \tag{3.1}$$

By ignoring the damping coefficient and excitation, the natural frequencies and mode shapes can be calculated by solving the homogeneous equation $[J]\ddot{\theta} + [K]\theta = [0]$. With orthogonal decomposition of the matrix $[J]^{-1}[K]$, the eigenvalues of it relate to the torsional nature frequencies, and the eigenvectors relate to the mode shapes for the corresponding nature frequencies. Tab.1 shows the inertia and stiffness for the components in the above simplified model. The natural frequency and mode shapes are shown in the Tab.2 and Fig.15-Fig.17.

In Fig.15 the natural mode of oscillation for the natural frequency f1 = 11.85Hz is depicted. We can see that the torsional vibration of mass 1 (motor rotor) and mass 2 (left coupling elbow) are higher. But they are in phase, so the twisting angle of the motor

shaft is relative small. The maximum twist angle occurs at the coupling for this natural resonance. Fig.16 shows the natural mode of oscillation for the natural frequency f2 = 103.58Hz, the maximum twist angle is at the motor's shaft and coupling. While the twisting angle of the load shaft is quite small. or the natural frequency f3 = 166.70Hz, Fig.17 presents that the twist angle of the motor's shaft is relatively small while the twist angles of the load shaft and coupling are quite big.

Tab.1 Inertia and stiffness for system components of simplified model

Mass No.	Inertia ($kg \cdot m^2$)	Between nodes	Stiffness e+6 ($N \cdot n / rad$)
J1	182	1 -- 2	8.414
J2	25	2 -- 3	1.282
J3	17.5	3 -- 4	17.73
J4	3100		

Tab.2 Natural Frequencies for simplified model

Mode	**Natural Frequency (Hz)**	**Mode mass ($kg \cdot m^2$)**	**Modal Stiffness E+5 ($N \cdot n / rad$)**	
1	11.85	711		
2	103.58	6214.8		
3	166.70	10002		

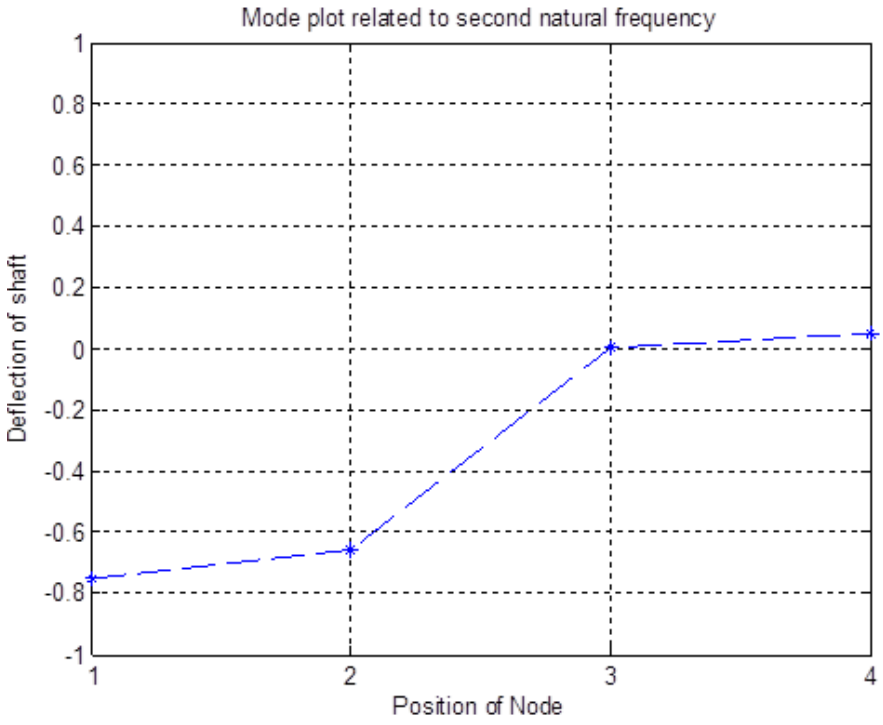

Fig.16 Mode shape related to natural frequency f1

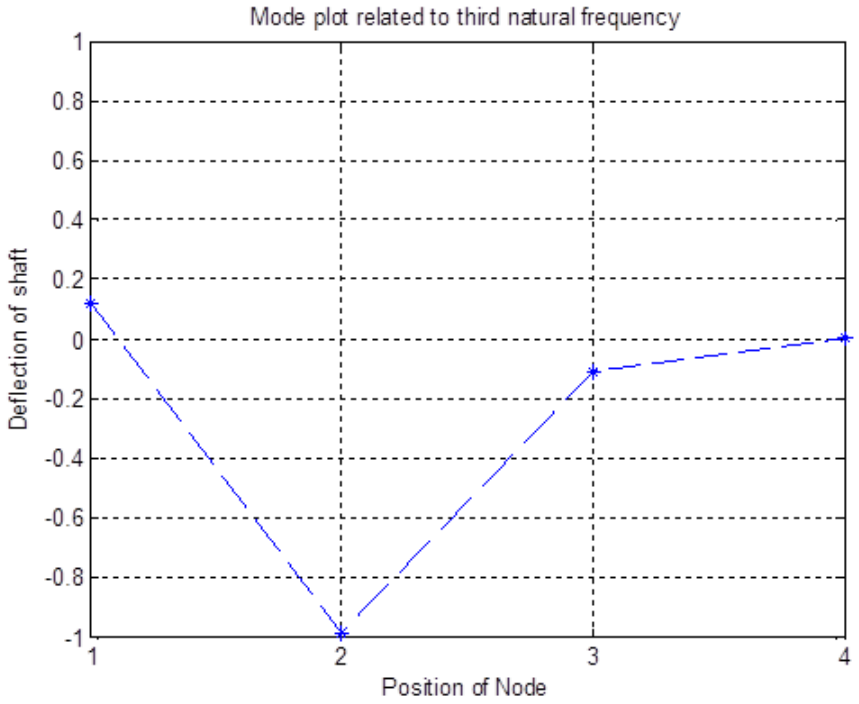

Fig.17 Mode shape related to natural frequency f2

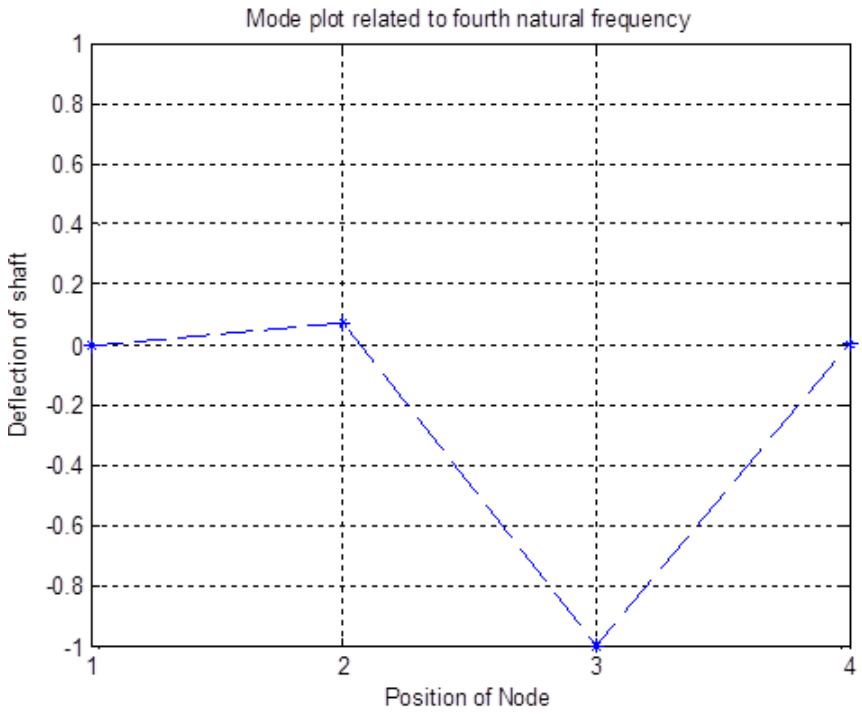

Fig.18 Mode shape related to natural frequency f3

So if the frequencies of one or more of oscillating torque harmonics coincide with one or more of the natural frequencies of the mechanical system, resonance will occur and tremendous shaft torques and stress could be induced. The weakest points are those experienced maximum twist angle and with less stiffness.

After the natural frequencies are calculated, they can be plotted on a so called interference diagram shown in Fig.18, where we can check possible coincidence between the expected excitation frequencies and the calculated torsional natural frequencies within the operating speed ranges. In Fig.18, each upward sloping line on the interference diagram represents a single mechanical or electrical excitation frequency or harmonics, which usually multiply times of rotating frequency. When they cross a torsional natural frequency (horizontal line), a torsional resonance would occur. The

solid circle identifies the possible torsional resonant condition. The speeds corresponding to the solid circle are called critical speed. The synchronous motor should avoid running at or close these critical speeds for steady state operation. The possible sources of excitation forces will be covered in the section B.

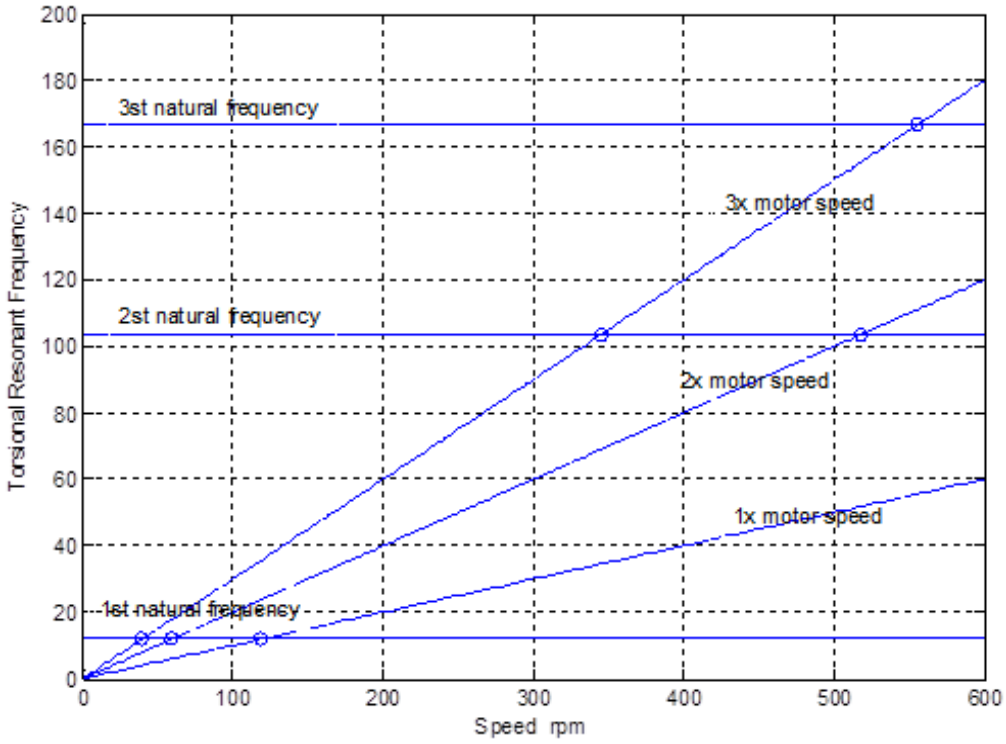

Fig.19 Interference diagram for the simplified system

2. Generalized Lumped Torsional Model

For more complicated system, torsional dynamics are modeled as an assemblage of massless shaft elements connecting inertia stations, couplings, maybe gears such as the example in Fig.19. The model consists of a total of n stations whose locations are based on the shaft geometry and the connected component properties. For example, each

significant shaft diameter change is represented, usually, by one station. Stations are also located at any significant component location such as bearing locations. The kth shaft element represents a linear torsional spring of stiffness k_k, and material damper of coefficient c_k that connects the inertia elements J_k and J_{k+1}. At bearing location, a station with the bearing viscous damping or windage friction damping d_k is assigned. It should be noted that if a gear system is involved, the model parameters should be referred to either side of the gearbox by multiplying each inertia coefficient, damping coefficient and stiffness coefficient by γ^2 and multiplying each torque by γ, where γ is the speed ratio. The model in Fig.19 removed the gear by multiply gear ratio to the element parameters.

The equations for the lumped torsional model can be represented in a compact matrix form as follows:

$$[J]\{\ddot{\theta}\}+[C]\{\dot{\theta}\}+[D]\{\dot{\theta}\}+[K]\{\theta\}=\{T(t)\} \tag{3.2}$$

where $[J]$ = diagonal inertia matrix,

$[C]$ = triple band diagonal damping matrix, dependent on station to station damping coefficient

$[D]$ = diagonal matrix of station to ground damping coefficient,

$[K]$ = triple band diagonal system stiffness matrix, dependent on individual stiffness.

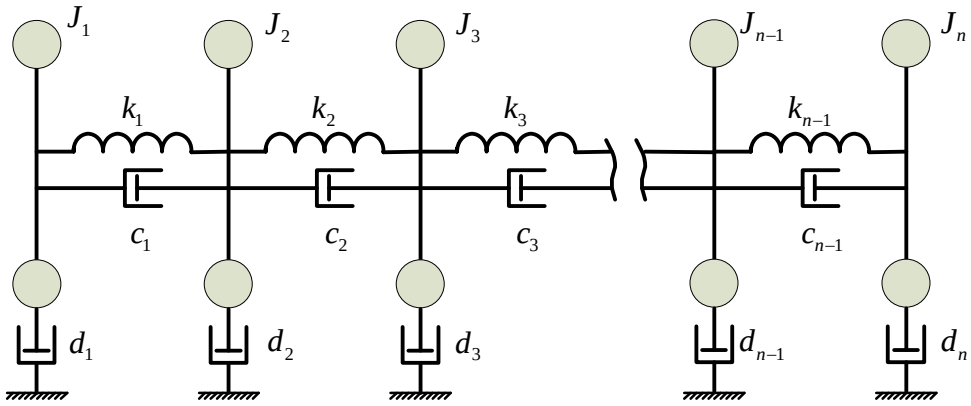

Fig.20 Representation of generalized torsional dynamics model

The system torsional deformations and torque vectors can be represented as

$$\{\theta\} = \{\theta_1, \theta_2, \cdots, \theta_n\} \tag{3.3}$$

$$\{T(t)\} = \{T_1(t), T_2(t), \cdots, T_n(t)\} \tag{3.4}$$

The torsional damping can be modeled with discrete damping of any particular element can be simulated as torsional damper, elastomeric coupling or bearing viscous damping and rotor windage damping which can be estimated based on the horse power loss in bearings and friction loss.

To calculate the natural frequency of system, a homogeneous equation can be considered.

$$[J]\{\ddot{\theta}\} + [K]\{\theta\} = \{0\} \tag{3.5}$$

Therefore, the complex eigenvalues and eigenvectors, including the rigid body motion are calculated from the following equation:

$$\left[\left[\omega^2\right] - [J]^{-1}[K]\right]\{\Phi\} = 0 \tag{3.6}$$

where ω^2 are the eigenvalue of the matrix $[J]^{-1}[K]$, $\omega = [\omega_1, \omega_2, \cdots, \omega_n]$ are the natural frequencies of the system. $[\psi] = [\{\psi\}_1, \{\psi\}_2, \cdots, \{\psi\}_n]$ are the eigenvectors of the matrix $[J]^{-1}[K]$ also the torsional vibration modal shape.

Usually the proportional damping assumption is made for the damping matrix as $[C] = a[J] + b[K]$, so that the equation of motion for damped and forced system can be decoupled into n independent one-degree-of-freedom system. Then closed form of solution can be easily achieved. When a system contains non-proportional damping, the previously used formulation of the eigenvalue problem will not yield modal vectors (eigenvectors) that uncouple the equations of motion of the system. A technique used to circumvent this problem was first documented by Duncan [58] and involves the reformulation of the original equations of motion, for an n-degree of freedom system, into an equivalent set of 2n first order differential equations known as Hamilton's Canonical Equations.

In the above closed form of solution, analytic force excitation need to be assigned. While for a torsional system under monitoring, the electromagnetic torque excitation should be numerically estimated, which is more accurate than the toque curve provided from motor manufacture. So it is necessary to apply numerical approach to find solution of twisting angles of shaft at different locations for shaft stress and fatigue analysis. The section C will cover this numerical approach by electrical circuit analogy.

B. Source of Torsional Excitation

Once the system has been modeled and the natural frequencies have been determined, then the forcing or exciting functions need to apply. The forcing functions represent dynamic torque applied at locations in the system that likely to generate torque variations. Identification and quantification of all possible sources of dynamic torque is an important step in diagnosing an existing vibration problem or avoid problems at the design stages.

The main sources of exciting forces are loads such as reciprocating or centrifugal equipment and primary drive such as induction or synchronous motors. In this research, only synchronous motor is analyzed, especially during its start-up transient.

1. Load Torque Excitations

The common loads include reciprocating compressor or pump, centrifugal pump or compressor and fan. All of these equipment produce oscillating torque, more or less. A brief discussion of the origin of the torques from each of these items will be included in this section.

Reciprocating Compressor or Pump

The conversion of reciprocating power to rotating power through a crank mechanism generates a varying torque because of the geometry of the system. The geometry of reciprocating equipment can be simulated along with the gas pressure caused torques (power or compressor cylinder) to define the dynamic torsional energy introduced into the shaft system.

An important effect from the view of torsional vibration is the inertial torque produced by the motion of the reciprocating masses. The inertia of the reciprocating parts creates primary and secondary harmonic torque [59].

Although reciprocating pumps and compressor have a steady discharge pressure resisting the rotation, the changing pressure from suction to discharge level causes a torque variation. Interaction between the pumped fluid and the piping system can produce pressure pulsations that may affect the dynamic torque of the machine and produce higher harmonics.

The torsional excitations generated by reciprocating compressors are a function of the compressor loading condition, the physical geometry of the cylinder, the crankshaft geometry, and the thermo-physical properties of the gas or liquid. The harmonic frequency excitation from the complex wave of pressure versus crank angle can be accurately calculated.

The torsional dynamics of any reciprocating machine deserve careful attention because of multiple frequencies or harmonics. The multitude of excitation frequencies produced increases the probability of exciting a system torsional natural frequency.

Centrifugal Compressor or Pump

In the centrifugal compressor or pump, torsional excitation at the equipment operation speed can result from turbulence or load variations, but is generally less than one percent zero-peak of the steady-state torque. Therefore, for 1x running speed, a one percent torque excitation is used to calculate the shaft torsional deflections and stresses.

The excitation is typically distributed across the masses in the piece of equipment with the maximum calculated amplitude at that frequency to obtain the maximum calculated stress. Torsional excitation can also be applied at other potential excitation location on the driver, the gear, and the driven equipment. If torsional natural frequencies coincide with multiples of running speeds, the torsional stresses are calculated with an assumed excitation level of 1/n percent of the transmitted torque, where n is the harmonic.

Torsional excitation from centrifugal machines can occur due to the impellers or wheels passing a stationary discontinuity in the case, such as diffuser vanes, steam nozzles, cutwater, etc. these excitations are characterized by a discrete frequency related to the geometry and speed and rarely exceed one percent zero-peak of the steady state load torque unless amplified by acoustic interaction. For case where blade passing frequency coincides with torsional natural frequencies, an excitation level of 1/(number of blades) percent zero-peak of steady state torque is used for calculate the possible maximum shaft deflection and stress. But these assumed excitations are based on experience and may have to be verified for critical applications.

Except motor and load excitation, the gears and coupling in the power transmission could also induce torsional. Misaligned or eccentric couplings can produce a torque fluctuation, particularly if some backlash occurs in gear coupling, which is nonlinear and hard for analytical solution for the forced response of torsional dynamics. This is also the incentive for us to introduce numerical solution in section C.

In summary, the most likely dynamic torque excitations, the frequencies and magnitude of torque modulation, are listed in Tab.3.

Tab.3 Steady state load torsional excitation or transmission

Source	Frequency	Amplitude	Comments
Centrifugal Compressor	1x, 2x	1.0%	Misalignment, turbulence
Fan or pump	Bx, Px B= number of impeller P= number of diffuse vanes	(1/B)% (1/P)%	Assumes no acoustical resonance
Reciprocating compressor or pump	1x, 2x, …, nx	TEC*(1-3)	Torque Effect Curve(TEC) developed for each cylinder
Lobed Blowers	1x, 2x, …, nx	10-40%	Harmonic torque depend upon number of lobes and their timing
Gear	1x, 2x, …, nx	1%	Worn gear, bad alignment

2. Electromagnetic Torque Excitations

Above we discussed the torsional excitation induced by some reciprocating or centrifugal load and their modulation. These torque excitations will be modulated into and manifest itself in the current signature of synchronous motor through electromagnetic coupling, which is also the fundamental of this research. Actually the

synchronous motor could produce torsional excitation other than the load mentioned above.

The machine under study is a salient pole synchronous motor, which is assumed to have one equivalent damper winding circuit on both the d- and q- axis of the motor. The stator voltage equation is written as:

$$[v] = p([L][i]) + [R][i] = [L]p[i] + \left(\left[\frac{\partial L}{\partial \theta}\right]\omega_r + [R]\right)[i] \tag{3.7}$$

where p is the derivative operator

$$[v] = \begin{bmatrix} v_a & v_b & v_c & 0 & 0 & v_{fd} \end{bmatrix}^T = \begin{bmatrix} v_s & v_r \end{bmatrix}^T$$

if define $v_s = \begin{bmatrix} v_a & v_b & v_c \end{bmatrix}$ $\quad v_s = \begin{bmatrix} v_a & v_b & v_c \end{bmatrix}$

$$[i] = \begin{bmatrix} i_a & i_b & i_c & i_{kd} & i_{kq} & i_{fd} \end{bmatrix}^T = \begin{bmatrix} i_s & i_r \end{bmatrix}^T$$

if define $i_s = \begin{bmatrix} i_a & i_b & i_c \end{bmatrix}$ $\quad i_r = \begin{bmatrix} i_{kd} & i_{kq} & i_{fd} \end{bmatrix}$

$$[R] = diag\begin{bmatrix} r_a & r_b & r_c & r_{kd} & r_{kq} & (r_{fd} + R_{dis}) \end{bmatrix} = diag\begin{bmatrix} R_s & R_r \end{bmatrix}$$

if define $R_s = \begin{bmatrix} r_a & r_b & r_c \end{bmatrix}$ $\quad R_r = \begin{bmatrix} r_{kd} & r_{kq} & (r_{fd} + R_{dis}) \end{bmatrix}$

$$[L] = \begin{bmatrix} L_{aa} & L_{ab} & L_{ac} & L_{akd} & L_{akq} & L_{afd} \\ L_{ab} & L_{bb} & L_{bc} & L_{bkd} & L_{bkq} & L_{bfd} \\ L_{ac} & L_{bc} & L_{cc} & L_{ckd} & L_{ckq} & L_{cfd} \\ L_{akd} & L_{bkd} & L_{ckd} & L_{kkd} & 0 & L_{fdkd} \\ L_{akg} & L_{bkq} & L_{ckq} & 0 & L_{kkq} & 0 \\ L_{afd} & L_{bfd} & L_{cfd} & L_{fdkd} & L_{aa} & L_{ffd} \end{bmatrix}^T = \begin{bmatrix} L_{ss} & L_{sr} \\ L_{sr} & L_{rr} \end{bmatrix}$$

if define $L_{ss} = \begin{bmatrix} L_{aa} & L_{ab} & L_{ac} \\ L_{ab} & L_{bb} & L_{bc} \\ L_{ac} & L_{bc} & L_{cc} \end{bmatrix}$, $L_{sr} = \begin{bmatrix} L_{akd} & L_{akq} & L_{afd} \\ L_{bkd} & L_{bkq} & L_{bfd} \\ L_{ckd} & L_{ckq} & L_{cfd} \end{bmatrix}$, $L_{ss} = \begin{bmatrix} L_{kkd} & 0 & L_{fdkd} \\ 0 & L_{kkq} & 0 \\ L_{fdkd} & 0 & L_{ffd} \end{bmatrix}$

The elements of the mutual inductance matrix L_{sr} are functions of the rotor angular position, so that accordingly be affected by the torque modulation of exciting forces. It should be pointed out that $v_{fd} = 0$ at starting, while $R_{dis} = 0$ at normal running conditions.

The developed electromagnetic torque can be obtained as the partial derivative of the energy stored in the mutually coupled inductive circuits with respect to the angle θ. Accordingly, the electromagnetic torque can be estimated as:

$$T_e = [i]^T \frac{d[L]}{d\theta}[i] = [i_s]^T \frac{d[L_{sr}]}{d\theta}[i_r] \tag{3.8}$$

The electromagnetic torque and load torque can be substituted into the equ.(3.2) to get the solution of the forced response of torsional dynamics of the drive system.

Steady State Torque Excitation

During steady state operation, synchronous machines are subject to diverse sources of torque oscillations which applied to shaft assembly and stimulate twisting oscillations of the rotating shaft. The stimulus sources can be classified into mechanical and electromagnetic kinds.

Mechanical excitation forces may be generated from structural irregularities such as static or dynamic unbalance of rotating parts, asymmetrical mechanical parts, misalignment, loosening of bearings.

Electromagnetic excitation forces are those induced by unbalanced radial magnetic attraction between stator and rotor magnetic flux. The magnetic flux density in

the air gap can be expressed as the multiplication of magnetomotive force and permeance of air gap:

$$B_g = MMF_g \bullet P_g \tag{3.9}$$

The magnetmotive forces are determined by the pattern of stator and rotor winding patterns, stator current of three phase (balanced or unbalanced) and field DC current (whether has harmonics). The permeance is the inverse of air gap length, which is dependent upon the rotor shape (salient or round) and whether the air gap is concentric or eccentric. The magnetomotive force and permeance can be decomposed into Fourier series and the harmonics will be eventually shown in the current signature and torque excitation.

Due to above reasons, the electromagnetic torque can be decomposed as follow:

$$T_e(t) = T_{ave} + \sum_k T_k \cos(k\omega_e t + \varphi_k) \quad , k = 1, 2, \cdots \tag{3.10}$$

where T_{ave} is the DC component, and T_k, $k = 1, 2, \cdots$ are the harmonic torque components which must be considered whether they are coincident with the critical speed of the torsional dynamics.

Transient Torque Excitation

At subsynchronous speeds while operating as an induction motor, the synchronous machine transient electromagnetic torque consists of:

(a) An average or accelerating component and

(b) A twice of slip frequency oscillating component

(c) Components caused by switching the supply

(d) Oscillating components due to magnetic saturation

(e) An oscillating component due to magnetic saliency and non-uniform rotor windings

(f) Oscillating components due to higher harmonics of air gap permeance and winding magnetomotive force

The items (e) and (f) also exist during steady state operation. All above components will be affected by the drive acceleration process. The acceleration methods such as pony motor starting, starting by damper winding or soft startup by Variable Speed Drive (VSD) could produce different transient electromagnetic profiles. So that the torque-speed curve provided by motor manufacturers usually supply average torque data in the form of curves as functions of rated speed. When we conduct the forced torsional analysis, it is more reliable to use the electromagnetic torque estimated for real data.

When a synchronous motor starts, the excitations which vary from 120 Hz to 0 Hz are imposed upon the torsional system. This transient excitation cannot be avoided during the machine startup for the natural frequencies below 120 Hz. So that for frequent startup and shutdown process, the shaft assembly of drive system may suffer fatigue failure.

3. Modulation of Torsional Excitation to Current Signature

In the previous section, we discussed the electromagnetic torque excitation resulting from the machine stator winding pattern, rotor shape and input power quality.

Actually the load torque oscillation could also affect the electromagnetic torque and be modulated into the current signature through the transmission of shaft assembly.

Assume that a mechanical load can lead to a periodically varying load torque at characteristic fault frequency f_{osc}. Considering only the fundamental component in the Fourier series development, the load torque can be described by:

$$\Gamma_{load}(t) = \Gamma_{const} + \Gamma_{osc}\cos(\omega_{osc}t) \tag{3.11}$$

where Γ_{osc} is the amplitude of the load torque oscillation and $\omega_{osc} = 2\pi f_{osc}$ is related angular frequency. The mechanical speed $\omega_r(t)$ is obtained by solving the mechanical equation of motion and contains an oscillating term resulting from the torque oscillation. Consequently, the mechanical rotor position $\theta_r(t)$ includes an oscillating term as well:

$$\theta_r(t) = \frac{\Gamma_{osc}}{J\omega_{osc}^2}\cos(\omega_{osc}t) + \omega_r t \tag{3.12}$$

These oscillations lead to a phase modulation of the rotor magnetic field expressed in the stator reference frame whereas the stator magnetic field is not directly affected. In presence of load torque oscillations, the synchronous motor stator current can be considered as the sum of a phase modulated sinusoidal signal $i_{rt}(t)$ and an unmodulated signal $i_{st}(t)$.

$$i_{pm}(t) = i_{st}(t) + i_{rt}(t) = I_{st}\sin(\omega_s t + \varphi_s) + i_{rt}\sin\left[\omega_s t + \beta\cos(\omega_c t)\right] \tag{3.13}$$

$i_{st}(t)$ and $i_{rt}(t)$ denote the stator current components resulting from the stator and rotor magnetic field with amplitudes $I_{st}(t)$ and $I_{st}(t)$. β is the phase modulation index

proportional to $\frac{\Gamma_c}{J\omega_c^2}$.

Forces excitation whether from the electromagnetic torque or from load torque, could considerably amplify the shaft torque by the torsional resonance of rotor shaft assembly if the excitation frequency is coincide with the system critical speed. The resulting large shaft torque will be transmitted to the electromagnetic torque and draw large current. This could lead to shaft mechanical failure and machine breakdown. So by studying the electromagnetic torque or current profile, we can exam the possible coincidence of the frequencies of force excitations and system natural frequencies and avoid possible torsional resonances.

C. Coupling Between Electromagnetic Torque and Rotor Dynamics

As we discussed in section B, the analytical solution for the torsional dynamic equation maybe hard to be obtained for generalized damping. In this section, a numerical method by electrical analogy will be considered. This electrical equivalent circuit approach to solve the differential equations consists essentially of deriving a network, composed of linear circuit elements such as resistors, inductors, capacitors and voltage sources. The equivalent electrical network model of the torsional dynamics can be easily implemented in the Matlab/Simulink for both the transient and steady state solution. The results can be easily and intuitively explained and by from the basics of RLC circuit.

Similar to section B, we revisit the simplified case shown in Figure 3.1. According to Newton's law, the dynamically balanced equation of the system is given in

the eq.(3.14). By applying Laplace transform to eq.(3.14), the mass-rotor speed can be written as shown in eq.(3.15). T_{12}, T_{23} and T_{34} correspond respectively to the torques of the shaft segments between the motor and coupling, coupling elbows, coupling and compressor load respectively.

$$\begin{cases} J_1 \dfrac{d\omega_1}{dt} = T_e - k_{12}\int(\omega_1-\omega_2)dt - c_{12}(\omega_1-\omega_2) \\ J_2 \dfrac{d\omega_2}{dt} = k_{12}\int(\omega_1-\omega_2)dt + c_{12}(\omega_1-\omega_2) - k_{23}\int(\omega_2-\omega_3)dt - c_{23}(\omega_2-\omega_3) \\ J_3 \dfrac{d\omega_3}{dt} = k_{23}\int(\omega_2-\omega_3)dt + c_{23}(\omega_2-\omega_3) - k_{34}\int(\omega_3-\omega_4)dt - c_{34}(\omega_3-\omega_4) \\ J_4 \dfrac{d\omega_4}{dt} = -T_L + k_{34}\int(\omega_3-\omega_4)dt + c_{34}(\omega_3-\omega_4) \end{cases} \tag{3.14}$$

$$\begin{cases} \omega_1 = \dfrac{T_e - T_{12}}{sJ_1}; \qquad \omega_2 = \dfrac{T_{12} - T_{23}}{sJ_2} \\ \omega_3 = \dfrac{T_{23} - T_{34}}{sJ_3}; \qquad \omega_4 = \dfrac{T_{34} - T_L}{sJ_3} \end{cases} \tag{3.15}$$

$$\begin{cases} T_{12} = \dfrac{k_{12}(\omega_1-\omega_2)}{s} + D_{12}; \qquad T_{23} = \dfrac{k_{23}(\omega_2-\omega_3)}{s} + D_{23} \\ T_{34} = \dfrac{k_{34}(\omega_3-\omega_4)}{s} D_{34} \end{cases} \tag{3.16}$$

$$\begin{cases} C_{12} = c_{12}(\omega_1-\omega_2); \qquad C_{23} = c_{23}(\omega_2-\omega_3) \\ C_{34} = c_{34}(\omega_3-\omega_4) \end{cases} \tag{3.17}$$

These torque components can be expressed as eq.(3.16). The above relationships can be converted into block diagrams, which shown in the Fig.20. By recalling the modeling of RLC circuit and considering the shaft damping, we can translate the above mechanical equation of motion into electric circuit diagrams presented in Fig.21. The

equivalent circuit can be converted into simulink block, and the subsystem—torsional dynamics of shaft assembly are shown in Appendix I.

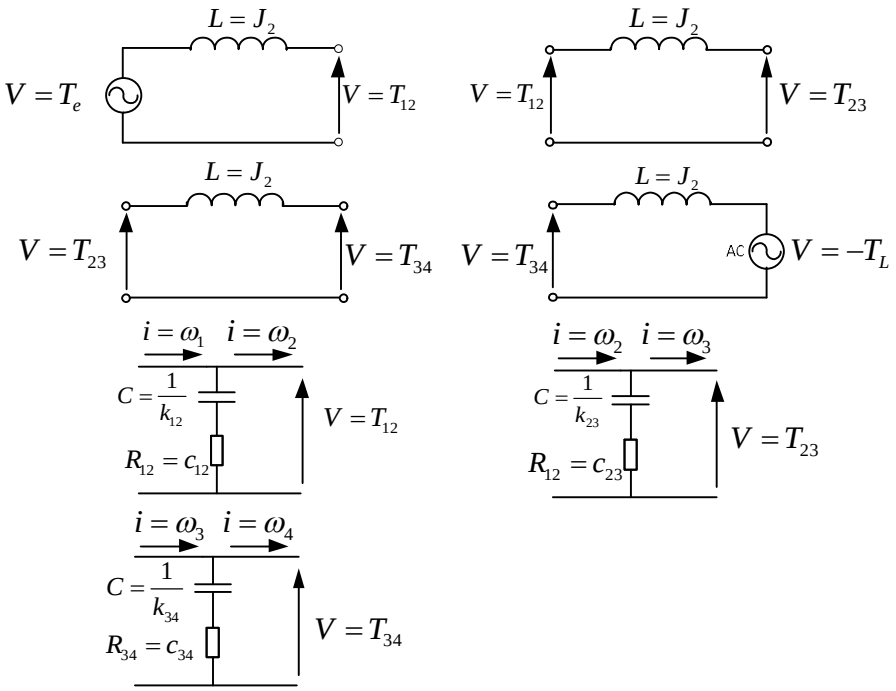

Fig.21 Electromechanical similarities for a flexible shaft system

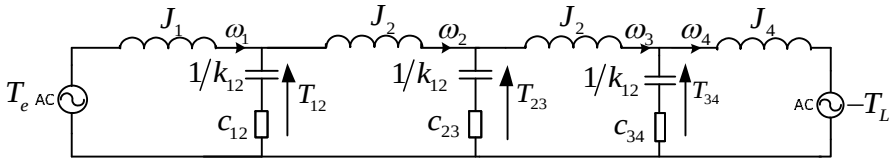

Fig.22 Equivalent circuit diagram of the motor driven compressor system

From the simulink block, we can find that the electric system and mechanical system are interfaced by electromagnetic torque T_e and mechanical speed ω_m. The shaft torque, electromagnetic torque and load torque will interact with one another just as shown in equivalent circuit. The per-unit model for synchronous motor is used. It can be

appropriately scaled to couple with mechanical shaft assembly. Below we will discuss the transient and steady state response of forced torsional dynamic systems under damping and undamped situation.

1. Torque Amplification during Resonance

Above when we studied the transient force response of torsional dynamics, we assumed the load torque is constant when it applied. From its results, we can find that the speed, field current and electromagnetic or shaft torques will eventually converge, and the stator currents also resume to sinusoidal. There are no steady state oscillations in above variables because we assumed no excitation during steady state. Now we will add steady state oscillation to load torque and exam its steady state response. Here the constant electromagnetic torque output is assumed.

The load will be applied at the 8^{th} second together with the oscillating excitation at the first natural frequency. The Fig.22-Fig.24 shows the shaft torques amplification when the oscillating load torque frequency is settled on the natural frequency f1 = 11.85Hz under the condition without damping. The torsional vibration resonance occurs and the coupling torque will continue to accumulate until the coupling is snapped. Actually this case is not practical in the field. The damping is mainly caused by the elastomer-type coupling. Fig.25-Fig.27 illustrates shaft torque profiles when the resonance happens under the condition with damping. The torque will be damped more or less depends on how big the damping is. Similar results can be obtained for the excitations at other two natural frequencies.

When the excitation frequencies are close to natural frequencies, even if the torque can be damped to some extent, there are still some possibilities that the shaft fatigue failure could occur.

Note that the shaft torque transmitted from the section between load and coupling to coupling, and to the section between coupling and machine with power loss. It can be seen from the comparison among the profiles of shaft current, either with or without damping. The power loss is stored in the coupling or shaft as strain energy. As the torsional mode is excited, the torsional angular displacement of rotor and strain energy will keep increase until the coupling or shaft break. Usually the shaft is much stiffer than coupling, so the strain energy will store more in coupling than shaft, and the coupling will be easier to fail, which can protect the rotor shaft.

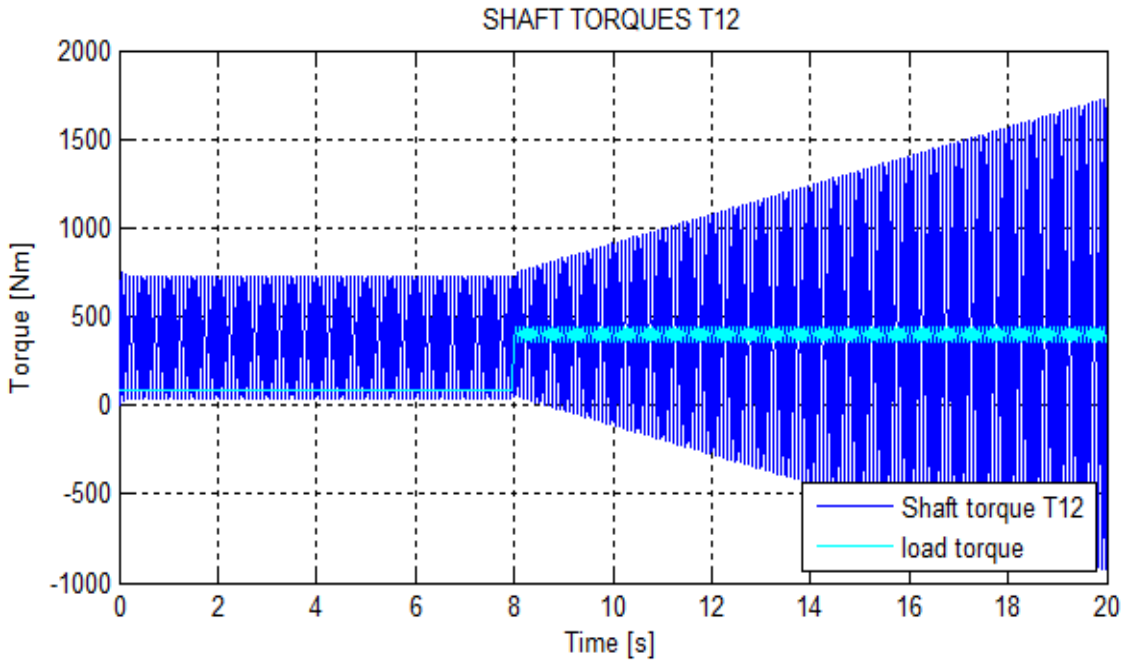

Fig.23 Shaft torque T12 without damping

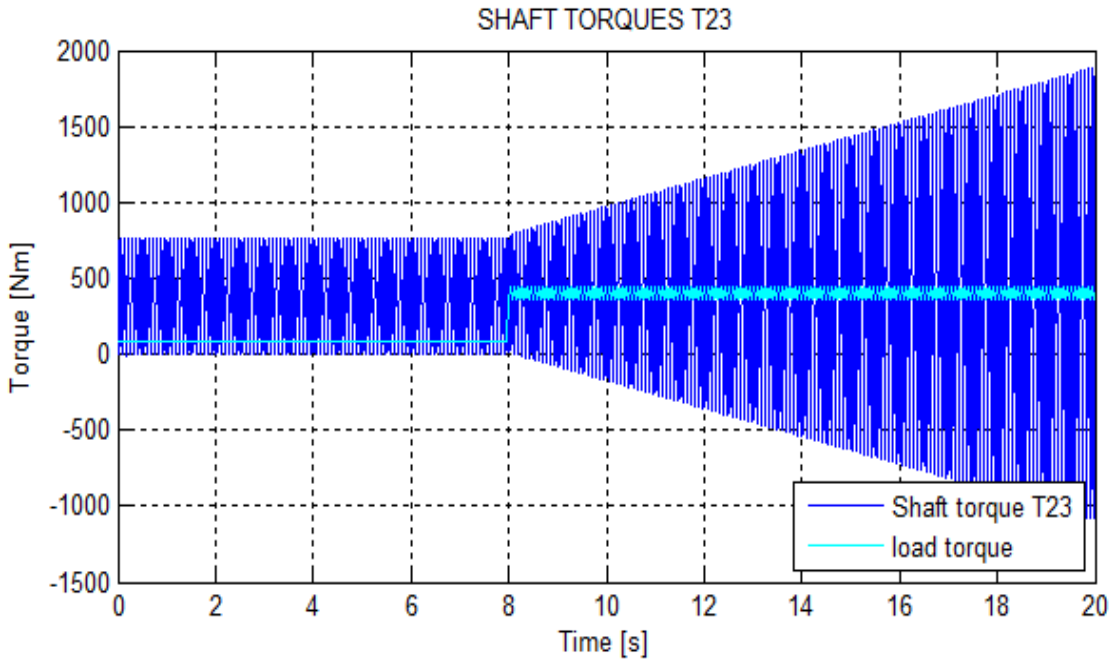

Fig.24 Shaft torque T23 without damping

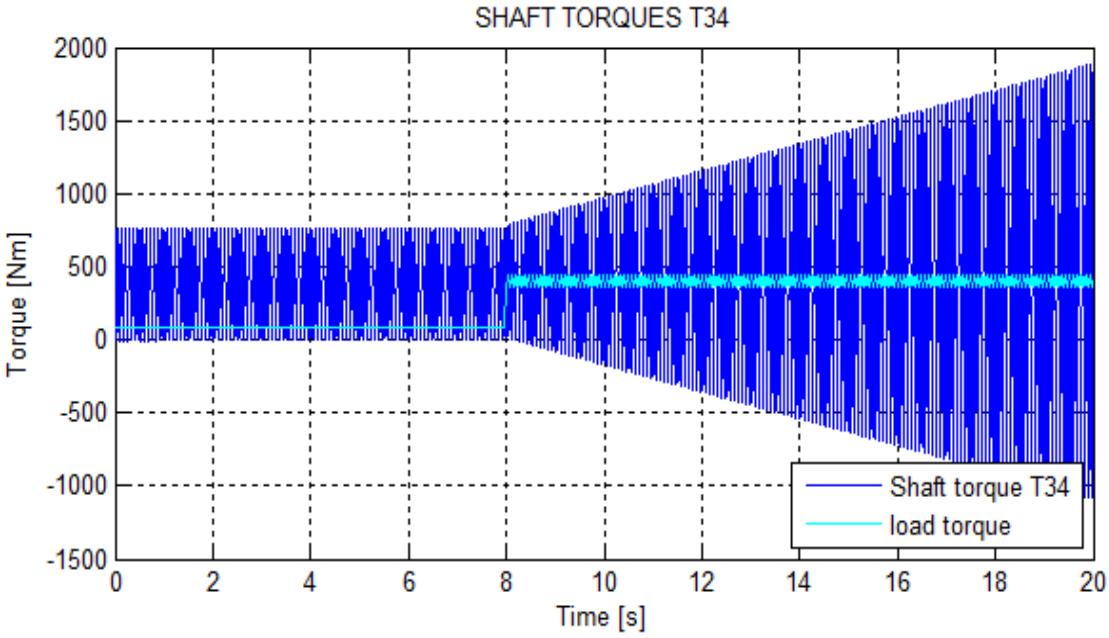

Fig.25 Shaft torque T34 without damping

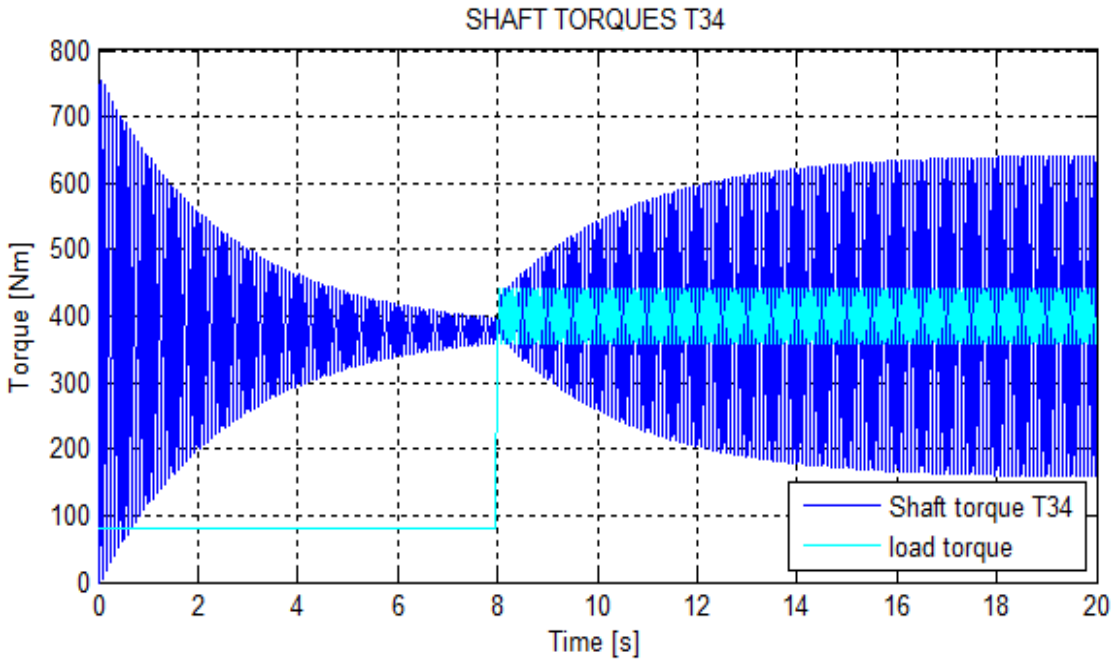

Fig.26 Shaft torque T12 with damping

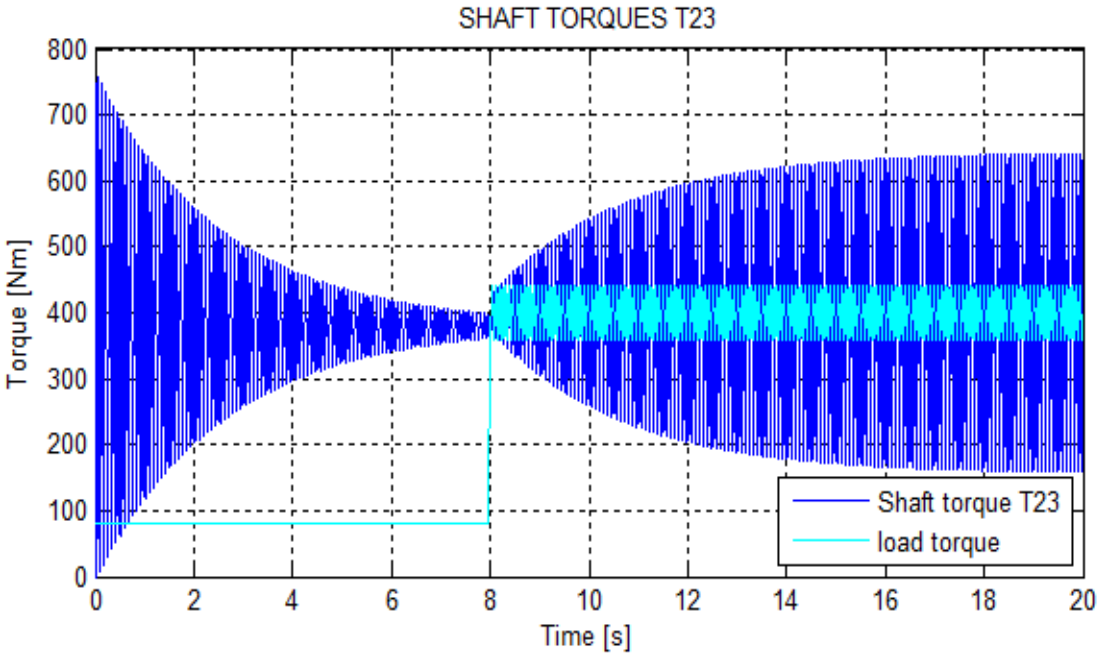

Fig.27 Shaft torque T23 with damping

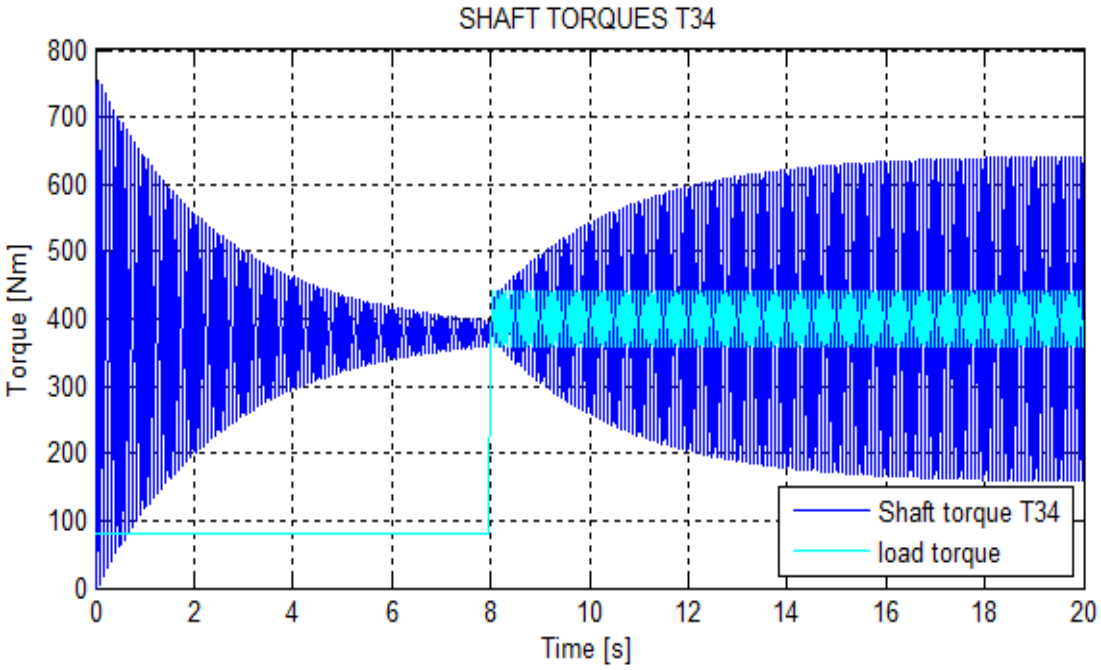

Fig.28 Shaft torque T34 with damping

If the coincidence of natural frequencies with one of excitation frequencies, we can intentionally introduce right damping to appropriate position so that the shaft stress can be move below the endurance limit.

To apply the ESA for torsional vibration monitoring, the relation between torsional excitation and it current signature should be investigated, which is shown in Fig.28. The oscillating torque frequency can cause rotor speed fluctuation, which will be modulated into the fundamental frequency (60Hz) of current carrier wave by electromagnetic coupling. The characteristic signature is the sidebands around the fundamental. Fig.29-Fig.30 below presents how the oscillating load level and frequency change affects its modulation to current signature. The sidebands around the current fundamental will go up as the oscillating torque magnitude increases from 0.1 to 1 times

of average torque in the Fig.29. The sidebands are at the frequencies $f_c \pm k \cdot f_{osc}$. Moreover, as the oscillating torque load level increase, the modulation index will become bigger, and more sidebands around the fundamental can be seen from current spectrum. The Fig.30 presents how the frequencies of oscillating load affect its modulation to current signature under the same oscillating load magnitude. Because the inertia could damper the higher frequency torque oscillations, the sidebands in the current spectrum will decrease as the oscillating frequencies increases from 1 Hz to 30 Hz. Similarly, there will be more sidebands around the fundamental as the excitation frequency is lower. This is also why low frequency band usually carry more information of system health condition than higher frequency of current signature, and is employed for fault signature analysis.

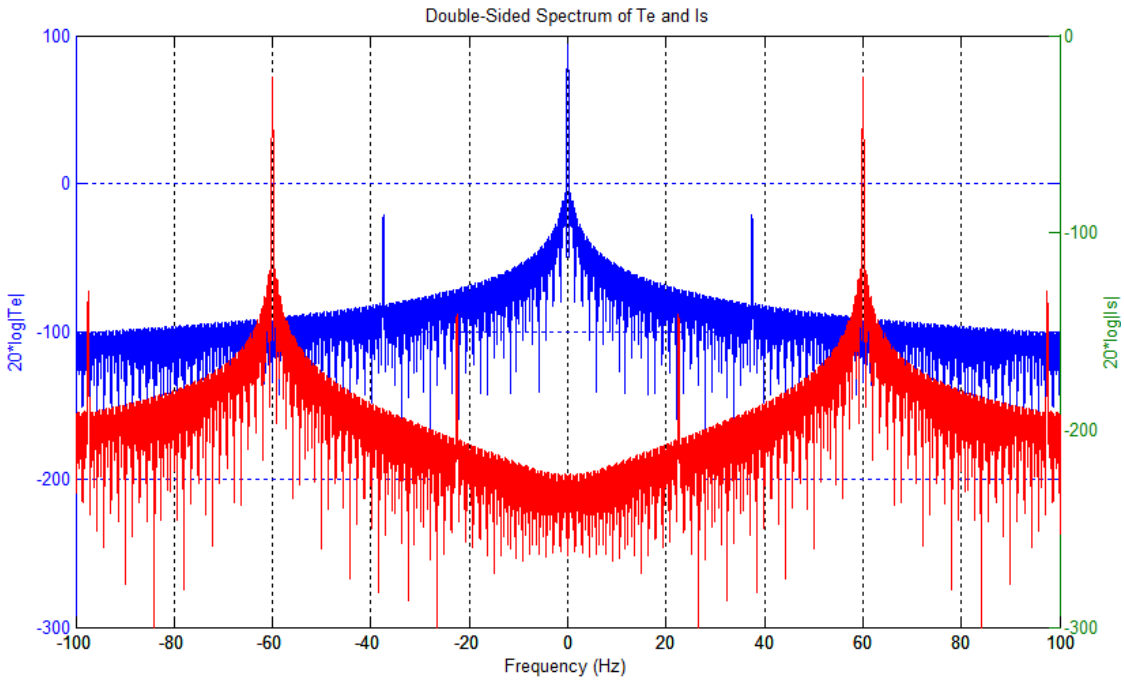

Fig.29 Relation between the EM torque and current spectrum

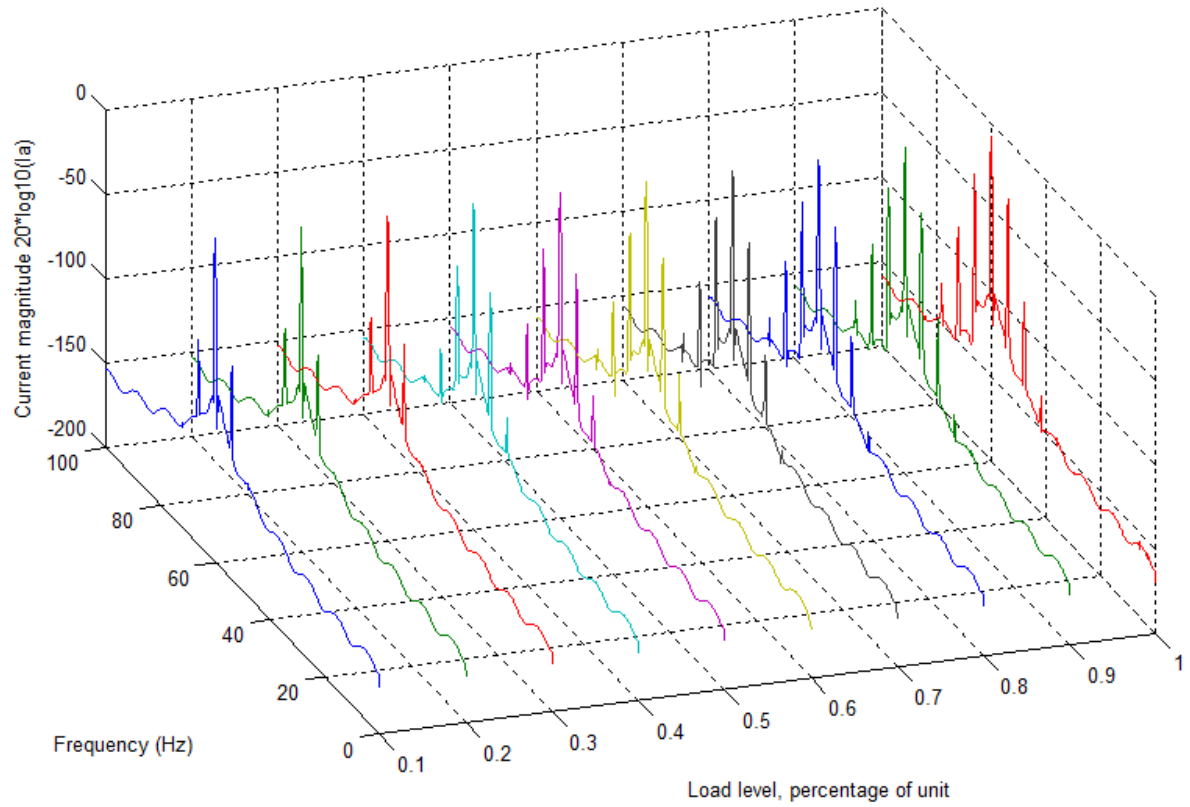

Fig.30 Torque modulation under fixed oscillating frequency and different load levels

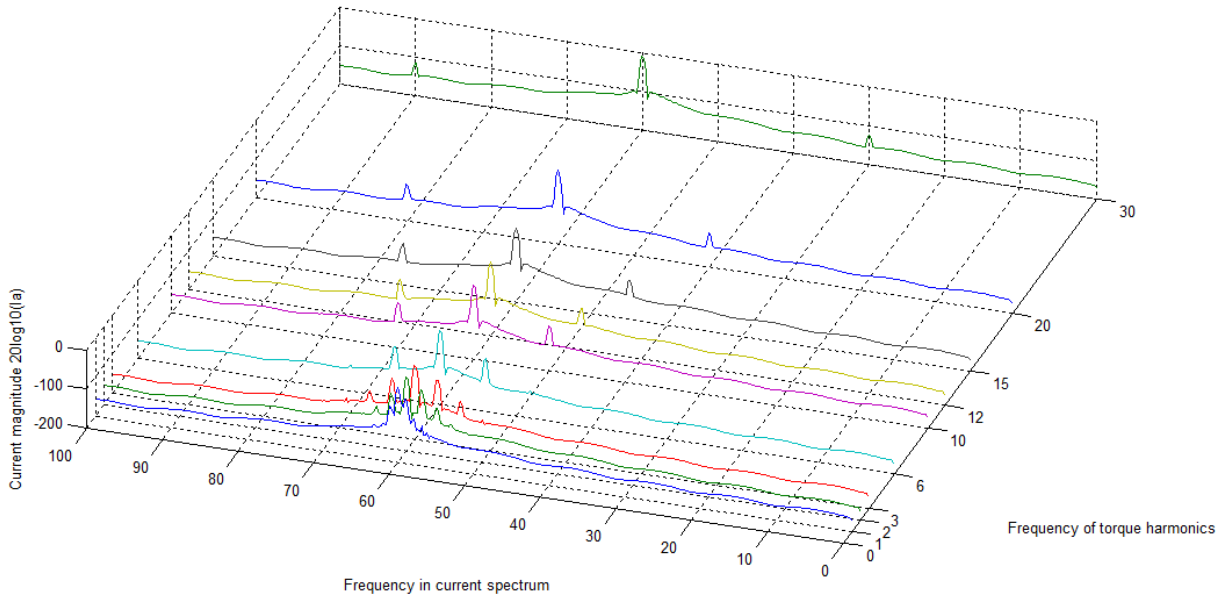

Fig.31 Torque modulation with changing frequency under fixed load $0.2T_{ave}$

In a similar way, the equivalent electrical network approach can also be extended to the generalized lumped dynamic torsional model, as shown in Fig.31. The bridge between two adjacent loops consists of capacitor $1/k_i$ and resistor c_i which are inverses of stiffness of shaft and damping between two masses respectively. The inductor J_i and resistor d_i are in the ith loop. In the circuit network, the source will be positive if it is a drive unit, and be negative if it is a load. When all the parameters are determined and all sources of oscillations are assigned, the simulation can be done to get the transient and steady state response, and lead to calculation of alternating shaft torque and stress, which can be used for torsional analysis of shaft assembly explained in the following sections.

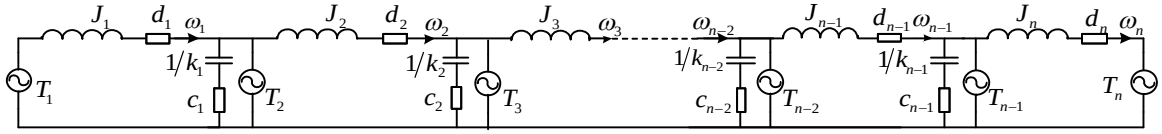

Fig.32 Equivalent circuit network of generalized torsional dynamics

2. Self-excited Torsional Vibration during Start-up

A salient pole synchronous motor is started from standstill at rated voltage with the dc field circuit shorted across an external field discharge resistor. When synchronization is almost attained, the discharge resistor is removed and a dc voltage is applied to the field circuit so that the motor will now run at synchronous speed. A load torque is then suddenly applied.

We can derive the interference diagram for the example in section 1. As shown in Fig.32, there are varying excitation frequencies from 120 Hz to 0 Hz equal to twice the slip frequency by transient electromagnetic torque. It indicates that the first two natural

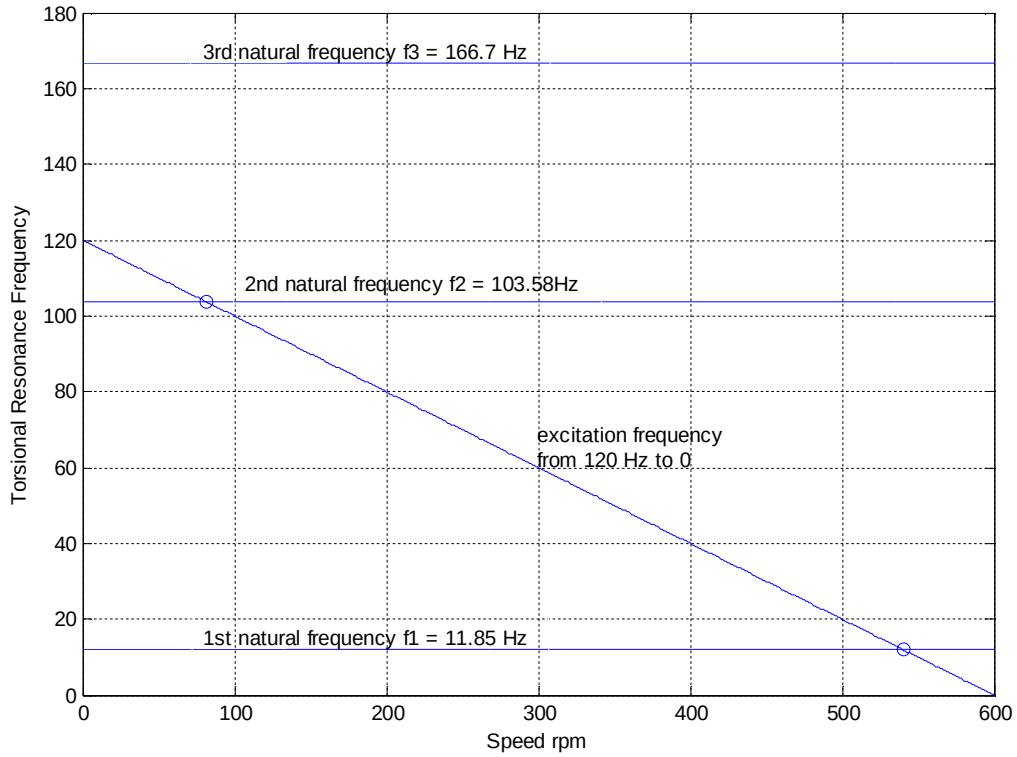

Fig.33 Interference diagram for transient 2x –slip frequency

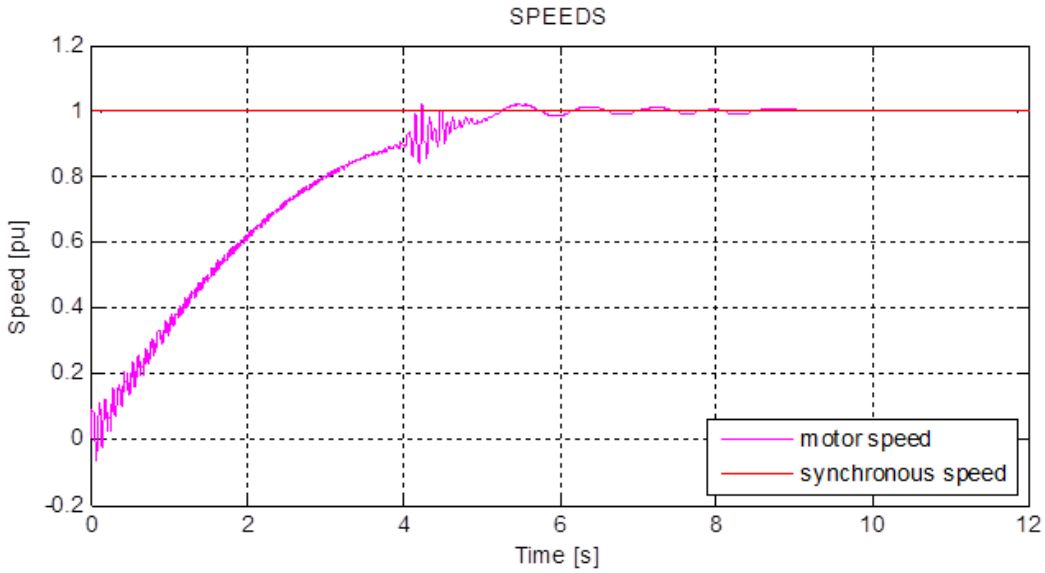

Fig.34 Motor speed during transient

torsional modes are expected to be excited during startup. The transient response is numerically simulated and the stress states for all 3 shaft segments are found.

Because we just study the transient excitation of electromagnetic torque in this subsection, we assume that the load torque is constant in simulation. During the transient, the machine is under no-load operation until the load is applied at 8^{th} second. From Fig.33, we can find that there are two locations where the speed fluctuates, which approximately correspond to the first two resonances modals.

The speed curve, stator and field current of the machine during the transient are shown in Fig.34-Fig.36. From the speed curve, we can find that the speed is oscillating at the beginning and around 4.2s. Similar to speed curve, the stator current contributing to armature flux and field current contributing to rotor field flux are resonant around the first two natural modals. We can exam the electromagnetic torque and shaft torques from Fig.37-Fig.40. These torques are approximate similar in profile, but the magnitudes are different. Due to resonance of shaft assembly, the peak shaft torque T12 is higher than that of electromagnetic torque.

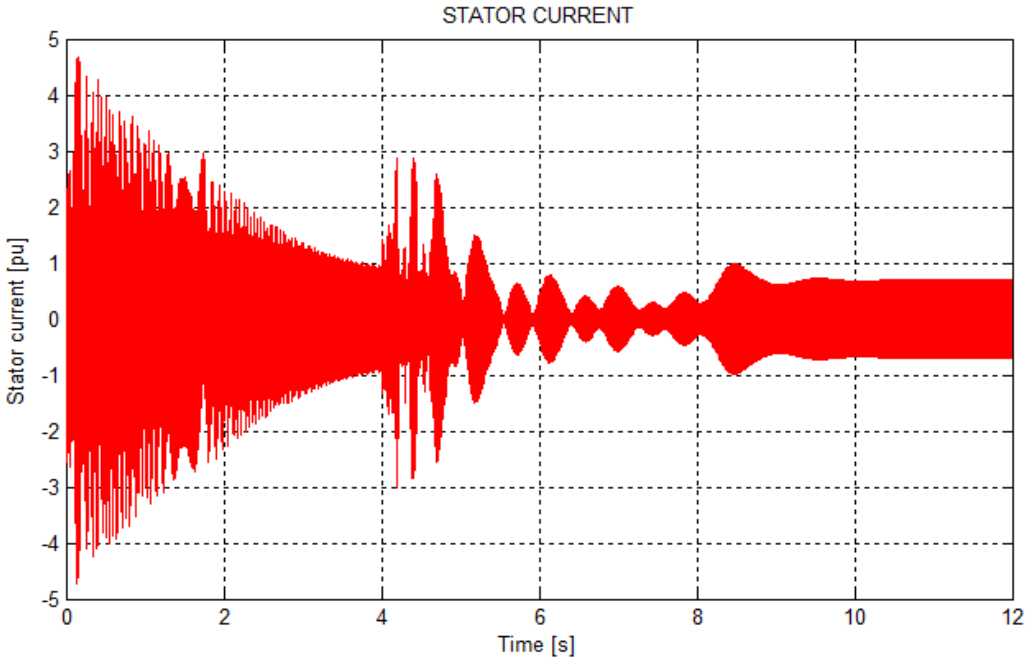

Fig.35 Motor current during transient

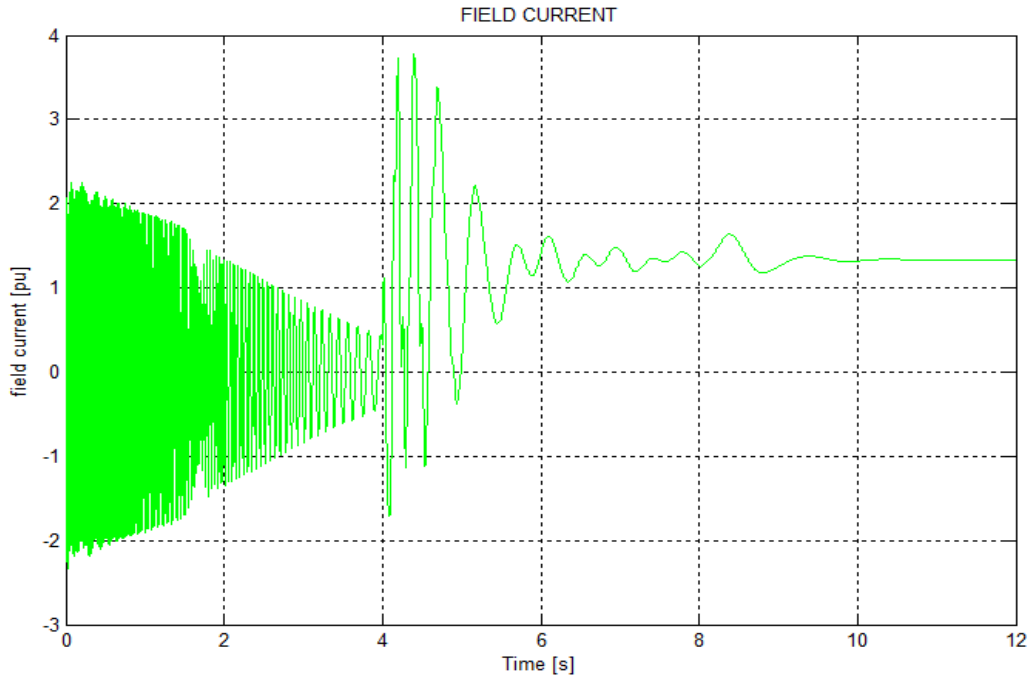

Fig.36 Field current during transient

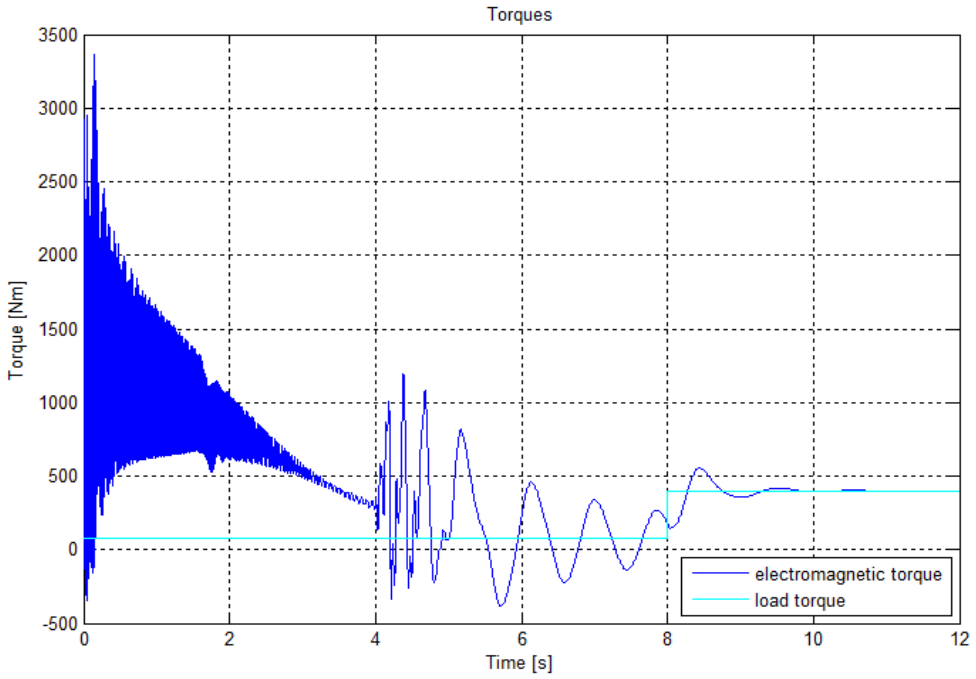

Fig.37 Electromagnetic torque during transient

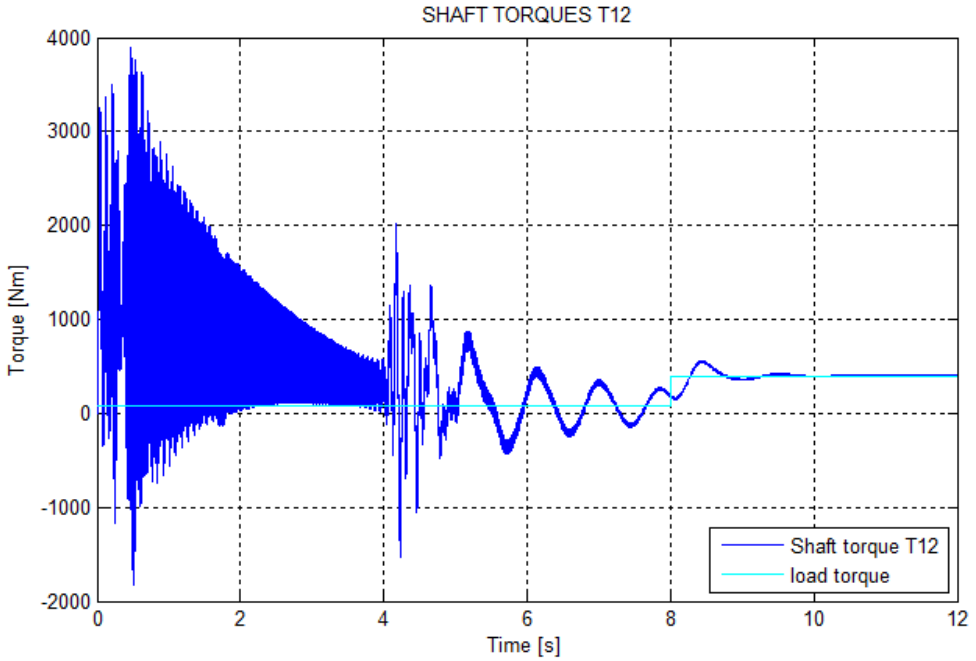

Fig.38 Shaft torque T12 during transient

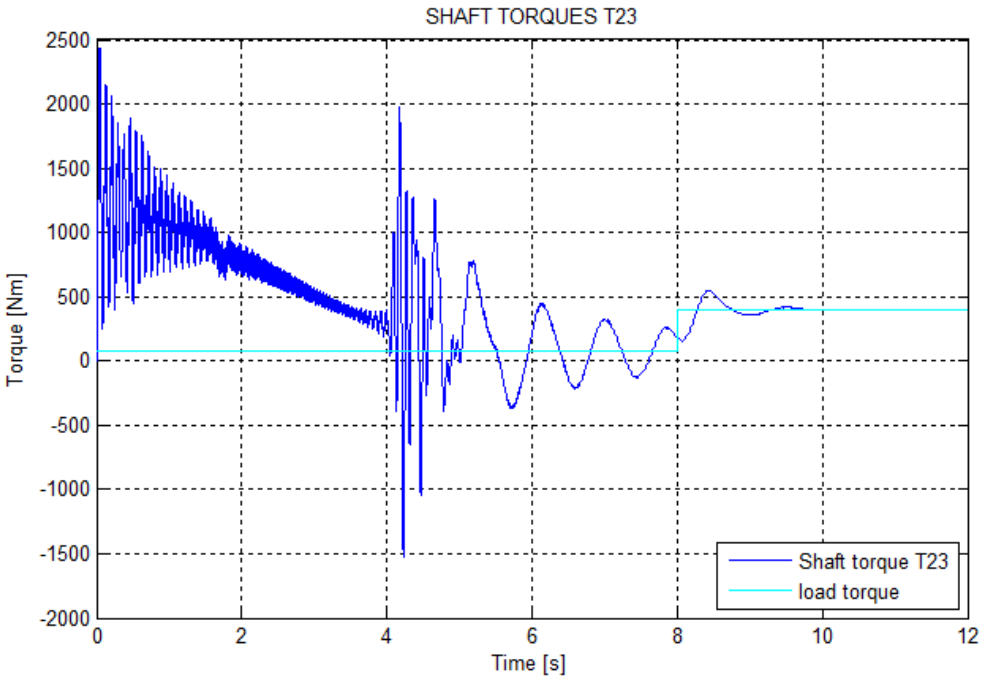

Fig.39 Shaft torque T23 during transient

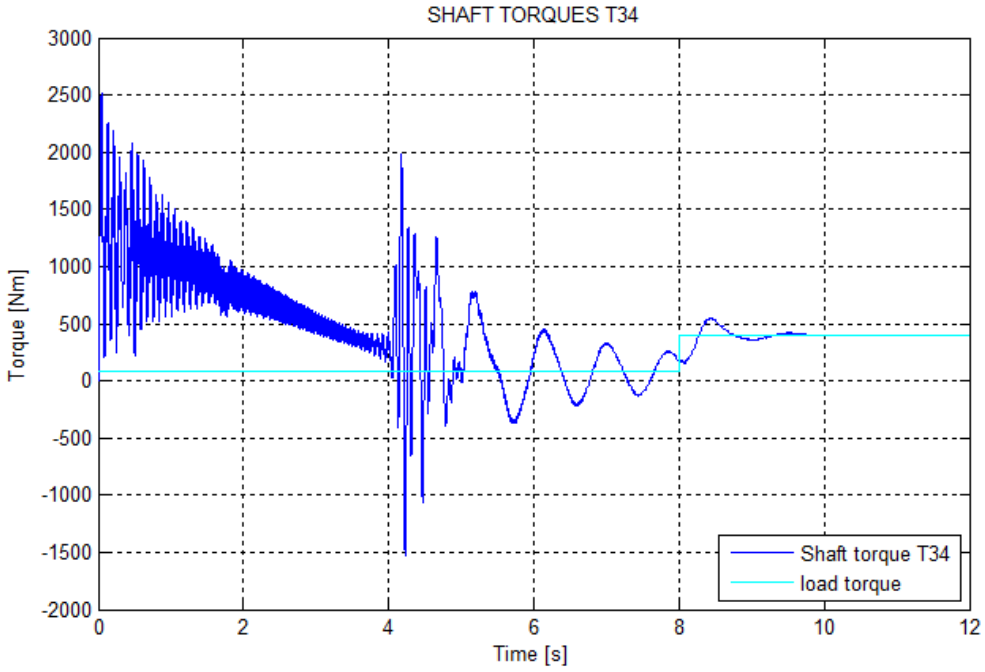

Fig.40 Shaft torque T34 during transient

3. Torsional Analysis Procedure

The drive train described in Section A is simulated under the excitation of electromagnetic torque and compressor position varying load in the above section. The electromagnetic torque can be estimated from the current and voltage signal of synchronous motor.

The objective of forced steady state torsional analysis is to evaluate the torque and torsional deflection at each mass and shaft segment. By the numerical approach introduced above, the dynamic torque at each shaft element can be computed from the simulation of coupled equivalent circuit approach.

Usually torsional resonance during steady state operation should be avoided at the design stage or be remedied by adding fly wheel, using higher damping or higher stiffness coupling to change the torsional dynamics of system. The fly wheel can be added at the appropriate position to change the resonance frequency around the operation speeds, and higher stiffness coupling can increase the natural frequency so that the excitation frequency cannot reach. The higher damping coupling can be used for torque damping to where the shaft stress is below the endurance limit.

While for a torsional system with multiply exciting harmonics or wide operating speed, there is an increasing chance for a coincidence of a speed or one of its harmonics with one of torsional natural frequencies. If sufficient separation margin cannot be achieved, then a detailed stress analysis should be performed to determine if the resulting stresses are below the endurance limit stress for the shaft material [60]. A detailed steady-state torsional analysis is summarized as follow:

(1) Calculation of torsional natural frequencies and torsional vibration modal shapes.

(2) Development of the interference diagram as shown in Figure 3.5.

(3) Definition of the coincidence of the excitation frequencies with the torsional natural frequencies, and the safety margin for each resonant frequency.

(4) Calculation of the dynamic torsional oscillations or deflections at all the masses and then the dynamic stresses in all shafts, based on the estimated dynamic torque modulations, stress concentration factors, and amplification factors [60].

(5) Comparison of the calculated results with application codes to determine compliance with regard to separation margin, stress and coupling dynamic torque and evaluate the possibility of fatigue failure.

(6) Parametric analysis to determine possible coupling modifications or mass modification by fly wheel when the separation margin, stress levels and coupling torque are not acceptable.

Even though the coincidence can be avoided during the design stage, the wear of mechanical parts such as gear or load blade or impellers and electrical or mechanical fault of synchronous motor during the operation within the machine's life cycle could induce unexpected excitations to the drive system. So the monitoring of the excitation frequencies from the electromagnetic torque can be informative for us to prevent the torsional resonance and shaft failure.

We know that the machine will produce harmonic torque range from 120Hz to 0 Hz during start-up when the rotor speed increase from 0 to synchronous speed. So the transient torsional vibration sometime is unavoidable if one of the natural frequencies of

shaft assembly below the 120Hz. The transient torque excitation usually is around 5-10 times of steady state torque, which could exceed the endurance limit. For the transient torsional analysis, we can investigate the coupling between electromagnetic and rotor dynamics, and the dynamic shaft torque obtained could lead to the cumulative fatigue analysis. This will be another research topic involving much of the structure and solid mechanics, and not be discussed in this research.

CHAPTER IV

CASE STUDY--- ESP DRIVEN CENTRIFUGAL PUMP

For downhole applications such as submersible multi-stage pumps and gas compressor driven by electric motor, the torsional vibration resonance or shaft fatigue maybe be experienced and lead to destructive effects on certain parts of rotor-shaft assembly. This section will cover the steady state and transient torsional analysis by ESA for an Electric Submersible Pump (ESP) system which include an electric motor and centrifugal pump.

A. Overview of ESP System

The Fig.41 shows the ESP system and detail configurations of motor and centrifugal. The submersible motor is the prime mover for the submersible pump system. Both induction and permanent magnet synchronous motor can be chosen as driver. Because of the size constraint of downhole environment, the diameter of these motor usually 4 to 8 inches in diameter and the motor should be longer. The power magnitude of the same series motors can be combined arbitrarily to fit with the power requirement of specific application. So it usually can extend to be 30 to 50 feet long. Besides the motors with single stage, motors may be stacked to be three stages: upper, middle and lower stages. They are fitted with spline coupling. These motors may also be combined according to the power magnitude required by the electric submersible pumps.

The submersible centrifugal pump is installed on the top of the electric submersible pump set. It can transfer the mechanical energy into the potential energy and the kinetic energy to lift up the well fluid to the surface out of the production well. The major components of multistage centrifugal pumps are nickel-alloyed iron stages that consist of rotating impellers and stationary diffusers. Selecting the correct number of stages will provide the required lift or head for the application, and the size of each stage will determine the volume of fluid through the pump. The Schlumberger and China Petroleum offer different series of centrifugal pump for various requirements [61,62].

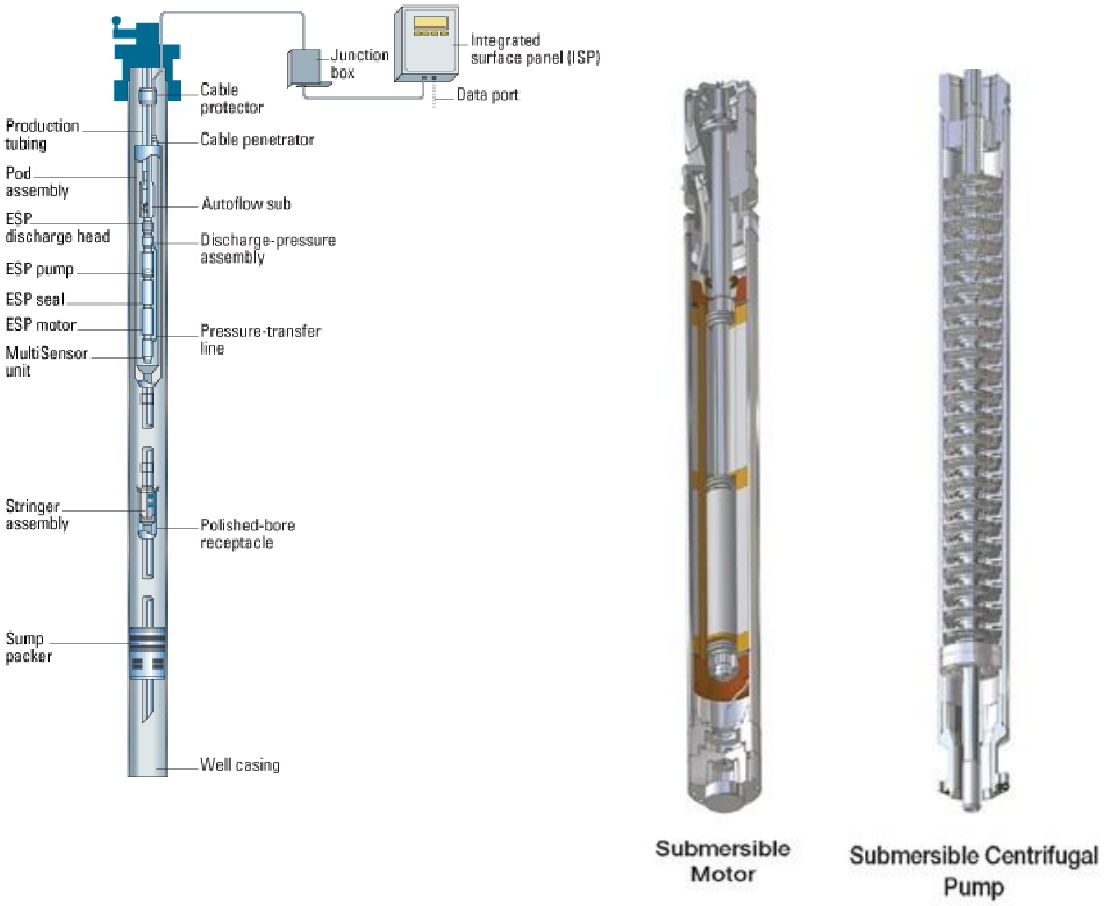

Fig.41 Electric submersible motor pump system

The submersible centrifugal pumps can be stacked to be upper stage, middle stage and lower stage and they are fitted with spline coupling to meet the requirements of combination of various series of electric submersible pump sets.

B. Modal Shape and Steady State Analysis

Due to the size constraint of downhole application, the long shaft of ESP could induce excessive torsional vibration under excitations. So we need to study the torsional dynamic of the ESP shaft assembly under possible load and electromagnetic torque excitations. Fig.42 illustrates the rotordynamic model for submersible motor and centrifugal pump. For completeness, each rotating mass was assigned a speed relative to the stationary pump housing. Coordinates and parameters were defined according to the electric analogy technique as discussed in section 3. The ESP housing is chosen as voltage reference. The rotors are stacked and connected with shafts to achieve power amplification, the rotor is assumed to be rigid, only the shaft can be twisted. The rotordynamic characteristics such as inertia and stiffness for rotor and impeller are specified in the Table I and II.

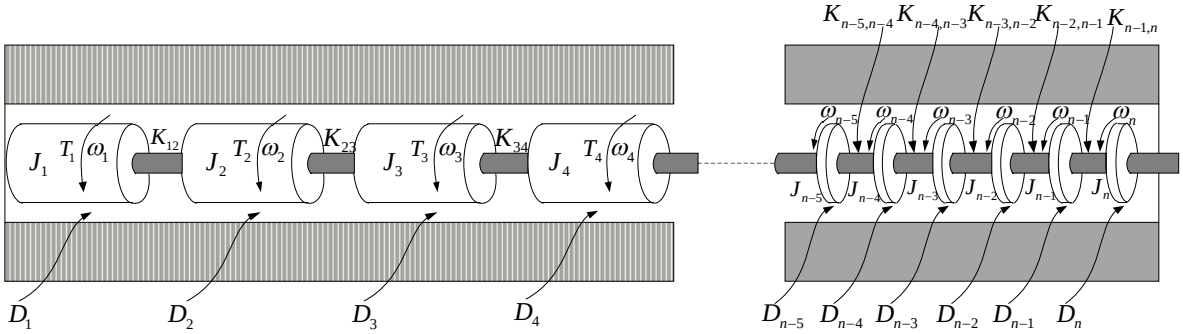

Fig.42 ESP model---the motor has multiply rotors

Tab.4 Electric submersible motor parameters (Series 456) [61]

Rotor				Shaft			
Rotor Length	Rotor Diameter	Rotor Power	Inertia (lb-in-s2)	Diameter (in)	Inside Diameter	Monel Compliance	Steel Compliance
13 in	2.414 in	5Hp	0.03242	1.181	0.38 in	8.02e-4	6.93e-5

Tab.5 Electric submersible pump impeller parameters (Series 540) [61]

Impeller				Shaft		
Impeller Diameter	Flow (gal/min)	Load (Hp/stage)	Inertia (lb-in-s2)	Diameter (in)	Monel compliance (lb-in-s2)	Steel Compliance (lb-in-s2)
4.00 in	73	1.26	0.00417	0.87	2.70e-4	2.33e-4

Similar to section 1, the modal shape analysis can be conducted for the ESP. For the chosen rotor and impeller types, one motor rotor can drive 4 stages of impeller, as more rotors are stacked, more stages of impeller are be driven to provide more flow rate and head. Usually the coupling connecting motor and pump is less stiff than that of shaft between rotating masses, as more rotating masses are stacked together, the ESP system will become longer and more flexible. As a result the natural frequencies of the system will decrease. The Fig.43 shows how the first natural frequency is affected by coupling

stiffness and the number of rotors stacked. We can found that the first natural frequency will drop as the number of rotor increases, but drop less as more rotors stacked.

The first natural frequency will decrease as the coupling become more flexible. The modal shape analysis shows the second natural frequency will drop just below 120Hz as the coupling stiffness decrease to $300\,lbf \bullet ft / rad$. The higher natural frequencies usually are not the serious concern unless the higher order harmonics from Variable Frequency Drive (VFD) match with these natural frequencies. This is not the main concern in this study. The Fig.44 presents the first modal shape of ESP system shaft assembly when coupling stiffness is chosen as $K_C = 1000\ lbf \bullet ft / rad$. The coupling will have maximum deflection when the first modal shape is excited and resonance is induced. We will find later that the harmonics of the starting torque will excite the natural frequencies below 120Hz during the start-up. The selection of coupling stiffness should not be too lower so that more natural frequencies are below 120 Hz. The stiffness, however, cannot also be too higher, so that excessively higher starting shaft torque experienced will break the shaft of rotor or experience fast shaft fatigue failure, and the principle purpose of flexible coupling to protect shaft cannot be justified. The starting torque will be discussed next.

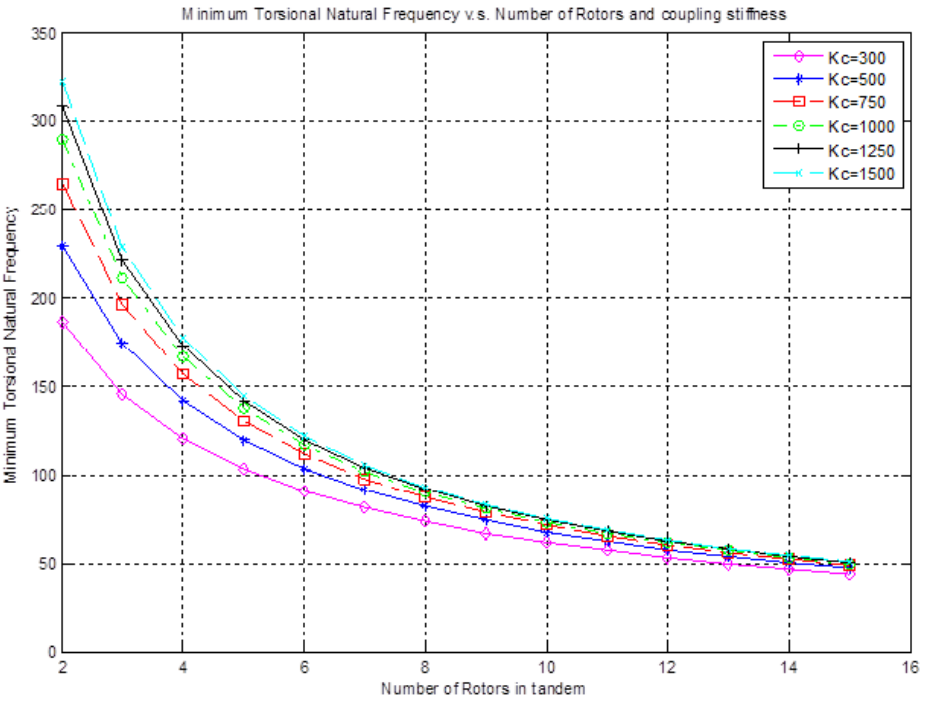

Fig.43 The first natural frequency of ESP v.s number of rotor in tandem

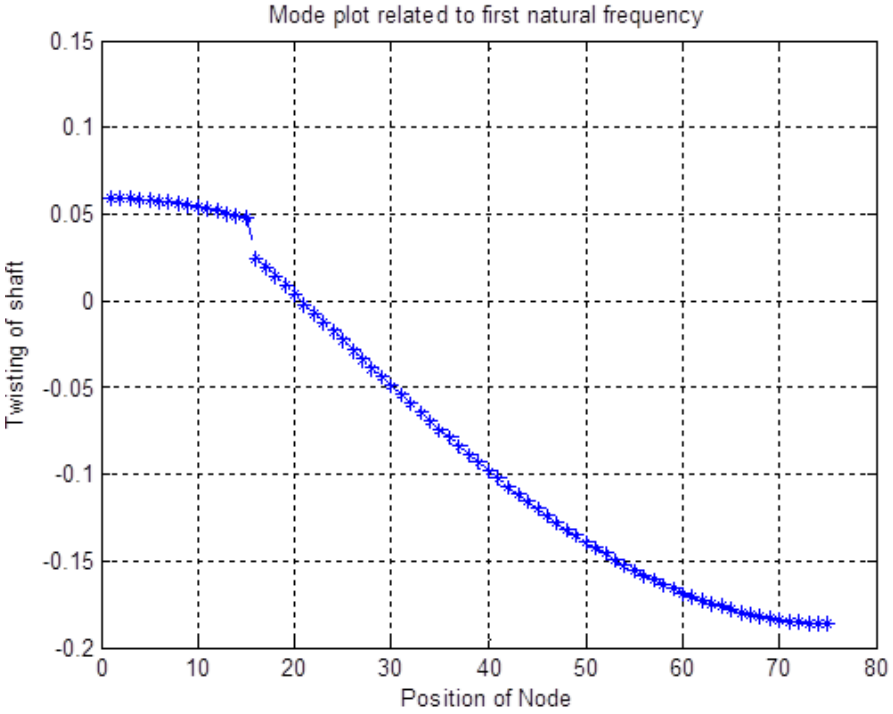

Fig.44 Natural mode for ESP with 15 rotors in tandem

C. Electromagnetic-Rotordynamic Coupling

The stator is common to all rotors, and mutual coupling between each rotor and stator depends on the angle θ_k between $\omega_k = d\theta_k / dt$. Self-inductance and resistance parameters L_{rr} and R_r is specified per rotor. Taking $\bar{v}$, $\bar{\lambda}$ and $\bar{i}$ as voltage, flux linkage and current vectors produced by the applied three phase voltages with $L_{sr}(\theta_k)$ the mutual inductance per rotor then

$$\begin{bmatrix} \bar{\lambda}_s \\ \bar{\lambda}_{r1} \\ \bar{\lambda}_{r2} \\ \vdots \\ \bar{\lambda}_{rn} \end{bmatrix} = \begin{bmatrix} L_{ss} & L_{sr}(\theta_1) & L_{sr}(\theta_1) & \cdots & L_{sr}(\theta_n) \\ L_{sr}(\theta_1) & L_{rr} & 0 & & 0 \\ L_{sr}(\theta_2) & 0 & L_{rr} & & \\ \cdots & & & L_{rr} & \\ L_{sr}(\theta_n) & 0 & \cdots & & L_{rr} \end{bmatrix} \begin{bmatrix} \bar{i}_s \\ \bar{i}_{r1} \\ \bar{i}_{r2} \\ \vdots \\ \bar{i}_{rn} \end{bmatrix} \tag{4.1}$$

The instantaneous torque per rotor is

$$T_k = \frac{3}{2}(\lambda_{qrk} i_{drk} - \lambda_{drk} i_{qrk}) \tag{4.2}$$

After converting to dq0 coordinate and referring rotor quantities to the stator, subscripts d, q, s, r and k denote direct axis, quadrature axis, stator, rotor and rotor number respectively. Similar to what we did in chapter V, the machine model can be coupled with rotordynamics of rotor shaft and be simulated in Matlab/Simulink. We choose ESP model with 15 rotor stacked and 60 stages centrifugal pumps for simulation. The electromagnetic torque, stator current and shaft torque can be obtained to justify the explanation above, which are presented in the Fig.45, Fig.47 and Fig.49. The time-dependent spectrum implemented by short-time Fourier Transform can be employed to show the harmonics profile shifting during the start-up transient. The related stator

current, electromagnetic and shaft torque spectrogram are shown in Fig.46, Fig.48 and Fig.50.

From the spectrogram of electromagnetic and shaft torque, we can find that the first natural frequency f1 = 50 Hz is excited, which can be justified from the time domain profile of the shaft torque T_{MC}. In the Fig.49, the shaft torque T_{MC} experienced the other amplification around 2.5 second due to the excitation of its first natural mode by the electromagnetic torque. From the spectrogram of electromagnetic torque shown in Fig.45, we can find that there are abundant torque harmonics below 120Hz during the transient. The harmonics start with 120Hz and converge to 0Hz when the rotor speed synchronizes with the rotating MMF in stator.

The stator current is amplified during the transient start-up. The second amplification is due to the coupling with the resonance of shaft torsional vibration, which occurs around 4.2 sec as presented in the Fig.49. The spectrogram of stator current shows that the principle component 60Hz mixes with harmonics 0~60Hz and converge to 60Hz as the speed reach to synchronous speed.

We can find that the second amplification of electromagnetic torque and stator current lag behind the second amplification of shaft torque in time. A possible explanation is that the rotor inertia will delay the transmission of shaft torque amplification to electromagnetic torque and stator current. It also can be justified from the point view of the coupled equivalent circuit. The time constant resulting from the rotor inertia delay the response (current or electromagnetic torque) to excitation input (shaft torque and load torque).

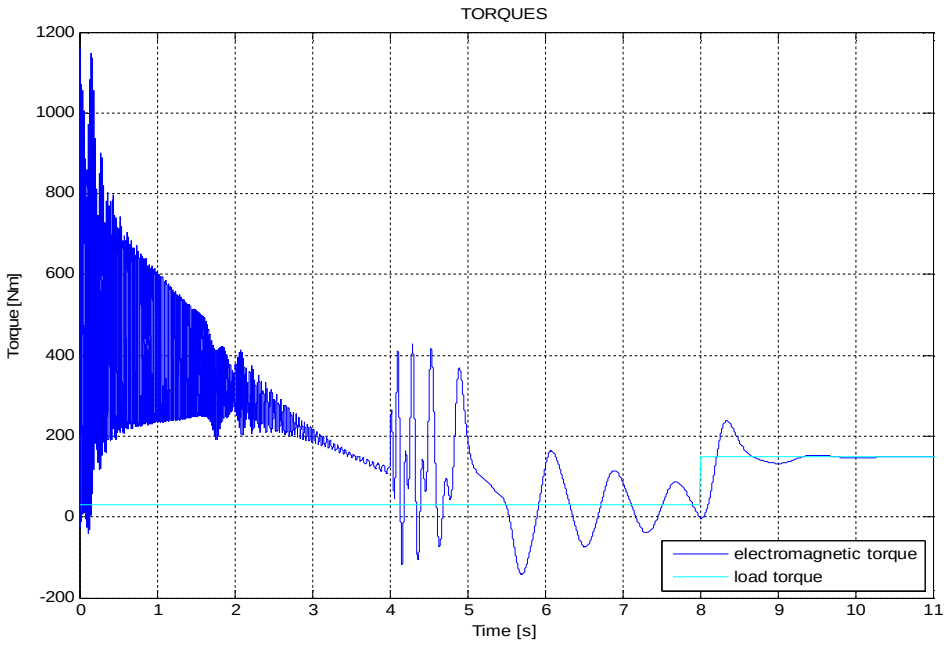

Fig.45 Electromagnetic torque Tem

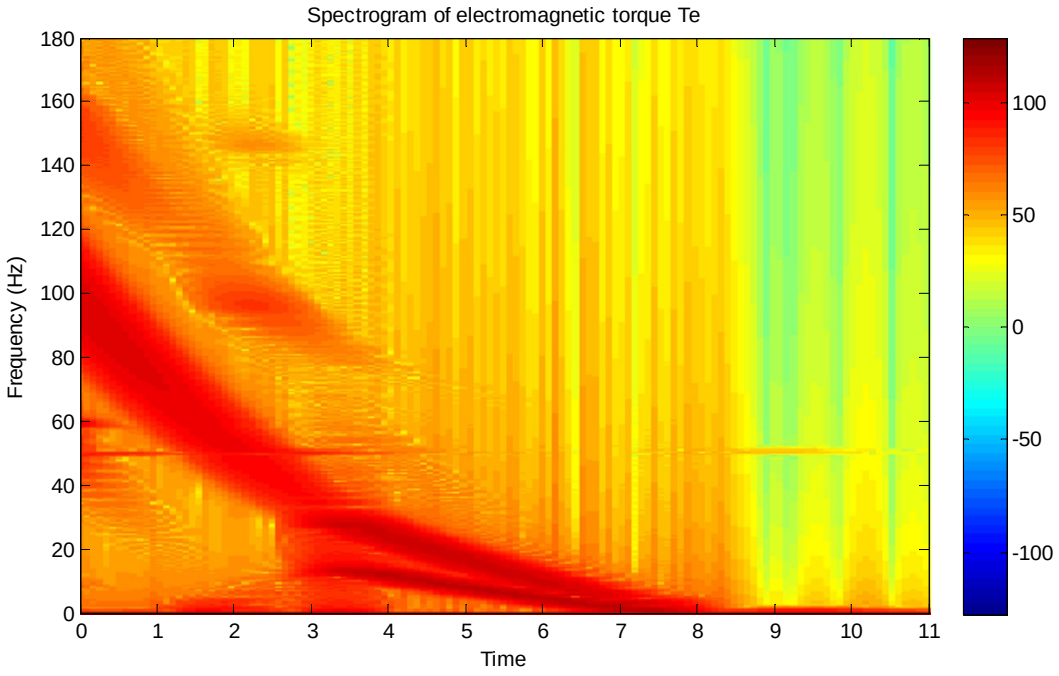

Fig.46 Spectrogram of electromagnetic torque

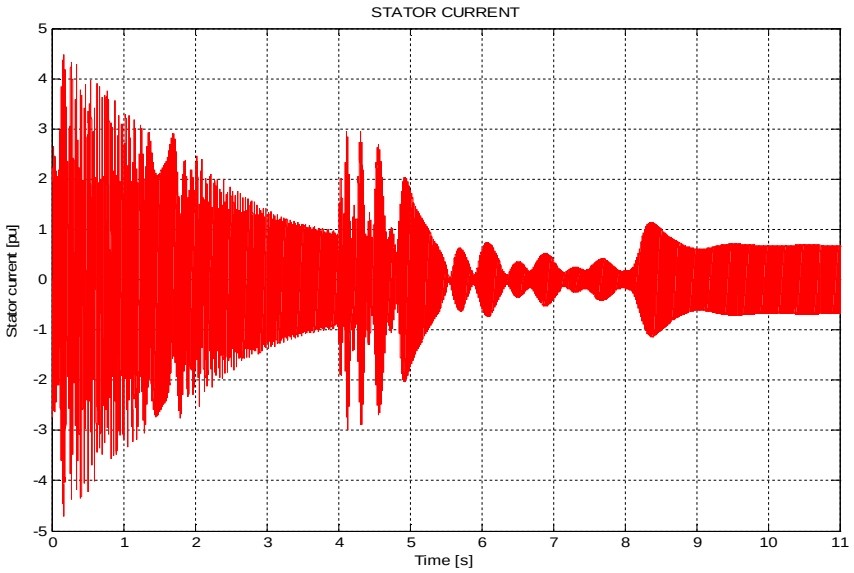

Fig.47 ESP motor stator current

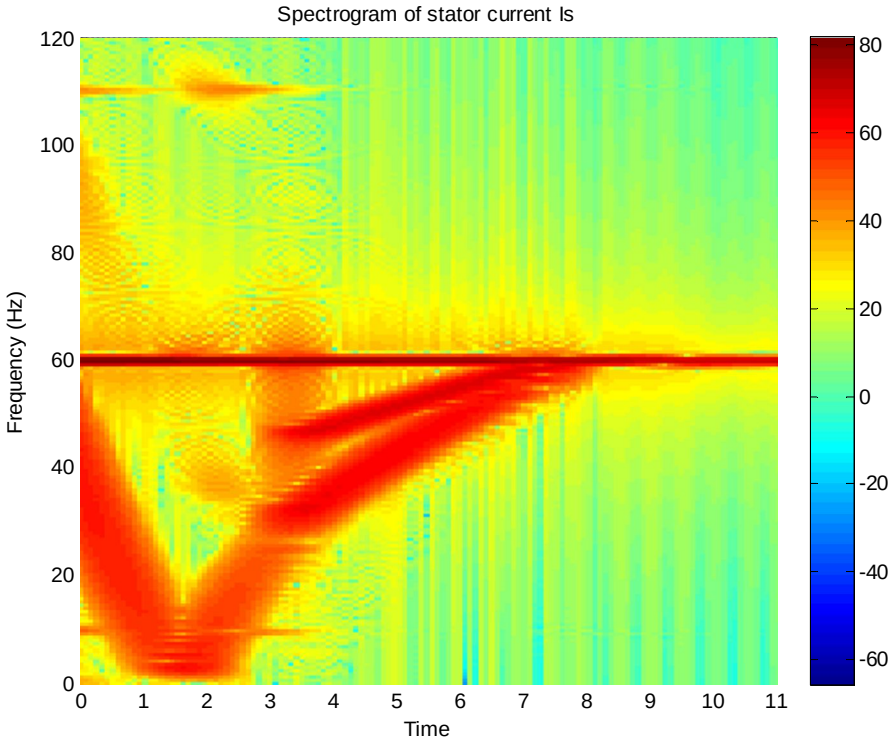

Fig.48 Spectrogram of ESP motor stator current

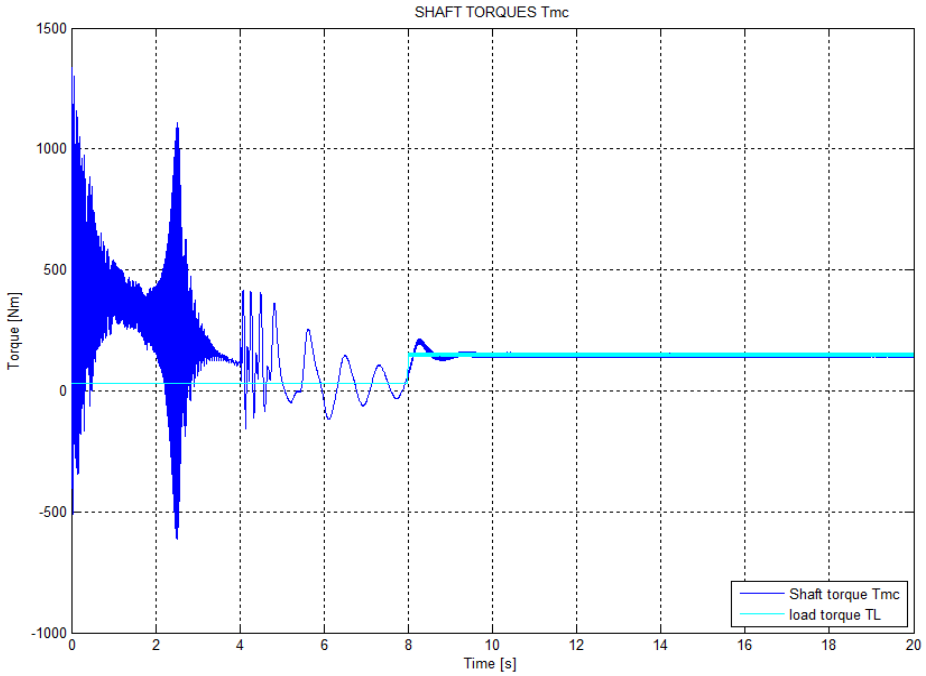

Fig.49 Torque on shaft between motor and coupling

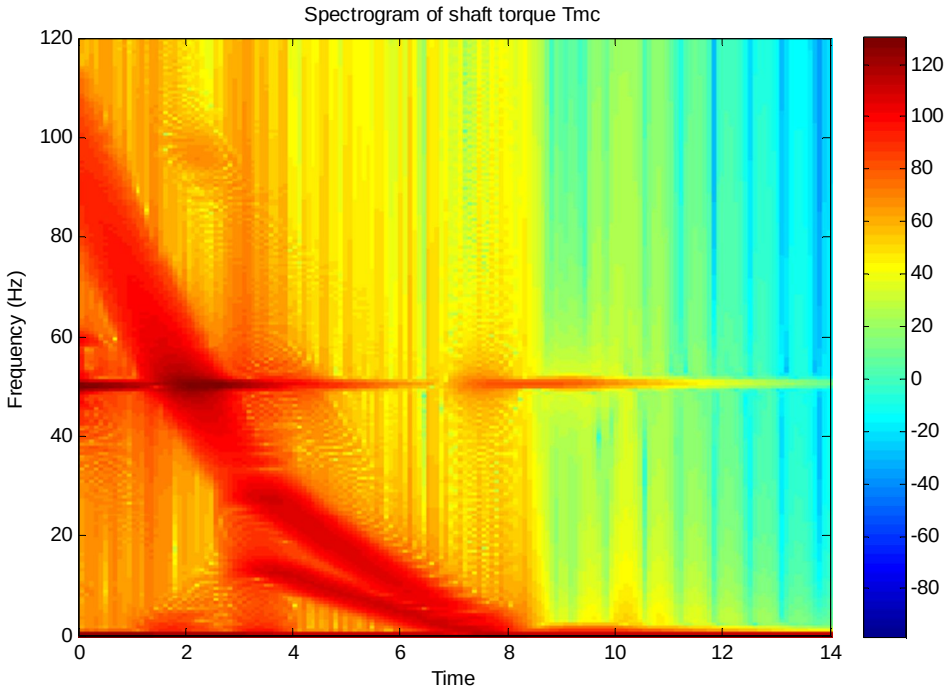

Fig.50 Spectrogram of shaft torque between motor and coupling

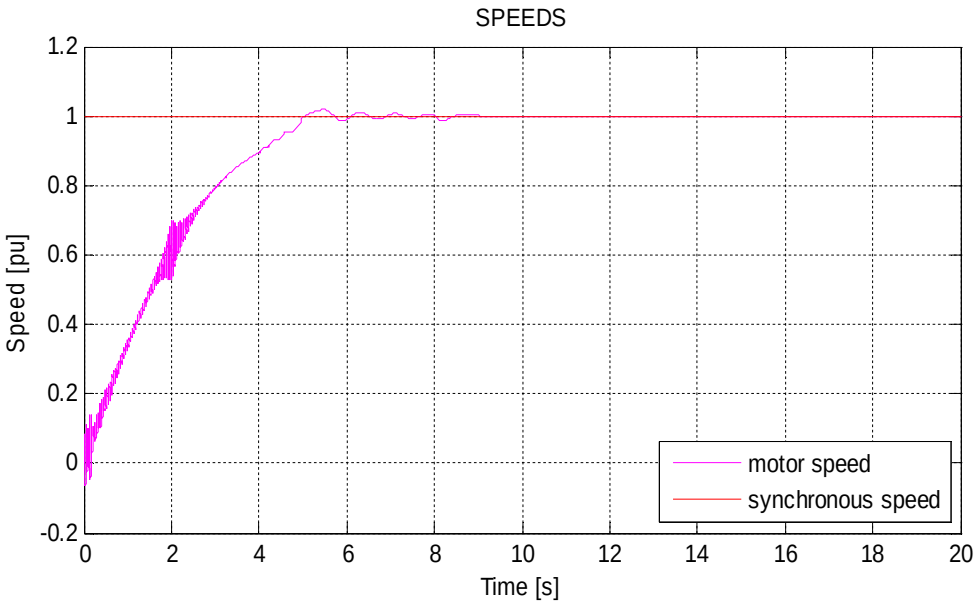

Fig.51 Rotor speed in time domain

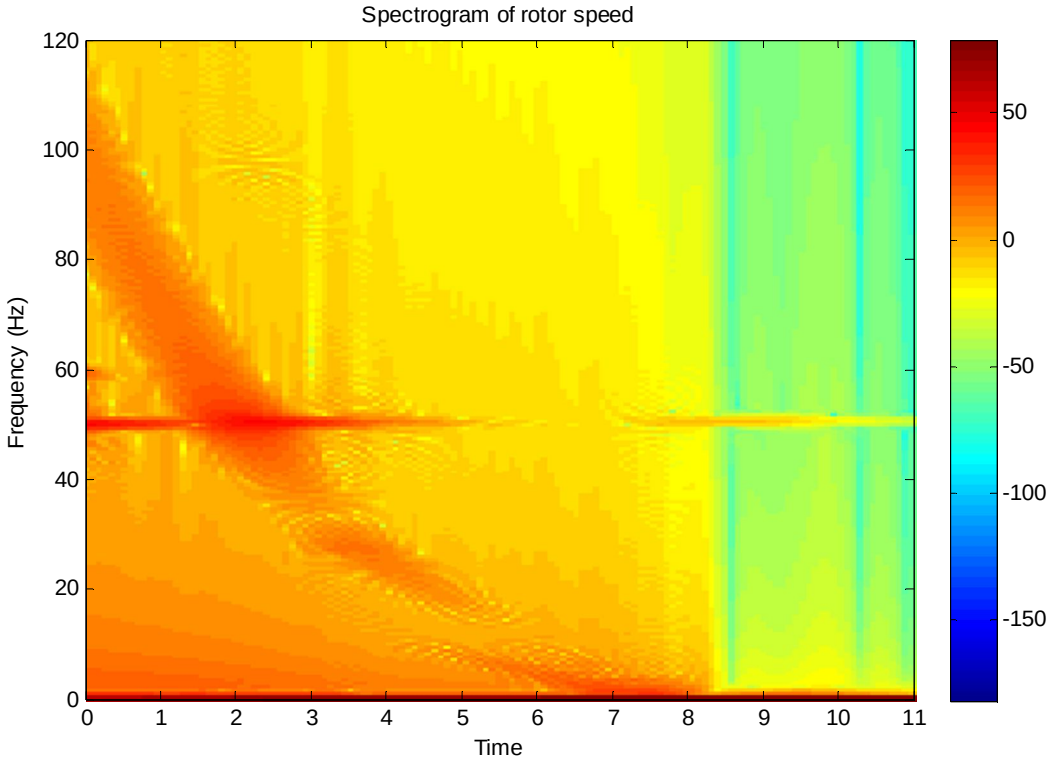

Fig.52 Spectrogram of rotor speed

From the spectrogram of shaft torque Tmc in the Fig.50, we can find that the shaft is resonant at it first natural frequency f1=50Hz. As the rotor speed reaches the synchronous speed, the resonance will disappear and the shaft torque reaches to a constant torque.

From the Fig.53~Fig.55, we can find that the stiffness of coupling will affect the starting electromagnetic and shaft torque significantly. As the coupling become stiffer, the starting torque will be bigger. So there is a trade-off to select the coupling by weigh the amplification of starting torque and lowering of natural frequency of ESP system.

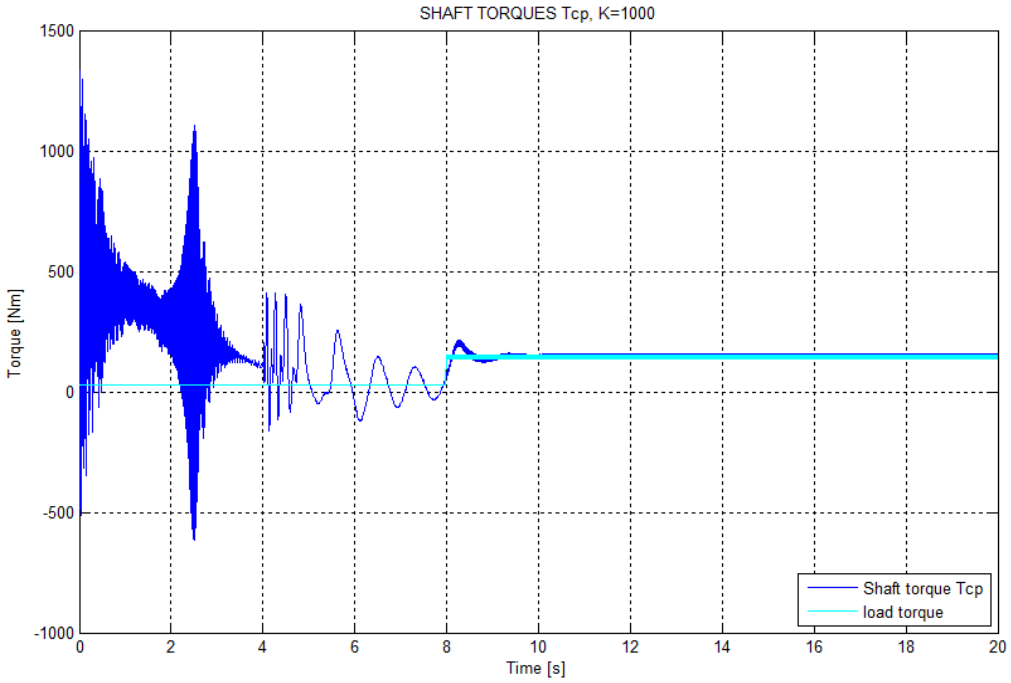

Fig.53 Torque on shaft between coupling and pump Tcp, K=1000 lbf· ft/rad

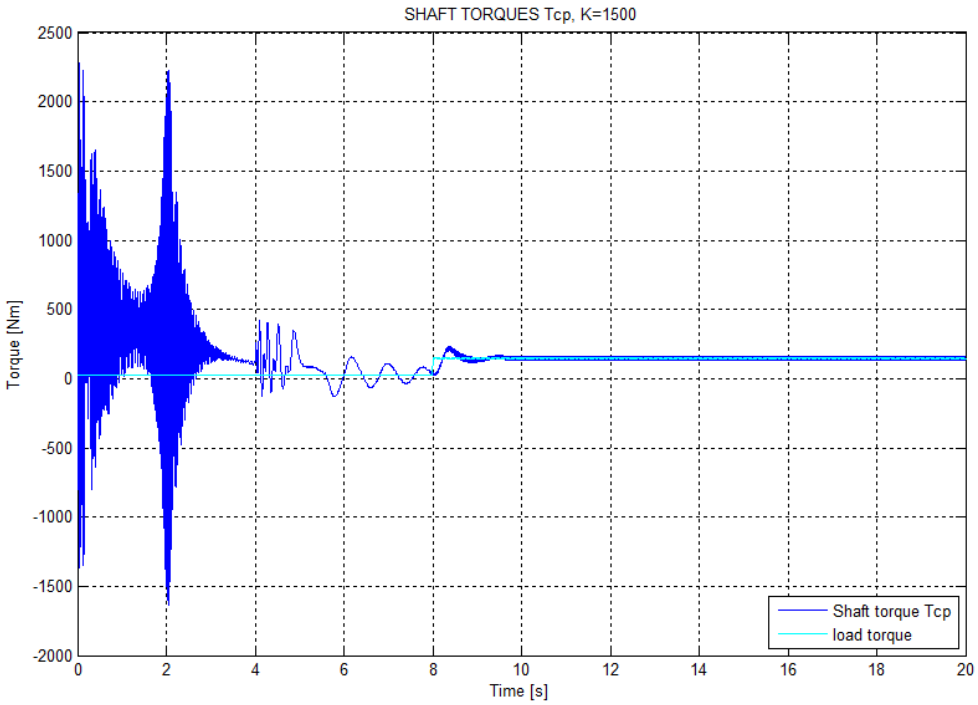

Fig.54 Torque on shaft between coupling and pump, K=1500 lbf▪ ft/rad

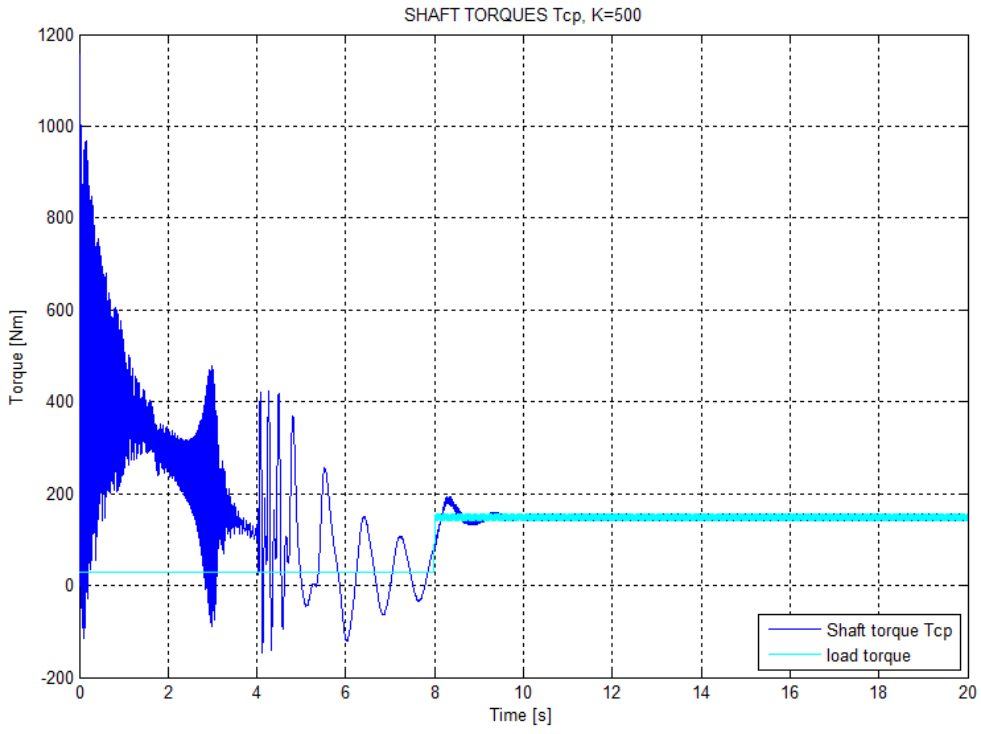

Fig.55 Torque on shaft between coupling and pump, K=500 lbf▪ ft/rad

CHAPTER V

ESA OF GENERALIZED ROUGHNESS BEARING ANOMALY UNDER NONSTATIONARY POWER INPUT

In this chapter, first we will investigate the nature of the generalized roughness bearing defect and its physical link to current signature. The power quality variation will be illustrated to show how the nonstationarity of power input could affect the ESA of subtle current signature of generalized roughness bearing defect. The discussion on the nonstationary, locally and piecewise stationary signal lead to the signal segmentation to isolate the influence of nonstationary power input.

A. Nature of Generalized Roughness Bearing Anomaly

As previous discussed, it is impossible to identify a specific frequency in the electrical signature for generalized roughness bearing defect, while unpredictable broadband changes in vibration and stator current spectrum could be induced. There are two physical explanations behind it. One of them is that vibration induced radial motion cause non uniform subtle air-gap operation and therefore machine inductance oscillates. Because of this oscillation, the line current becomes noisy and the noise floor of current spectrum becomes higher as the severity increases.

Rather than causing air-gap eccentricity, the other physical link between bearing defect and current harmonics is more practical. The generalized roughness defect will induce the torque ripple that produces a speed ripple which could be observed from

torque and speed measurements [27], even though the defect cannot produce detectable air-gap eccentricity and characteristic frequency. The speed variation will induce current harmonics by phase modulation. The Fig.56 shows that the influence of noisy torque pulsation on the stator current spectrum. So the bearing-fault related vibration is seen as a torque or speed component that generates in the current a chain of components. This fault mechanism is best suited for generalized roughness defect, while the air-gap eccentricity fault model is best suited for single point defect. In practice, however, both fault mechanism could manifest for bearing fault more or less depends on how the bearing defects looks like.

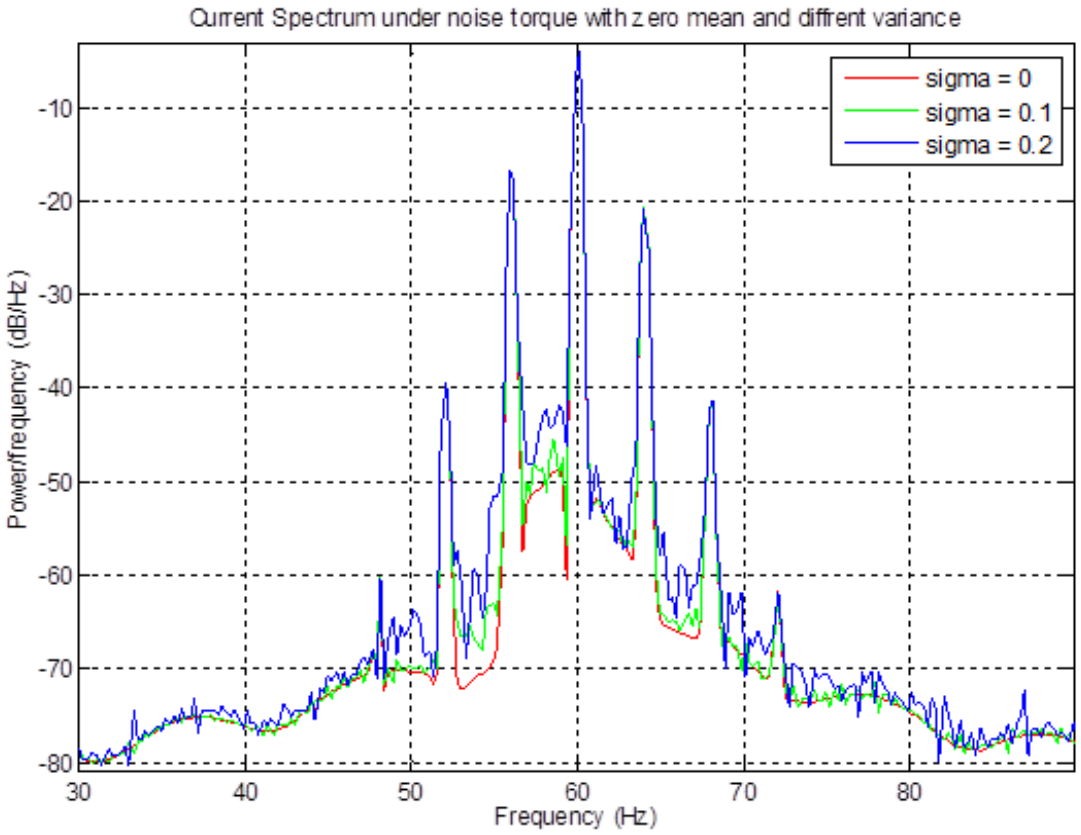

Fig.56 Current signature of generalized roughness under torque oscillation

The unpredictable broadband change in vibration spectrum can be detected by means of the temporal vibration signal Root Mean Square (RMS) analysis. As some works and standards set out, a RMS vibration value evaluation also provides a good indicator for motor health, allowing machine overall fault diagnosis.

Current signatures induced by generalized-roughness defects are usually recognized to occur in stationary conditions, and do not provide a specific fault signature. Time–frequency analysis is best suited to identify when a specific disturbance appears such as single point defect. Because of these limitations, techniques involving whole-spectrum energy content have been proposed to detect faults [28], which based on removing the non-bearing faults components from diagnostic signal and utilizing the residuum or on seeking and utilizing the frequency bands with high probability of presence of bearing faults components. Fabio [29] investigated the spectral kurtosis statistical properties of machine signals in order to identify in what bandwidth that disturbance is more suitable to appear. This approach is believed to be more effective for the specific characteristics of generalized-roughness faults. Unfortunately experimental results can verify this approach only effective for vibration signal, not for current signature.

The signatures induced from the generalized roughness defect are often subtle and low energy signals, compared with the significant frequency components in the power spectrum such as fundamental and harmonics which could be considered as noise in the bearing anomaly detection. Moreover, the above articles did not consider the influence of power quality of non-stationary input on the subtle current signature of

generalized-roughness bearing defect. Because of the influence and overwhelming of non-stationary voltage input, this current signature is hard or failed to be picked up by commonly used spectral analysis approaches, such as in [28,29]. So it is necessary to isolate the influence of nonstationary power input for improving the ESA of generalized roughness bearing defect. In this chapter, a segmentation procedure will be proposed to isolate the impact of nonstationary input voltage later.

B. PQ Variation and Nonstationarity of Power Input

Because the power supply system can only control the quality of the voltage, it has no control over the currents that particular loads might draw. So the power input we refer is actually the voltage input. The ideal voltage input is pure sinusoidal, which is the implicit assumption of almost all articles of MCSA of electric machine anomalies. This assumption, however, is not valid in practical applications and could lead to misleading results of MCSA. Actually voltage and current waveforms usually deviate from their nominal values. Any power problem that is manifested in voltage, current, or frequency deviations and results in the failure or incorrect operation of customer equipment is a PQ problem. PQ disturbances consist of two different types: PQ variations and PQ events.

In this dissertation, PQ problem of course should and actually is easy to be identified and detected. But main concern should be put on mild or gentle PQ variations [47] because they are pervasive through the long term service of electric machines. The mild or gentle PQ variations could not lead to failure or incorrect operation of equipment, but will impose influence on the MCSA of electric machine anomalies. As

discussed in previous section, the current signature of generalized roughness bearing anomalies usually subtle, so it is vulnerable to the influence of PQ variation. It is critical to isolate the influence of PQ variation for ESA of generalized roughness bearing defect.

Locally and piecewise stationary processes are important concepts leading to understand "slowly changing" nonstationary process, which can be dealt by signal segmentation technique [48]. Below will cover how a slowly changing nonstationary process can be model as a series of piecewise stationary process where we can use conventional signal processing techniques.

1. Power Quality Variation of Input Voltage

AC power systems are designed to operate at a sinusoidal voltage of a given frequency (typically 50 or 60 Hz) and magnitude. During the operation of electric machine, there are always slight deviations in the waveform magnitude, frequency, or purity, which are not a PQ problem, but will be important for MCSA of electric machine anomalies. The major PQ variations occur in practical power system are transient, voltage unbalance and it variation, voltage RMS variation in short or long duration and distortion by harmonics or inter-harmonics and its variation [49].

Transient

Transient usually caused by switching phenomena within end-user facilities, such as large inductive or capacitive load start-up. Some power electronic devices also generate significant transients when they switch. Transient can be generated at high

frequency (load switching and lightning), medium frequency (capacitor energizing), or low frequency. A transient with a primary frequency component less than 5 kHz, and duration from 0.3 to 50 ms, is considered a low-frequency transient, which will affect the effectiveness of MCSA of electric machine anomalies. The data section containing transient should be identified and removed so that the influence of transient on MCSA can be eliminated.

Short and Long Duration Voltage Variations

Short-duration voltage variations are caused by some events such as the energization of large loads which require high starting currents, or intermittent loose connections in power wiring. Depending on the fault location and the system conditions, the event can cause either temporary voltage drops (sags), voltage rises (swells), for durations from 0.5 cycle to 1 min for the equipment on the bus. Long-duration variations encompass RMS deviations at power frequencies for longer than 1 min. The boundary between them is no clear, however, their influences on MCSA are quite similar.

When a neighbor high power rating motor starts up, the motors have the undesirable effect of drawing several times their full load current. This large current will by flowing through system impedances, causes a voltage sag in the bus line and power supplied to other equipment in the same bus. The RMS variation of the voltage input to synchronous motor in our test rig is shown in the Fig.57, which present us that the RMS value of synchronous motor input voltage is varying during about 240 hours normal operation service.

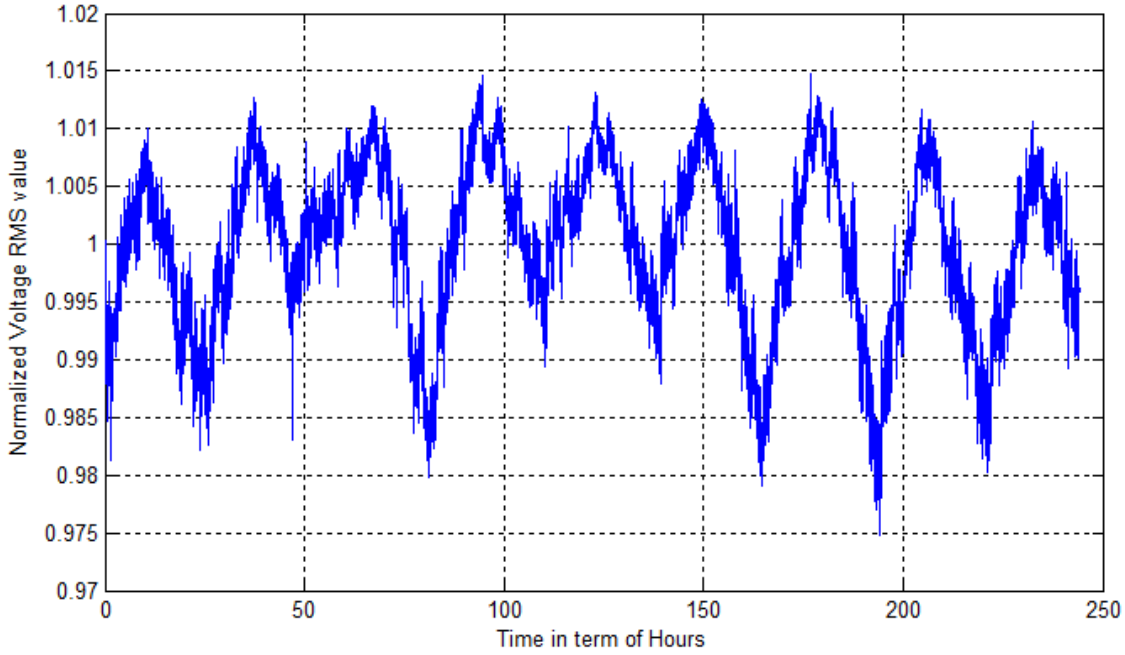

Fig.57 Normalized voltage RMS variations v.s. Time

Voltage Unbalance

The practical three phase voltage shows voltage unbalance and the slow variation of this unbalance. Voltage imbalance or unbalance is sometimes defined as the maximum deviation from the average of the three-phase voltages or currents, divided by the average of the three-phase voltages or currents, expressed in percent. Imbalance is more rigorously defined in the standards [49] using symmetrical components. The ratio of either the negative- or zero sequence components to the positive-sequence component can be used to specify the percent unbalance. The Fig.58 shows unbalance variation of the voltage input to synchronous motor in our test rig. We can find that the voltage unbalance of motor input voltage is varying during 240 hours normal operation service.

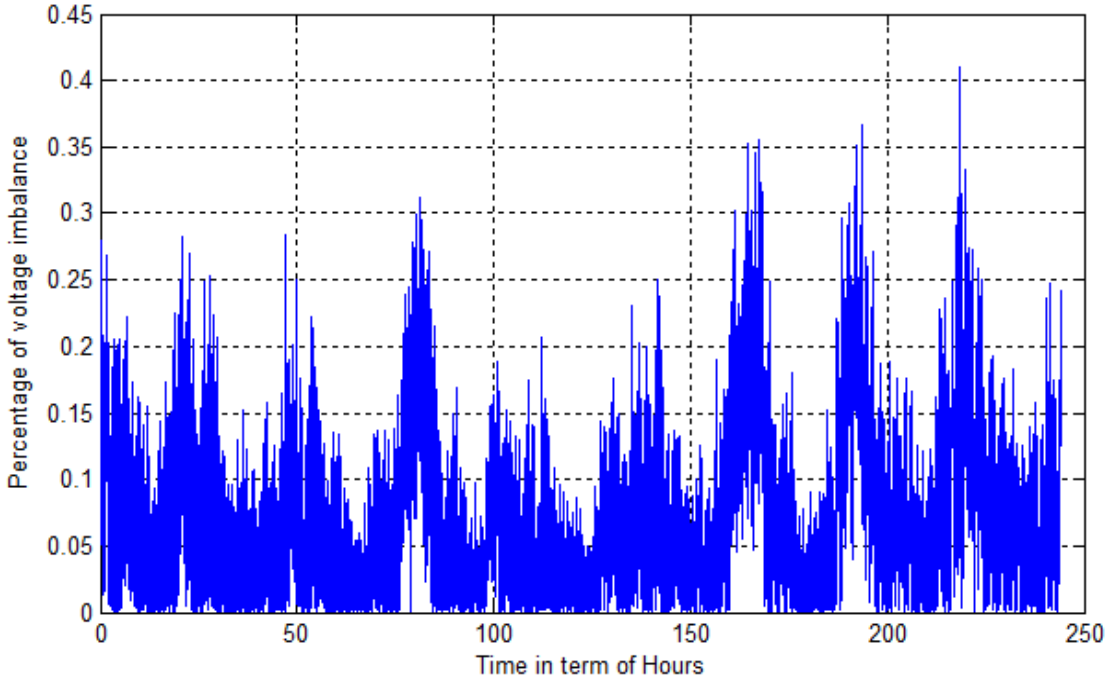

Fig.58 Percentage of voltage imbalance variations v.s. Time

Distortion by Harmonics or Inter-harmonics

The voltage from the utility power line always has harmonics, even though the machine is not driven by VFD. Moreover, distorted currents from harmonic-producing loads also distort the voltage as they pass through the system impedance. Thus a distorted voltage is presented to other end users. Waveform distortion is defined as a steady-state deviation from an ideal sine wave of power frequency principally characterized by the spectral content of the deviation.

Periodically distorted waveforms can be decomposed into a sum of the fundamental frequency and the harmonics. The harmonic distortion usually measured by

the total harmonic distortion (THD). The Fig.59 illustrates the THD variation for the synchronous motor voltage input for 240 hours normal operation.

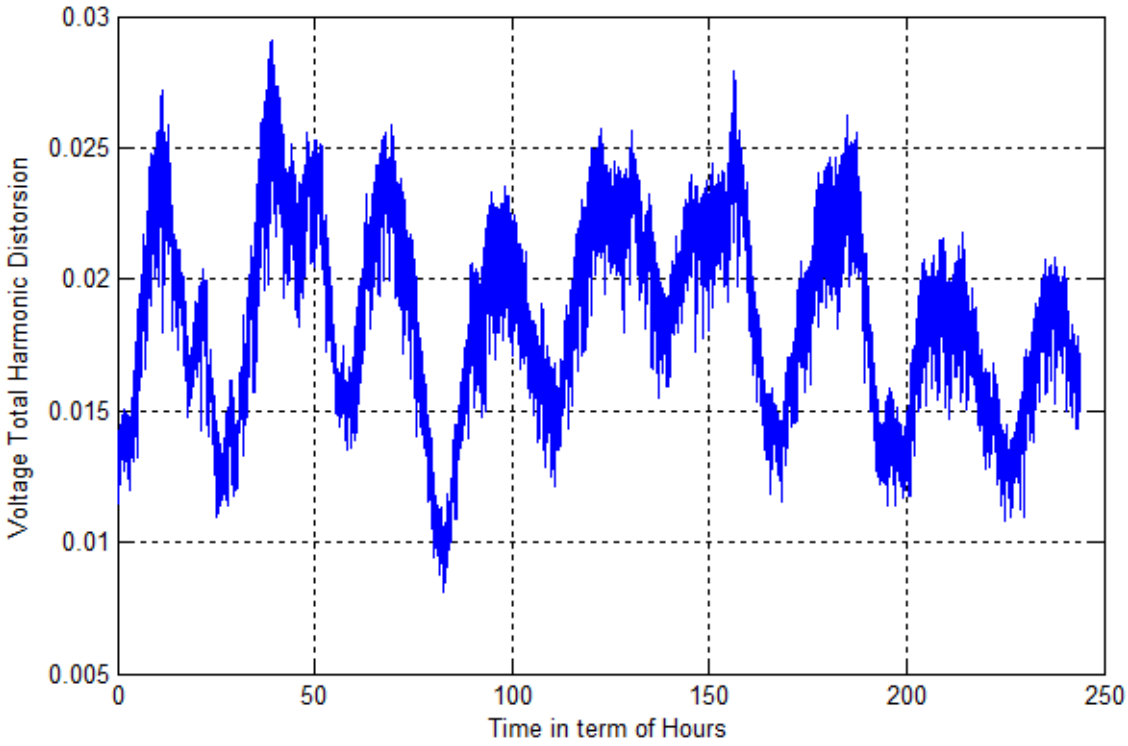

Fig.59 Voltage THD variations v.s. Time

On the other hand, voltages or currents having frequency components that are not integer multiples of the frequency called inter-harmonics. They can appear as discrete frequencies or as a wideband spectrum. The main sources of inter-harmonic waveform distortion are static frequency converters, cycloconverters, induction furnaces, and arcing devices. There is now a better understanding of the origins and effects of inter-harmonic distortion. It is generally the result of frequency conversion and is often not constant, and varies with load. In the motor driven applications, inter-harmonics usually come from VFD drive [49]. In this case, the inter-harmonics could have significant influence on it, because the signature of generalized roughness is broadband signal.

2. Representation of Non-stationary Signals

As we discussed above, the voltage and current signals carrying mechanical anomalies signature are inherently non-stationary, which is a non-property and no unique way to describe it. Since we are aiming at describing non-stationary carrier wave which close to sinusoidal wave, we seek a stochastic representation which preserves as much as possible physical understanding.

In the stationary case, Wold's decomposition [50] uniquely describes any stationary stochastic process as the output of a causal, linear, and time-invariant system excited by strict white noise:

$$Y(t) = \int_{-\infty}^{t} h(t-\tau)X(\tau)d\tau \tag{5.1}$$

Wold's decomposition imposes no other restriction on $X(t)$ than having a flat spectrum almost everywhere. However, for sake of simplicity, we shall also assume that $X(t)$ has a symmetric probability density function. The frequency counterpart of Wold's decomposition is known as Cramer's decomposition, i.e.

$$Y(t) = \int_{-\infty}^{+\infty} e^{j2\pi ft} H(f)dX(\tau) \tag{5.2}$$

where the transfer function $H(f)$ is the Fourier transform of $h(s)$ (s is a dummy variable for time) and $dX(f)$ is the spectral process associated with $X(t)$ i.e.

$$X(t) = \int_{-\infty}^{+\infty} e^{j2\pi ft} dX(\tau) \tag{5.3}$$

In Eq. (5.2), $e^{j2\pi ft} H(f)dX(\tau)$ may be interpreted as the result of filtering $Y(t)$ with an infinitely narrow-band filter centered on frequency f. This representation of a stationary

process has the advantage of being physically meaningful. A natural solution for extending the Wold–Cramer decomposition to non-stationary processes is to make the filter $h(s)$ time-varying. Specifically, let us define $h(t,s)$ the causal impulse response at time t of a system excited by an impulse at time $t-s$, then

$$Y(t) = \int_{-\infty}^{t} h(t, t-\tau) X(\tau) d\tau \tag{5.4}$$

Such a representation has been shown to hold true for any non-stationary process and, most importantly, to be unique under mild regularity conditions of the impulse response $h(t,s)$. Here again, this decomposition is physically meaningful --- $h(t,s)$ has the physical interpretation of a Green's function—and has been intensively discussed in the literature. The frequency counterpart of (5.4) is

$$Y(t) = \int_{-\infty}^{+\infty} e^{j2\pi ft} H(t, f) dX(\tau) \tag{5.5}$$

where $H(t, f)$ is the Fourier transform of the time-varying impulse response $h(t,s)$ and $dX(f)$ is the spectral process associated with $X(t)$. The Fourier decomposition (5.5) evidences an obvious similarity with the stationary case (5.2), except that a non-stationary process is now expressed as a time-varying summation of weighted complex exponentials. In (5.5), the time-varying transfer function $H(t, f)$ may be interpreted as the complex envelope or complex demodulate of process $Y(t)$ at frequency f, i.e. such that $e^{j2\pi ft} H(t, f) dX(\tau)$ is the output at time t of an infinitely narrowband filter centered on frequency f.

The non-stationary carrier wave can be defined through a Cramer-like representation similar to (5.5). This allows for an interpretation of the time-dependent

spectrum as a decomposition of the (time-varying) energy of the process over frequencies. This class of processes, which can be approximated by piecewise stationary processes, rigorously defines the previously heuristic notion of "slowly changing processes".

3. Locally and Piecewise Stationary Process

The input voltage of electric machine is non-stationary in nature, which will mix or even overwhelm the subtle signature in current signal of generalized roughness bearing defect. Fortunately the process is slowly varying in its spectral characteristics, the process can be approximated (in some sense) by a stationary one if the interval is short enough. Dahlhaus [51]) employed so-called locally stationary processes as a tool to model systems where the behavior varies as a function of time.

Definition 1 (Partition) Let $I \subset \mathbb{R}$ be an interval (possibly $\mathbb{R}$). A partition of I is a countable collection of subintervals $\{J_1, J_2, \cdots\}$ where $\{J_k \subset I\}$ is an interval for each $k \in \Theta$, some countable index set, such that

1. $J_i \cap J_k = \varnothing$ (the empty set) for all $i \neq k$ in Θ.
2. $\bigcup_{k \in \Theta} J_k$ (the empty set) for all $i \neq k$ in Θ.

Recall that countable includes finite, thus the index set Θ may be the finite counting set $\Theta = \{1, 2, \cdots, K\}$ for some positive integer K and the partition is $\{J_1, J_2, \cdots, J_K\}$. We will denote a partition of the interval I by P, and we let

$\Im_I$ represent the collection of all possible partitions of the interval I. Thus $P = \{J_1, J_2, \cdots, J_K\} \in \Im_I$ is a specific instantiation of the collection.

Definition 2 (Locally stationary on an interval) Let $I \subset \mathbb{R}$ be an interval (possibly $\mathbb{R}$). A stochastic process $\{ X(t) : t \in I \}$ is said to be locally stationary on I if there exists some partition $P \in \Im_I$, and at least one subinterval $\{J \in P\}$ such that the stochastic process $\{ X(t) : t \in I \}$ is stationary on J.

Definition 3 (Piecewise stationary on an interval) Let $I \subset \mathbb{R}$ be an interval (possibly $\mathbb{R}$). A stochastic process $\{ X(t) : t \in I \}$ is said to be piecewise stationary on I if there exists some partition $P \in \Im_I$ such that on all subintervals $\{J \in P\}$ the stochastic process $\{ X(t) : t \in I \}$ is stationary on J.

This assumption of locally stationarity has led to the popularity of windowed Fourier transforms and spectrograms in the estimation of time-dependent spectra. However, the spectrograms used to estimate the time-varying spectrum have to be adapted to the nature of the stationary interval. It means that the window width for the spectrogram must be adapted to the bound on the length of the stationary interval.

It is clear that together with the assumption of local stationarity, an adaptive approach is required to adjust at each time point t to use only the data from the stationary interval at t. This adaptive approach is so called signal segmentation technique, which is widely used in speech and image processing, EEG signal processing. It can adaptively partition the nonstaionary signal set into locally stationary process, which can be concatenate into a set of piecewise stationary signal for processing.

C. Signal Segmentation Procedure

In the previous section, piecewise locally stationary processes are introduced to represent a slowly changing time-dependent spectrum. So a piecewise locally stationary time series can be partitioned into approximately stationary intervals within which it is close to being a stationary process. This suggests that in estimating the time-dependent spectrum of a non-stationary process, a segmentation procedure that partitions the time series into approximately stationary intervals can be used. The purpose of the segmentation algorithm is to detect changes in the spectra of the process over time and to estimate these change points.

1. Parametric Method

In practice, many stationary processes encountered can be closely approximated by AR models. The AR model can be estimated for a specific time interval within which the signal is approximately stationary. The change of model parameter or some specific indicator extracted from model can be used for signal segmentation to detect the change of signal and the time interval. There are different approaches to detect the changes in non-stationary signals. One useful approach for change detection consists in filtering of the observed data through a known or identified AR filter, and in looking for changes in the residual signal of innovations, $\{\varepsilon_t\}$. Actually, the use of CUSum (Cumulative Sum) [52] techniques based upon the innovations (one-step prediction errors), $\{\varepsilon_t\}$, or the squared innovations, $\{\varepsilon_t^2\}$, is a standard approach for change detection in AR models.

Such a technique, using $\{\varepsilon_t^2\}$ is based upon the fact that, before the change $E\{\varepsilon_t^2\} = \sigma_1$ and thus: $E\{\varepsilon_t^2 / \sigma_1 - 1\}$.

To conclude, statistical whiteness tests can be used to test if the residuals are white noise as they should be if there is no change. The filter residuals are transformed to a distance measure that measures the deviation from the no-change hypothesis. The stopping rule decides whether the deviation is significant or not. The most natural distances are listed below:

• Change in the mean or RMS. The residual itself is used in the stopping rule and $s_t = \varepsilon_t$.

• Change in variance. The squared residual substracted by a known residual variance λ is used and $s_t = \varepsilon_t^2 - \lambda$.

• Change in correlation. The correlation between the residual and past outputs and/or inputs are used and $s_t = \varepsilon_t y_{t-k}$ or $s_t = \varepsilon_t u_{t-k}$ for some k.

For the ESA, the distance measure can employed the quantities which reflect the power quality variation, such as voltage and or current RMS value, imbalance, THD and inter-harmonics.

2. Nonparametric Method

A tree-based adaptive segmented spectrogram algorithm (TASS) is proposed that partitions the data into approximate stationary intervals of possibly varying lengths, depending on the "degree of nonstationarity" in each interval. The procedure described

in this chapter also has the advantage of being truly nonparametric, as it does not rely on any model assumptions.

Initially, a complete tree is grown that recursively halves each segment of the data into very short segments (with possibly overlapping segments). The spectrum in each segment of the tree is estimated and an optimal pruning algorithm used to recombine adjacent segments for which the spectra are the same.

Growing the Complete Tree

The segmentation algorithm outlined here is based on the notion of trees and optimal pruning as is used in Classification and Regression Trees (CART) and as introduced by Coifman [53] to the signal-processing literature. The segmentation draws on the ideas of CART in as much as using a penalized minimization and cross-validation to find the optimal segmentation. However, it avoids the time- intensive part of CART, which is to grow the tree by recursively searching for the best subdivision. In that respect, we follow Coifman and choose to recursively halve the data; that is, grow the complete tree to maximum depth. By avoiding the recursive search procedure of CART's growing algorithm, the algorithm is almost as efficient as the FFT used for estimating spectra of stationary time series. The diagram of tree-based signal segmentation is shown in the Fig.60 and the detail steps are expressed below.

Step 1: Set D = Maximum depth to which tree is grown

Step 2: Set $m = N / 2^{D+1}$ [# Maximum overlap of segments]

Step 3: For $d = 0:D$, divide the data into 2^d block: block(b,d), $b = 0,\cdots,2^d - 1$, each block overlapping the next one over $2m-(23)$ data points; block(b,d) corresponding to node(b,d) of the tree

Step 4: For $d = 0:D, b = 0:(2^d - 1)$, compute an estimate, $\hat{f}_{b,d}(\lambda)$, of the spectrum in block(b,d)

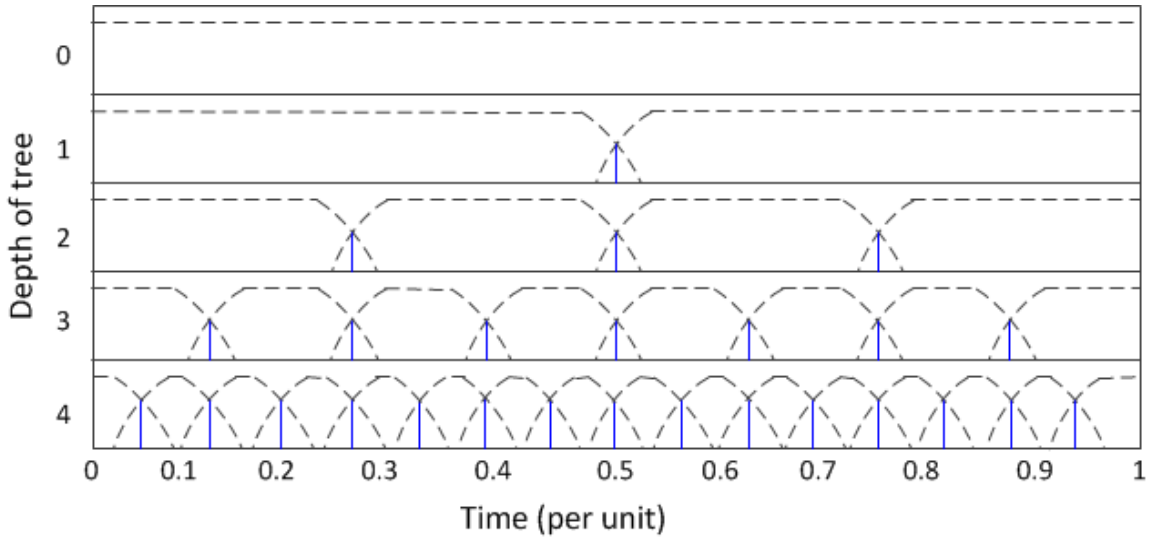

Fig.60 Diagram of tree-based signal segmentation procedure

The local spectral estimates on the segmentation block (b,d) is expressed as:

$$\hat{f}_{b,d}(\lambda) = \frac{1}{N/2^d}\left|\sum_{t\in block(b,d)} w_{b,d}(t) X_t e^{-i2\pi\lambda t}\right|^2$$

$$D_{b,d(d+1)} = 20\log_{10}\left|\frac{\hat{f}_{b,d}(\lambda_s)}{\hat{F}_{b,d}(\lambda_I)} \Big/ \frac{\hat{f}_{b,d+1}(\lambda_s)}{\hat{F}_{b,d+1}(\lambda_I)}\right|$$

$F_{b,d}(\lambda_I) = \int_{\lambda_I} \hat{f}_{b,d}(\lambda) d\lambda$: The spectrum at selected bands

$\hat{f}_{b,d}(\lambda_s)$: The spectrum at fundamental or harmonics

This algorithm is used in the segmentation of locally stationary time series of dyadic length, that is, $N = 2^J$ for some J. It is different from the tree-growing algorithms of CART, which find the best possible subdivision of each data segment by a search procedure that evaluates a splitting criterion at all points in the data segment. If such a search procedure were to be used here, it would necessarily involve estimating the spectra for all possible subdivisions of a data segment.

Optimally Pruning the Tree

For a given segmentation S, a measure of nonstationarity of the segmentation can be computed using

$$\sum_{segment \in S} distance(\hat{f}_{left}, \hat{f}_{right}) \tag{5.6}$$

where $\hat{f}_{left}$ and $\hat{f}_{right}$ are the estimated spectra from the left and right halves of the segment and distance is a measure of discrepancy between the two spectra. This measure as defined by (5.6) quantifies the discrepancy between the given segmentation S and the ideal segmentation, which is a stationary segmentation in which all intervals are stationary or at least approximately so. The modified objective in using the optimal pruning algorithm is used to find the most stationary (dyadic) segmentation with the smallest number of segments S^*, where

$$S^* = \arg\min_{dyadic\_segmentation \in S} \times \sum_{segments \in S} distance(\hat{f}_{left}, \hat{f}_{right}) \tag{5.7}$$

It is clear that restricting the search to dyadic segmentations is equivalent to searching over all subtrees of the complete binary tree. Having estimated the spectra in

each block of the complete binary tree, the optimal pruning algorithm is used to find the best subtree, which gives the best dyadic segmentation.

The optimal pruning algorithm is as follows:

For $d = (D-1):-1:0, b = 0:(2^d - 1)$

Step 5: Compute $R_{b,d} = distance(\hat{f}_{2b,d+1}, \hat{f}_{2b+1,d+1})$, and set value $(b,d) = R_{b,d}$.

Step 6: If $d == D-1$, mark the block(b,d) as terminal. If $d < D-1$, and if value(b,d) < value$(2b,d+1)$ + value$(2b+1,d+1)$, mark the block (b,d) as terminal; otherwise, leave block(b,d) unmarked and set value(b,d) = value$(2b,d+1)$ + value$(2b+1,d+1)$.

After the whole data set is split into piecewise stationary subsets or groups within which all piecewise stationary segments can be considered as approximate stationary. So the rest of work is to process this approximately stationary data within some of subset which have most of data. This kind of selection can make sure the effective use of data and give more reliable result. Actually how this approximate stationary process is close to real one determined by how fine the segmentation we choose. If we choose finer segmentation, i.e. the distance the adjacent leafs is chosen smaller, this approximation is close to real stationary process. But the disadvantage is that less data will be left within the subset. This is harmful to the analysis of the data in subset, and could lead to results with low reliability. So there is always a tradeoff for the segmentation distance.

D. Processing of Approximately Stationary Segments

After the segmentation of slowly changing time-dependent electrical signal, the processing of the segmented approximately piecewise stationary data set can be considered as stationary signal. Because the current signature of generalized roughness bearing defect is nearly stationary, the extraction of it features for analysis and fault detection is much easier with the isolation of influence of nonstationary power input.

The signature of generalized roughness bearing defect is broadband changes in the current spectrum accompanied by the absence of the characteristic fault frequencies. However, the frequency band with the signature is selective and indeterminate [7]. So the specific band pass filter and spectrum analysis can effectively deal with the segmented electrical signal. And the broadband change can be employed to construct indicators for analyzing the generalized roughness bearing defect.

We know that the broadband change in current spectrum can result from both the power quality variation and bearing anomalies. Even though the data are segmented into a group of piecewise stationary subsets, the signals in any subset are still have some nonstationary tolerance comparing with the signal within that subset, which depends on segmentation distance. Statistical technique can be applied to deal with it. We know there is a correlation between the voltage and current spectrum broadband change if the machine is health. A statistical model was built for this correlation under health condition, so the deviation from the model for the future data can be considered as condition of bearing anomalies. This deviation or residual can be applied as the indicator to trend the health condition of bearing.

CHAPTER VI

EXPERIMENTAL PROCEDURE AND RESULTS

In this chapter, first the general diagram of the setup for generalized roughness bearing deterioration and shaft torsional vibration experiment will be illustrated. The fundamental of the existing bearing deterioration experiment will be explained. Its problem of shaft current will be examined and illustrated from three aspects: alternating electromagnetic field between stator and rotor, influence of shaft current induced heat on stiffness of clearance between bearing and bearing housing, vibration dynamics of rolling element bearing with lubricant film. Last an improved experimental procedure is introduced to closely resemble the practical bearing degradation process in the field.

A. Experimental Setup

The basic experimental setup is illustrated in Fig.61, wherein the experiments are performed for torsional effects induced by bearing generalized roughness. Motor terminal quantities are sensed through current/voltage transducers and fed into our customized data acquisition box and vibration signals are measured by NI DAQ device. In Fig.62 two Marathon Electric synchronous machines 281PDL1722 with 8.8Kw rated power, 240V/3 Phase is employed in the test-bed. One is for synchronous motor as primary drive and the other one as synchronous generator loaded by a water heater. The power control circuit is used for producing oscillating torque to excite torsional vibration of shaft assembly.

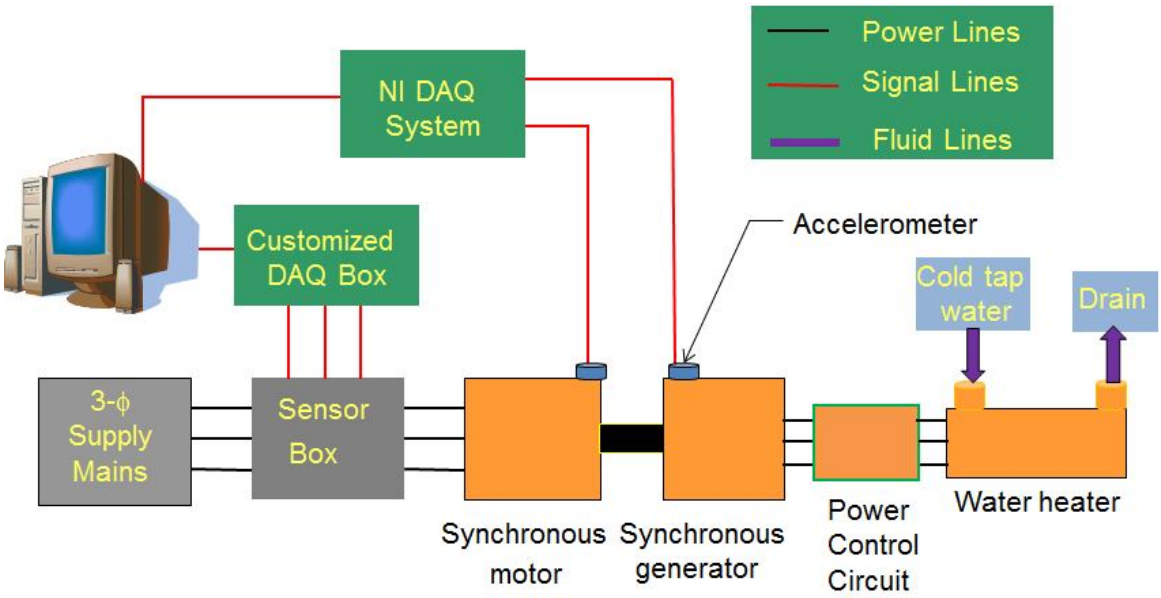

Fig.61 Diagram of experimental setup

Fig.62 Experimental setup snapshot

In the field, generalized roughness bearing defect is recognized as a more practical anomaly than single point defect. To emulate the generalized roughness bearing anomaly and avoid misleading and confusion vibration and electric signature induced from the offline removing and reinstalling the same bearing, an in-situ bearing deterioration method by using shaft current is introduced in [31]. The general diagram for its implementation is shown in the Fig.63.

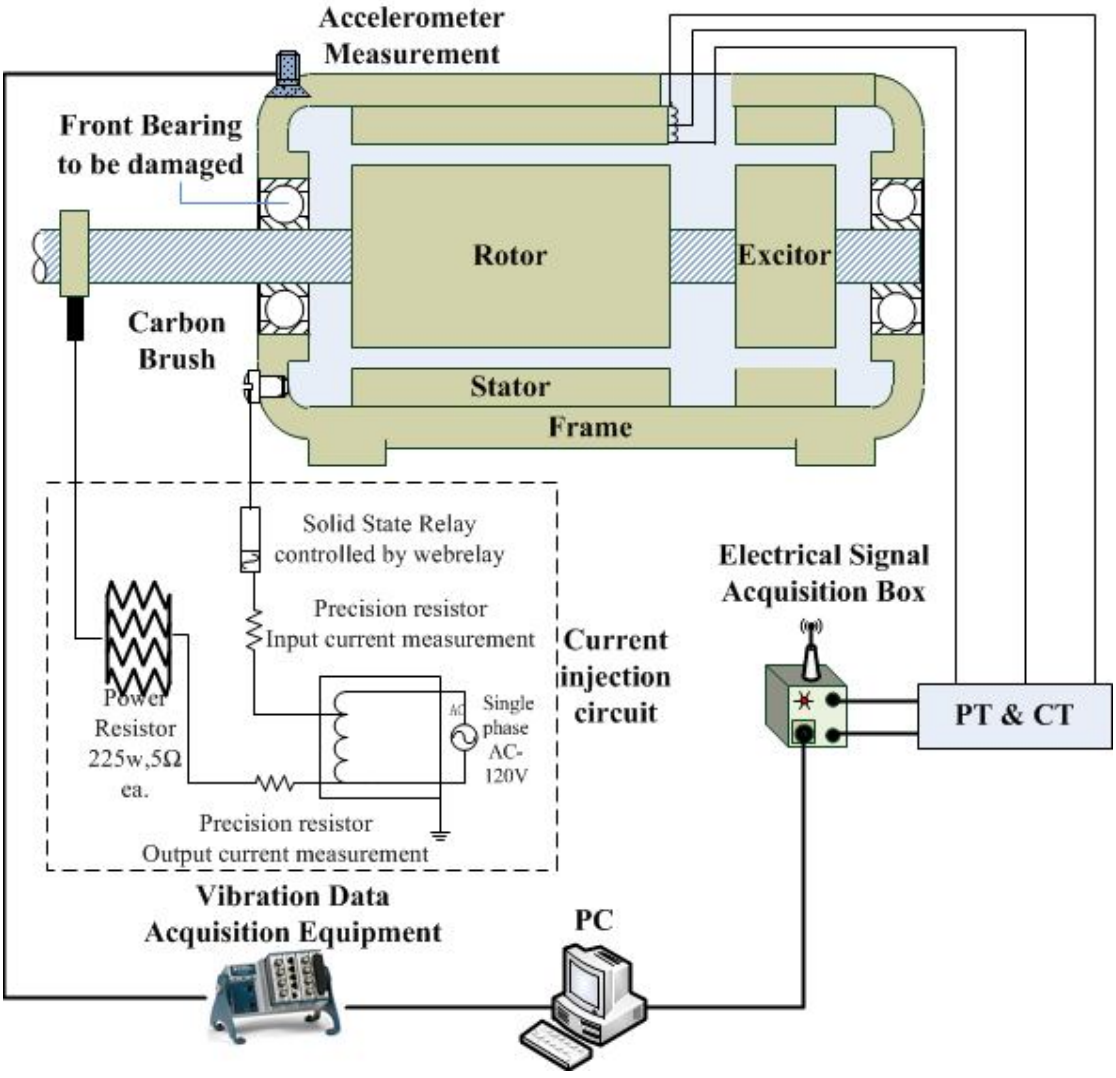

Fig.63 In-suite bearing deterioration setup by shaft current

In this setup, an external voltage source is applied to the shaft of the motor via a carbon brush. Because of convenience and availability, a single-phase, 120V 60Hz AC power adjusted by transformer is used for providing controllable shaft voltage. By replacing the NDE bearing with a ceramic one, a current will flow from the shaft through the drive end bearing, and return to the power negative from the stator frame. An aluminum disk is mounted on the shaft to provide a smooth contact surface for the brush.

1. Vibration Signal Acquisition for Benchmark

The vibration data acquisition system is used as a benchmark to control the process of experiment. This accelerometer is capable of measuring -50G to +50G with the sensitivity of 100mV/G from 0.2Hz up to 5000Hz. NI USB-9234 is ideal for a wide variety of portable applications such as industrial machine condition monitoring and in-vehicle noise, vibration, and harshness testing. It is a USB-based four-channel C Series dynamic signal acquisition module for making high-accuracy audio frequency measurements from sensors. The NI cDAQ-9174 is a four-slot NI Compact DAQ chassis designed for small, portable, mixed-measurement test systems. By plugging the USB-9234 module with cDAQ-9174, a custom digital I/O measurement system is shown in Fig.64. A Virtual Instrument (VI) program that runs under the NI LabView on PC saves the experimental measurements into data files.

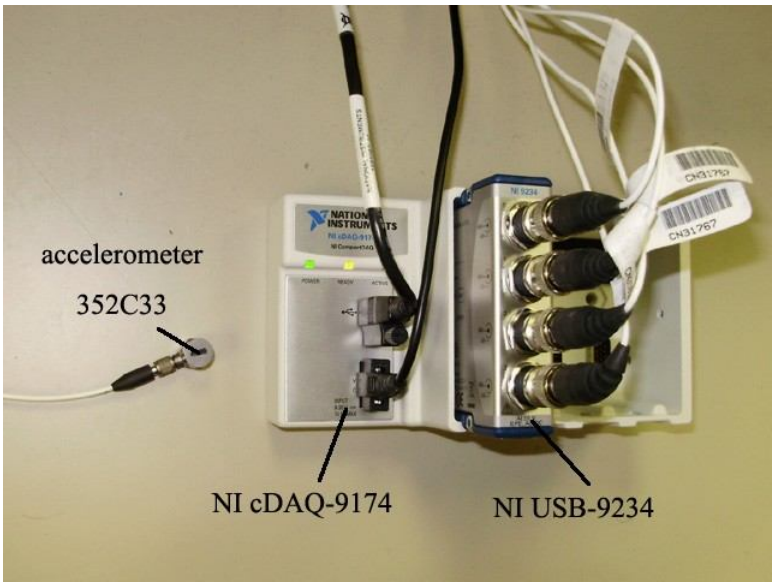

Fig.64 Vibration signal data acquisition system

2. Electrical Data Acquisition for ESA

In electric data acquisition system which is shown in Fig.65, the motor line voltages and phase currents are measured by using potential transducers (PT) and current transducers (CT), respectively. The AD73360 is a six-input channel analog front-end processor. It is particularly suitable for industrial power metering as each channel samples synchronously. With this one can sample 3 channels voltage signals and 3 channels current signals. Sampling rate is set at 8 kHz. A serial port allows easy interfacing of single or cascaded devices to industry standard DSP engines. The endpoint software is built around the Analog Devices VDK kernel. This is a multi-threaded kernel that provides the necessary support for the Ethernet interface. This support comes in the

form of driver software and a TCP/IP stack. The data transfer algorithm is based on win socket programming.

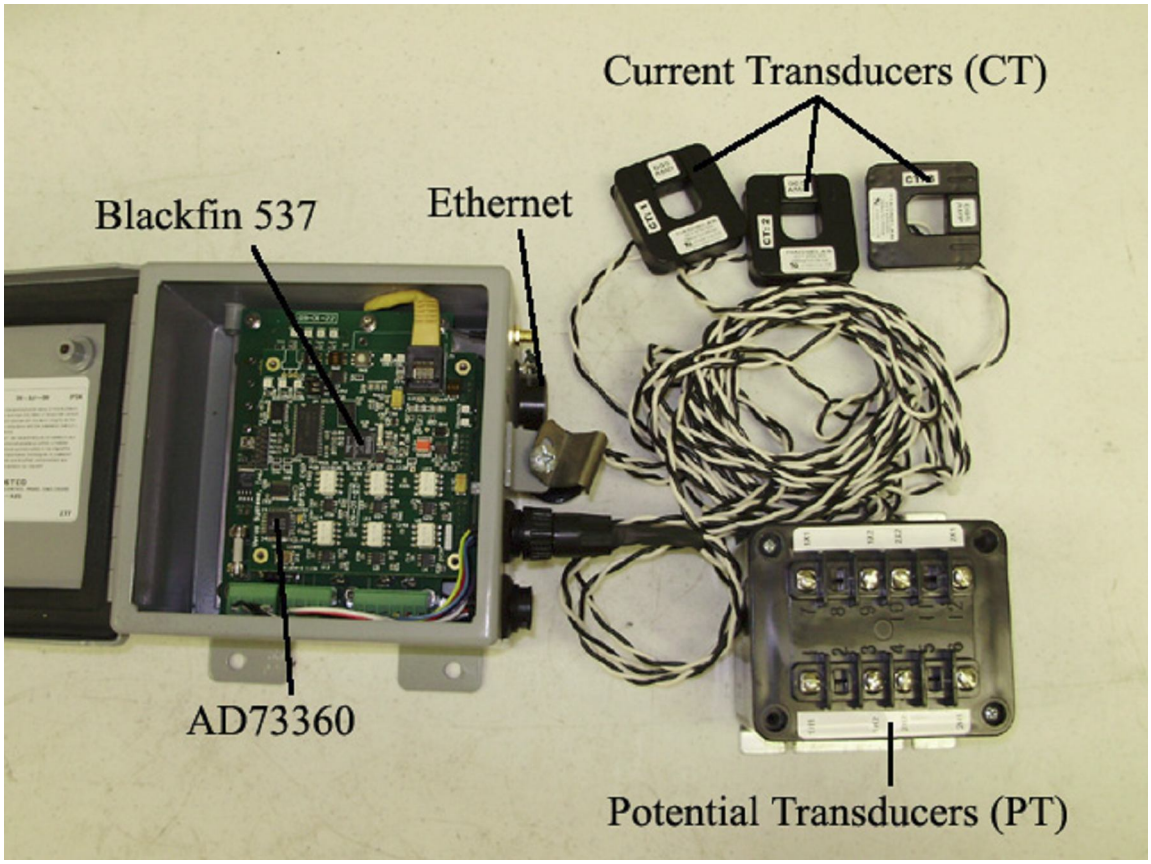

Fig.65 Electric signal data acquisition system

B. Explanation of In-situ Bearing Deterioration Experiment

The mechanism of accelerated bearing deterioration experiment conducted here is the so call Electric Discharge Machining (EDM). For EDM damage to occur, the rolling element must be separated from the raceways by a thin film of lubricant. When the current across the bearing exceeds the dielectric strength of the grease, EDM could

make the lubricant film ineffective, and pits could be etched on raceways and rolling elements.

Research indicates that a healthy bearing will possess a film of lubrication ranging from 0.2 μm to 2.0 μm thick at normal operating speeds. Given this thickness of lubrication, EDM currents can be caused by 60Hz shaft voltage as low as 0.2V to 2V peak [31]. Another study suggests that it is not the magnitude of the EDM current but the current density within the bearing that directly determines the rate of failure [54].

The factors affect the life expectancy of bearing under experiment consist of the amount of grease, the size of bearing, rotor speed, load level and the magnitude of shaft current. The amount of grease is measured in term of percentage of free space in bearing. The less grease packaged, the faster the bearing damage, but if the grease is too less, the EDM maybe exist. But two much grease will make the deterioration process longer. So the bearing is usually degreased to 3-5% of total free space and repackaged (The factory fill of grease of new bearing is about 25% of total free space). So the bearing will deteriorate faster. The bigger the bearing size, the longer the deterioration process. If the shaft current magnitude grows, the EDM will be more significant, and the life expectancy of bearing will be shorter. According to our experience, the higher rotor speed and load level will speed up the EDM and make the bearing fail faster. The load level is measured by percentage of rated load. The bearing reaction force will rise as the load level increases, and the probability of direct contact of the rolling bearing metallic surfaces also increases. In [31], research shows that the amount of grease and current magnitude is the most significant factor affects the life expectancy of bearing.

C. Influence of Shaft Current on the Rotordynamics of Machine

The intent to introduce the in-suit bearing deterioration approach by shaft current is to avoid the influence of offline removing and reinstalling the same bearing. The observation from experiment, however, shows that the applied shaft current across the machine bearing impacts the vibration signal. Fig.66 illustrates the trend of vibration indicator for 160 consecutive data sets which are acquired in 160mins. We can tell that the shaft current across the bearing will increase the vibration RMS value after it was applied. The vibration indicator will drop to original level after it was removed 40mins late. Actually the bearing heath condition cannot get worse during 40mins of current injection.

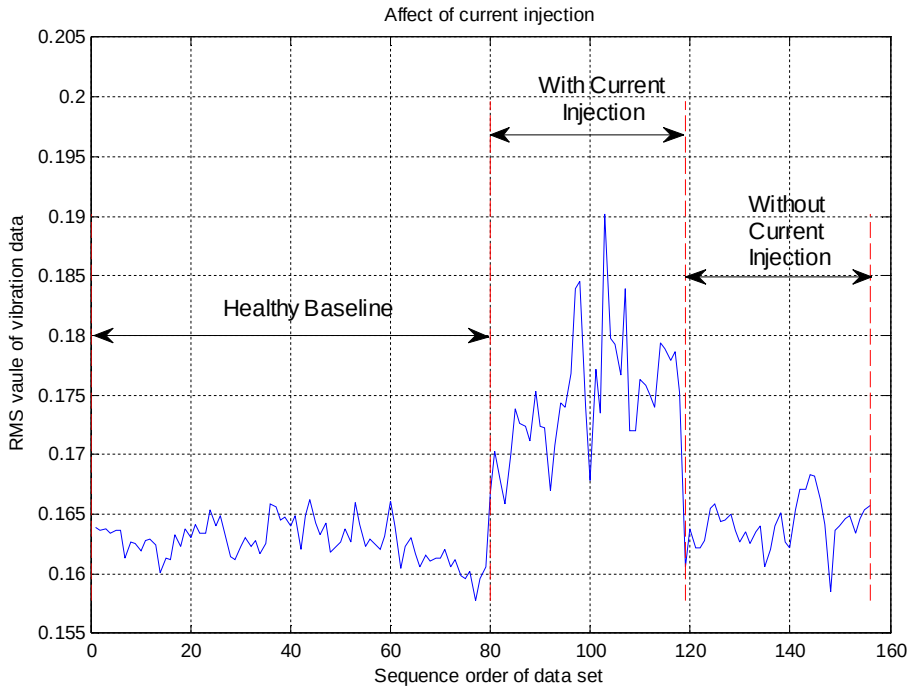

Fig.66 Influence of shaft current on vibration trend

The shaft current is the only external variable which could affect the vibration indicator. For electrical signal monitoring, the bearing anomaly signature is subtle, even a little noise induce from the shaft current could conceal the anomaly signature and give rise to misleading results. The researches produced in-situ bearing defect by an externally applied shaft current, and acquired data during the whole deterioration process. The shaft current, however, could affect the rotordynamics of machine under test in three ways: (a) Induce asymmetrical magnetic flux distribution in air-gap and UMP on rotor, change the excitation of rotor-bearing system; (b) Alter the rotordynamic coefficients (contact stiffness and damping) of rotor-bearing system due to thermal effect induced by shaft current; (c) Cause rotor shaft bending and rotor-stator rubbing due to the cumulative heat build-up produced by shaft current. Details of them will be covered below.

1. Unbalanced Magnetic Pull (UMP) Induced by Shaft Current

Fig.67 depicts the capacitive coupling model for the induction motor. The stator winding to frame capacitance (C_{sf}) is a distributed element representing the capacitive coupling to frame along the length of the stator conductors. For most investigations, magnetic coupling of the stator and rotor is sufficient. But with the high dv/dt present with modern power devices, capacitive coupling considerations cannot be ignored. Therefore, the stator to rotor capacitance (C_{sr}) and the rotor to frame capacitance (C_{rf}) are included.

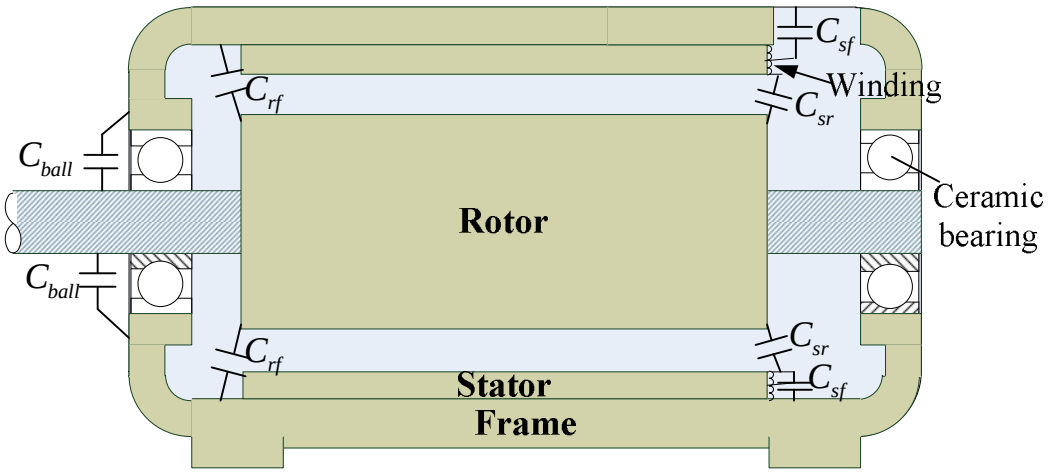

Fig.67 Capacitive coupling model of induction motor under shaft current

The equivalent circuit of the above coupling model is presented in Fig.68, which shows the capacitor coupling path from the stator neutral to ground modulation source through the end windings and stator slot openings, through the air gap to the rotor shaft, down through the inner bearing race, ball bearing, oil film, and out to the bearing outer ring to frame ground. The shaft current across the bearing could build a voltage potential between rotor and stator frame. So the air-gap between rotor and stator frame acts like a capacitor that periodically charges and discharges in the frequency of the shaft voltage.

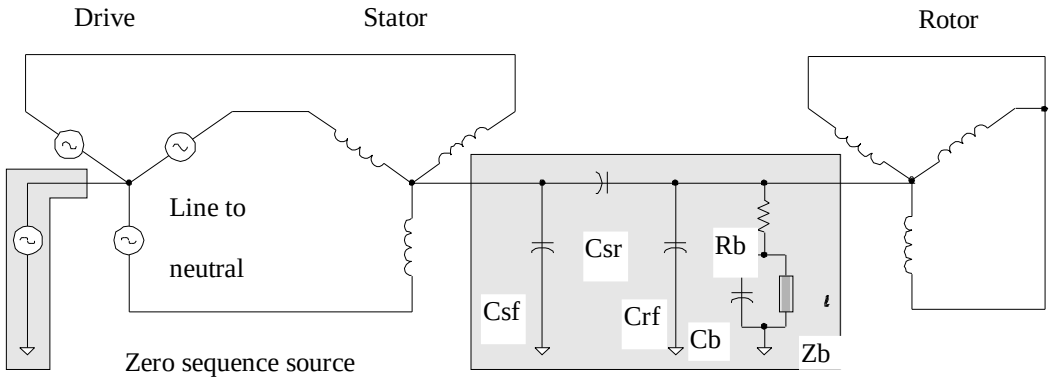

Fig.68 Capacitive coupling mechanisms for shaft voltages

This established alternating AC electric field between rotor and stator frame which could affect the magnetic field distribution [6] and induce UMP on rotor. Thus we can find that the vibration increases a little than it previous stage just after the shaft current was applied, as illustrated from the observation in our experiment.

Moreover, the stator current signal could also be affected by the electromagnetic coupling below due to flux Φ variation induced by shaft current.

$$V_s(t) = R_s I_s(t) + \frac{d\Phi(t)}{dt} \tag{6.1}$$

The research [3] analyzes the generalized roughness bearing anomaly by trending the change of electrical indicator. The trend change is not significant as the load increase because the electrical signal acquired is influenced by the shaft current during the bearing deterioration process, together with the power quality variation and machine manufacturing imperfections [7] and the interaction of both. The influence of these disturbances becomes much more significant when the load reach to full load condition.

2. Thermal Effect of Shaft Current on Rotordynamic Coefficients

In the rotor-bearing system, bearing have an excessive impact on the rotordynamics of the system. For rolling element bearing, there are several major factors could affect its stiffness and damping coefficients. In [8, 9], M. Sarangi investigated the influences of speed, load capacity, lubricant viscosity, surface roughness on the damping and stiffness of lubricated ball bearing. The influence of clearance on ball bearing dynamic stiffness is studied in [10].

To better understand the influence of thermal effect on rotordynamic coefficients, the illustration of asperity contact and lubrication regimes between rough surfaces are necessary, and shown in the Fig.69.

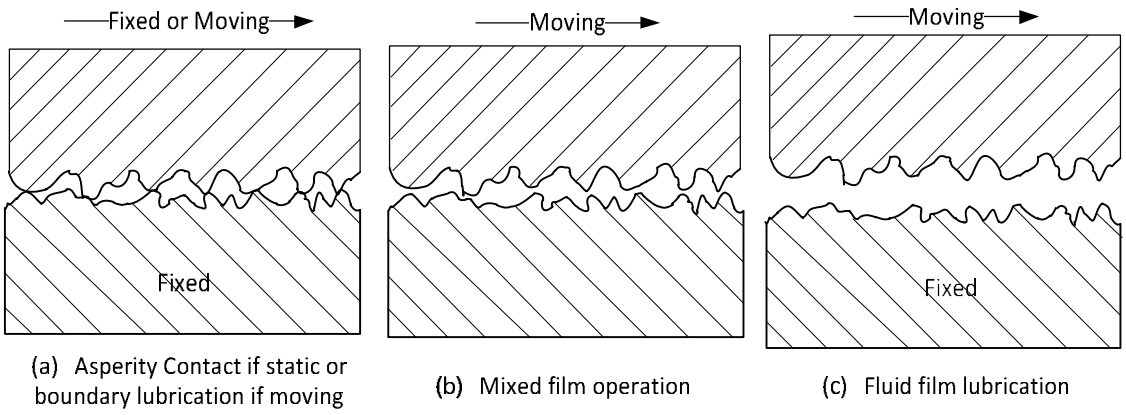

Fig.69 Schemes of asperity contact and lubrication regimes between rough surfaces

The Fig.69(a) illustrates the asperity contact or boundary lubricant depends on whether there is relative motion between the rough surfaces. In mixed film and boundary lubrication, the oil film is too thin to separate the rough metallic surfaces as shown in Fig.69 (a) and (b). Under full film lubrication conditions, no contact takes place between the rough metallic surfaces as illustrated in Fig.69(c). When the surfaces run together under thin film conditions, the lubricant is only capable of carrying part of the load, while the remainder is carried by contact between the two surfaces asperities. So the effective stiffness is the resultant of lubricant film and asperity contact. While in the other two case, the effective stiffness depends on either lubricant film or asperity contact. In practice, the contact of rolling element bearing usually falls into the mix lubrication case. Any factor affecting the clearance and lubricant property between rough surfaces could affect the effective stiffness and then rotordynmics of its.

Thermal Effect on Bearing Stiffness

Bearing manufacturers usually provide recommendations for bearing housing and shaft fits. In general, the rotating inner ring should have an interference fit on the shaft, and there should be a slight clearance in between the non-rotating outer ring and the housing. Ideally, the fit with a clearance should be as loose as possible without sacrificing vibration performance. The clearance between bearing outer ring and bearing housing is justified for easy assembly and vibration isolation.

The fit between bearing outer ring and housing can be considered as asperity contact. The effective stiffness of the fit depends on how they are assembled, and the clearance between the outer ring and housing. Because the asperity on the rough surfaces is irregular and random, the fit between outer ring and housing cannot be exactly the same for each disassembly and reassembly. So the effective stiffness will be different. This is why the offline approach to make bearing fail by the act to disassemble, reassemble and remount the bearing will change the vibration and current signature of the machine health condition. Unfortunately the explanation was not provided in [1].

The thermal effect induced by shaft current could affect the clearance of bearing or between bearing and housing. The shaft current across the bearing could induce heat and build up a temperature field. The temperature gradient is pointing outward from shaft to bearing housing. So the temperature build up more in the shaft than inner ring, more in the inner ring than outer ring and more in the outer ring than housing. The part will expand more at where the temperature is higher, thus the bearing clearance and clearance between outer ring and housing will decrease due to the thermal effect.

The rolling element bearing can be modeled as spring elements shown in the Fig.70. The decreasing clearance between outer ring and housing will increases the contact stiffness because more asperities are made contact between rough surfaces. Furthermore the clearance reduction in bearing will make the lubricant film between race and roller thinner, so the effective stiffness of the race-ball contact will increase.

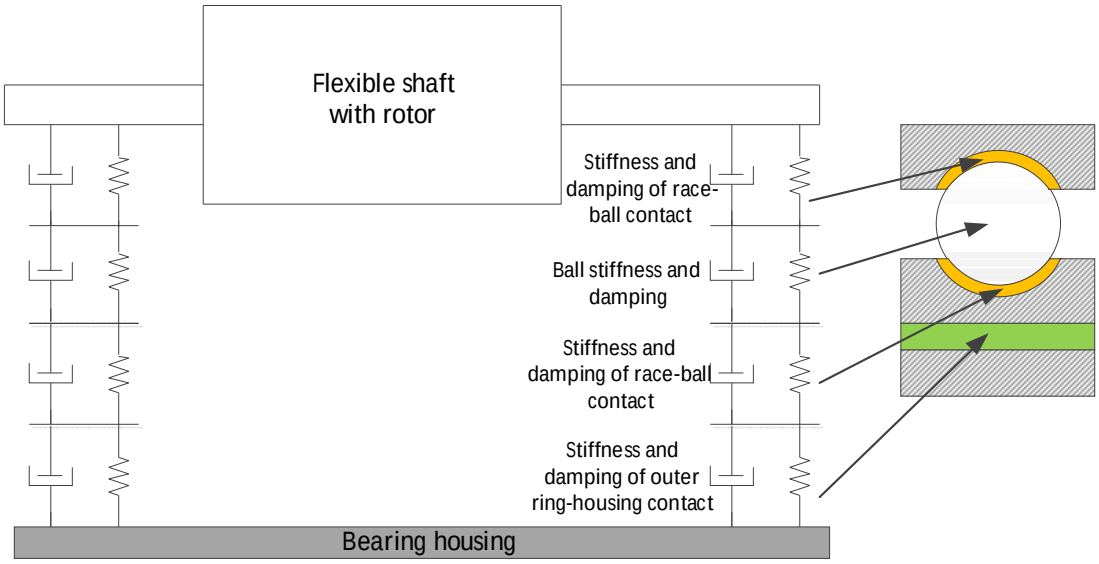

Fig.70 Simplified model for ball bearing of rotating machine

Recall the lateral vibration model of rotor-bearing system, considering that we just investigate the bounce or translation mode, so gyroscopic effect can be ignored. The model can be expressed in (6.2).

$$[M_T]\{\ddot{q}(t)\}+[C_T]\{q(t)\}+[K_T]\{q\}=\{f(t)\} \tag{6.2}$$

where $\{q\}=\{x,y,\theta,\varphi\}$, x,y denote translational movements of the rotor center of mass, θ,φ are the tilting angle along y and x axis. By assuming proportional damping, the system can be decoupled to four 1DOF problems. Just pick up the motion along x axis.

By substituting phasor quantities, give us the following equation

$$kX - cj\omega X + m\omega^2 X = F \tag{6.3}$$

$$X = \frac{F}{k - m\omega^2 + cj\omega} = \frac{F/k}{1 - \frac{\omega^2}{\omega_n^2} + 2j\zeta\frac{\omega}{\omega_n}} \tag{6.4}$$

where $\zeta = \frac{c}{2\sqrt{mk}}$ is the damping ratio.

Hence $$|X| = \frac{F}{k}\frac{1}{\sqrt{(1-\frac{\omega^2}{\omega_n^2})^2 + 4\zeta^2\frac{\omega^2}{\omega_n^2}}} \tag{6.5}$$

The transmitted force is the resultant of kX and the damping force $c\omega X$, its amplitude is

$$|F_T| = |X|\sqrt{k^2 + (c\omega)^2} \tag{6.6}$$

The transmissibility, i.e. the ratio of transmitted force amplitude to applied force amplitude, can be expressed as

$$Transmissibility = \left|\frac{F_T}{F}\right| = \sqrt{1 + 4\zeta^2\frac{\omega^2}{\omega_n^2}} \Big/ \sqrt{(1-\frac{\omega^2}{\omega_n^2})^2 + 4\zeta^2\frac{\omega^2}{\omega_n^2}} \tag{6.7}$$

The transmissibility can be shown as function of damping ratio ζ and frequency ratio ω/ω_n in Fig.71. The rise in contact stiffness could increase the natural frequency of rotor system, so that the vibration transmissibility will increase under the same operation speed and load (Note: the ratio ω/ω_n is generally between $2.5\sim5 > \sqrt{2}$ for transmissibility reduction). So we can observe that the vibration increase as the current applied on the shaft and cross the bearing.

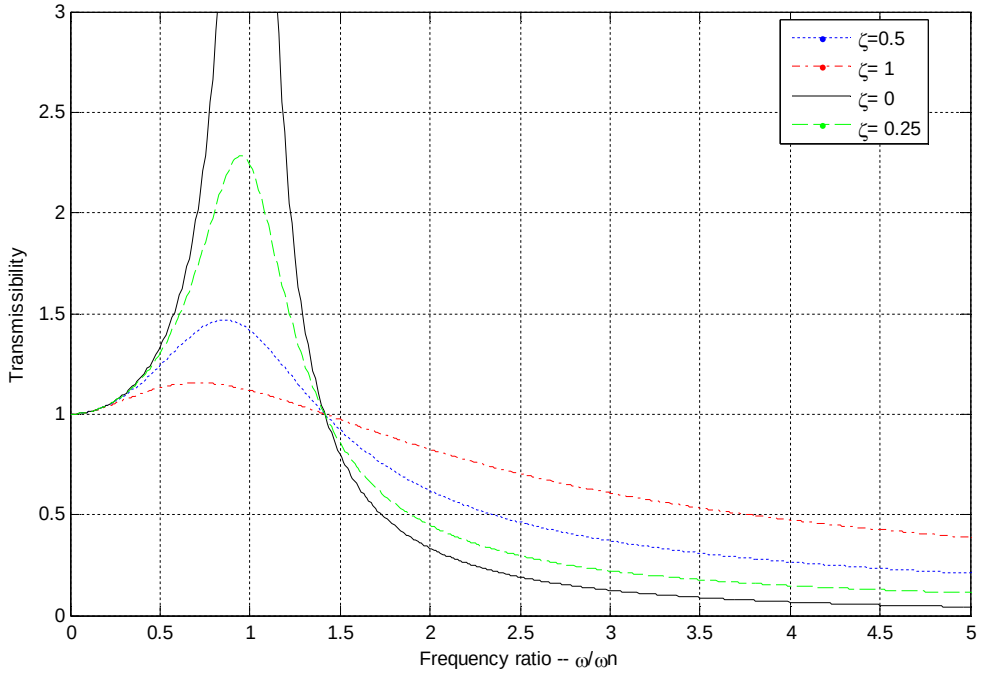

Fig.71 Vibration transmissibility v.s. frequency ratio

Thermal Effect on Lubricant Viscosity

Not only the thermal effects could affect the contact stiffness of the bearing support, but also affects the viscosity of lubricant, which is critical parameter to determine the ball bearing damping. Some researches [11] investigated the influence of lubricant viscosity on the rolling element bearing damping. As shown in Fig.71, the damping could also affect the vibration transmissibility of bearing. The temperature increase will reduce the lubricant viscosity or its damping, and increase the vibration level of rotor-bearing system.

One of the causes in vibration level variation with the change in lubricant viscosity can be correlated with the behavior of the lubricant film thickness of the lubrication conditions. The values corresponding to the minimum film thickness between

the inner race and the roller represents the most critical tribological contact in the rolling element bearing. In the R.Serrato's research [12], gradual decrease in film thickness can be observed along the test time as temperature increase. So the rolling element and race could lead to mixed film operation and even boundary lubrication condition. The reduction in film thickness could increase the probability of direct contact of the rolling bearing metallic surfaces. During such a contact, small impacts among surface irregularities can excite natural frequencies of the bearing elements, increasing vibration level, specifically that of the high frequency band. Moreover the direct contact with higher probability means more asperity contact, which will produce more friction and heat. The extra heat will in return decrease the lubricant viscosity further. This could form a vicious cycle and expedite the bearing deterioration process in nonlinear pattern.

In the bearing deterioration experiment, the shaft current applied is around 20-30 A (60Hz), which could induce extra temperature buildup than normal operation. The decrease in the lubricant damping could cause the vibration increase. This can be justified by the observation of vibration RMS value change in Fig.66.

3. Thermal Induced Rotor Shaft Bow

Another influence of thermal accumulation induced by shaft current is the shaft wrap or "bow". Sustained heat induced by shaft current could continue to build up temperature and soft the rotor shaft, and make the shaft bow. The bowed shaft will induce air-gap eccentricity and UMP, together with increased the unbalance response. The resultant effect is to drive the rotor bend more to the minimum air-gap length

direction until the rotor rubs with stator core. The rotor-to-stator rubbing will cause electrical insulation degradation of stator/rotor core or stator/rotor winding. In addition, the rotor-to-stator rubbing may generate sufficient heat to cause thermal aging of the stator winding insulation and a consequent ground fault.

Actually we observed this kind of anomaly in a bearing deterioration experiment. The shaft current around 30A is applied to finish the final stage bearing deterioration. The induction motor under test experienced a continuous increase in vibration amplitude at some time, and last until the rising stator current trigger the fuse protection. During the last 30~60sec before it trigger the fuse protection, we can find that the induction motor experienced almost doubled stator current.

However, it is surprising that we succeed in restart and operate the machine about 10 hours after the motor shut down. It hints us that the possible causes could be related to influence of thermal effects of shaft current. The thermal effect usually induces the rotor to bow, and rotor bow results in an imbalance condition with all its usual symptoms. It can usually be manifested by the fact that it goes away when the motor is cooled down.

After disassemble the machine, we find the inner race of drive end bearing almost melted with the shaft so that it cannot be disassembled by our manual bearing puller. Finally it was removed by a hydraulic puller from a local machine shop. After examination on this bearing, it can be found that the original silver metal color already darken totally on the fit surface of the inner ring, as shown in Fig.72. It shows that shaft experienced an extremely high temperature during the long-time current injection and

galling occurred between shaft and inner ring. The mechanism behind is that asperities may penetrate the opposing contact surface, and initiate friction or plastic deformation, which induces pressure and energy in a small area or volume called the contact zone. The thermal effect will increase the interference between shaft and inner ring, elevate pressure, energy density and heat level within the deformed volume. This leads to greater adhesion between the surfaces which initiate material transfer and galling, and made this interference fit tighter and harder to be disassembled. The high temperature experienced made the metal color dark, it is an irreversible process even cool down.

Fig.72 Galling between bearing and shaft under shaft current injection

D. An Improved Experimental Procedure

As explained before, the injected current could have two influences on the ESA of bearing anomaly. First it could affect the magnetic field distribution and stator current during the bearing deterioration. The other is that the induced thermal effect could impact the rotordyamics of bearing-rotor system. So the reliability of ESA of generalized

roughness bearing anomaly will suffer if the above influences of injected current cannot be removed for the data analyzed.

To counter this problem, an improved experimental procedure will be introduced. It consists of healthy and several different faulty baseline stages with increasing severity. In-between are the deterioration stages with current injection. Data are acquired for all the stages, but only health and faulty baselines are analyzed for health condition trend analysis. Actually the improved experimental procedure can closely resemble the degradation of rolling element bearing in the field, but alos help us to identify how effective the algorithm is, i.e. whether the approach can detect the anomaly at it earlier deterioration stage.

This experimental procedure is used to successfully generate online fault in the driven end bearing type-6208 of induction motor under full load condition. Vibration and electrical signal are measured simultaneously. The vibration signal was acquired by an accelerometer with band width 0–20 kHz. The intent of the wide bandwidth for accelerometer is to include vibration at higher frequency range, which can carry the characteristic signature during incipient bearing defect. The measurement meets the ISO 10816 machine vibration standard.

E. Experimental Results

The results of ESA of generalized roughness bearing anomaly based on signal segmentation of the experiments are presented in this chapter. To justify the effectiveness of the proposed approach, the electrical signals are analyzed under cases

with and without segmentation, together with analysis of vibration signal. The proposed approach is also applied to the bearing anomalies under different load levels, which could show how different load levels affect the ESA of the bearing anomaly.

1. Vibration and Electrical Signature of Bearing Defect

The nature of generalized roughness bearing defect is broadband increase in both the vibration and current spectrums. The Fig.73 and Fig.74 show the vibration and current spectrum comparison between health and the final faulty baseline for the same test bearing. The result shows that the current spectrum of the failed bearing has broadband increase, but it is less significant than that in vibration spectrum.

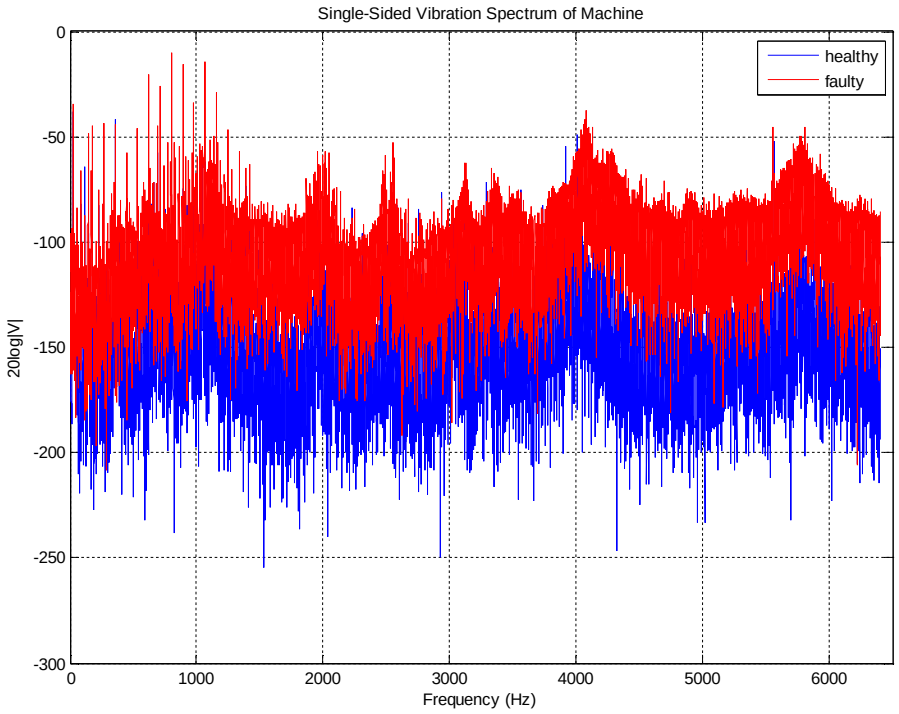

Fig.73 Vibration spectrum for bearing at health and failed condition

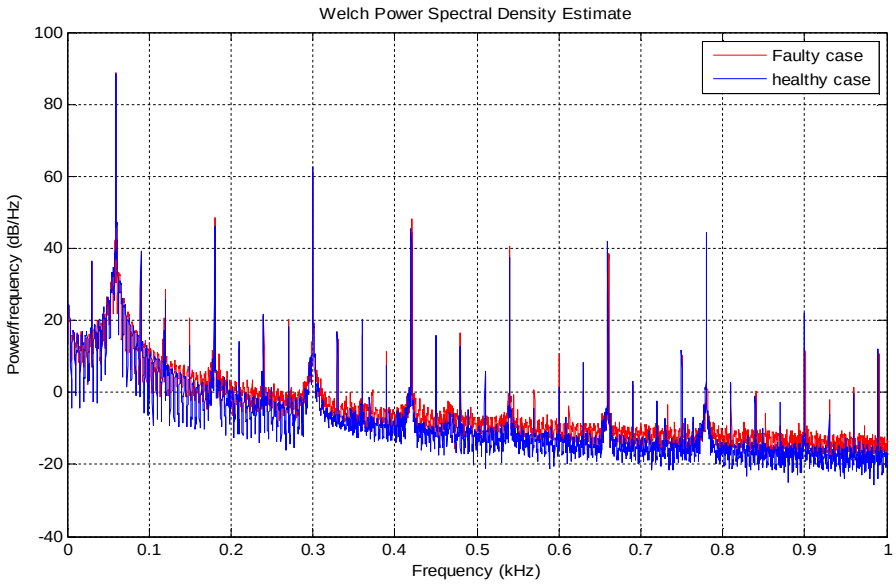

Fig.74 Current spectrum for bearing at health and failed condition

2. Vibration Indicator Trend Analysis

There is no need to segment the vibration signal because it is enough sensitive to the health condition change of bearing. The indicator for vibration signal is chosen as RMS value, the trend of vibration RMS is shown in Fig.75, which illustrates the increase in vibration versus samples in time sequence for the machine under test. Each data sample contains 60 sec of data. So the horizontal axis can also be considered as time frame. This figure represents the transition of health condition of this specific bearing during its operational lifetime. It tell us the vibration will goes up as the bearing deteriorates, and the vibration during the current injection rises up more than the bearing deterioration itself can justify. The extra increase of vibration results from the influence

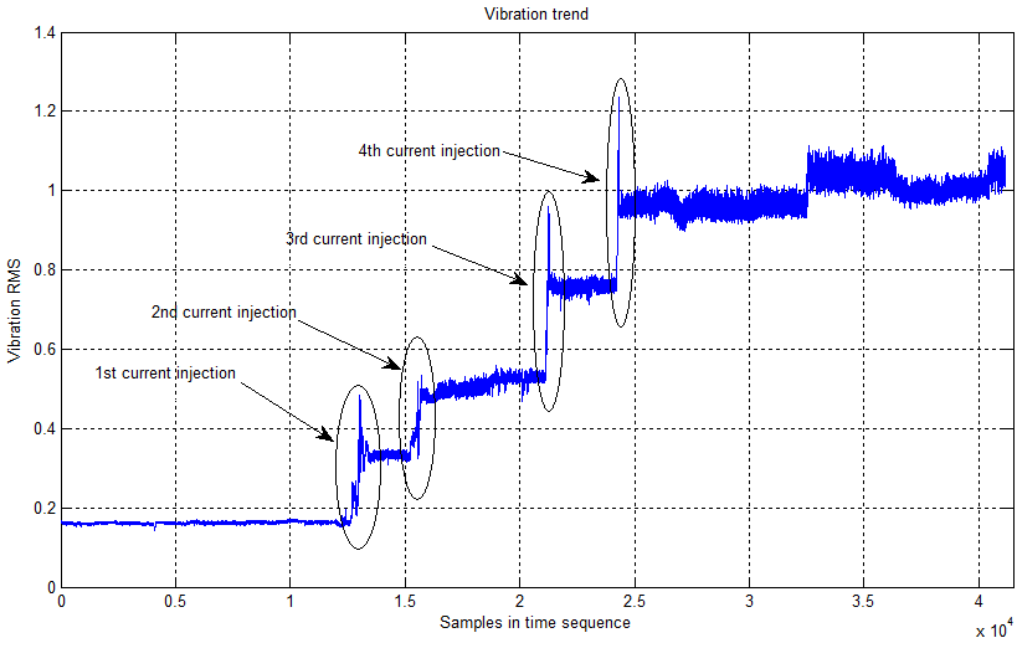

Fig.75 Trend of vibration indicator under full load

of shaft current on the rotordynamics of machine. This can be better illustrated from the zoom in view of the four stages of current injection as shown in Fig.76.

From the comparison among them, the duration for each stage of current injection are about 1000 samples (16.6 hours), 450 samples (7.5 hours), 150 samples (150 min) and 90 samples (90 min) respectively. The vibration RMS increments of each fault baselines relative to healthy baseline are listed in the Tab.6. It shows that the bearing will deteriorate faster as its health condition get worse and worse in nonlinear pattern. As the shaft current was removed, the thermal effect and its influence on the rotordynamic of machine will decline gradually as temperature drops. It is seen from figure 6.16 that the vibration indicator will drop to the value that reflects the next fault baseline. This phenomenon is more significant in the 3rd and 4th stage of fault baseline,

because the temperature gradient build up higher when the bearing health condition getting worse. The experiment result validates the analytical analysis above.

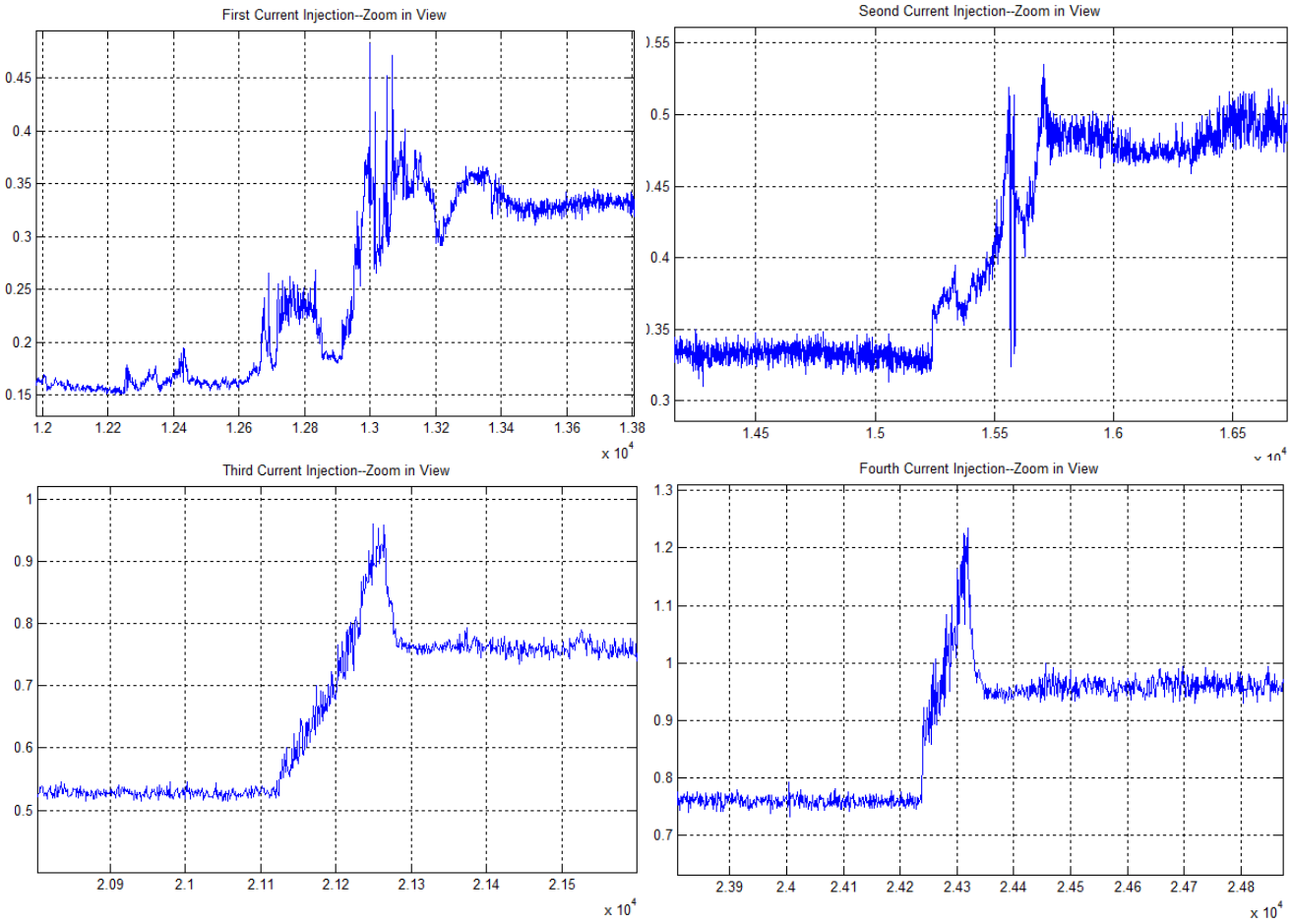

Fig.76 Zoom in view of vibration indicator during current injection

Tab.6 Vibration increment as health condition change

	1st baseline	2nd baseline	3rd baseline	4th baseline
Deterioration duration from prev. to	1000 min	450 min	150 min	90 min
Change from healthy baseline	125%	228%	375%	497%
Change from previous baseline	125%	54.4%	44.8%	25.7%

3. Electrical Indicator Trend Analysis

To analyze the bearing anomaly, we employ model-based method to trend the health condition change. The broadband change in current spectrum can result from both the power quality variation and bearing anomalies. Even though the data are segmented into a group of piecewise stationary subsets, the signals in any subset are still have some varying tolerance comparing with the signal within that subset. There is a correlation between the voltage and current spectrum broadband change. A statistical model was built for this correlation under health condition, so the deviation from the model for the future data can be considered as condition of bearing anomalies. This deviation or residual can be applied as the indicator to trend the health condition of bearing. The Fig.77 presents the trend of electrical indicator of bearing anomalies under full load.

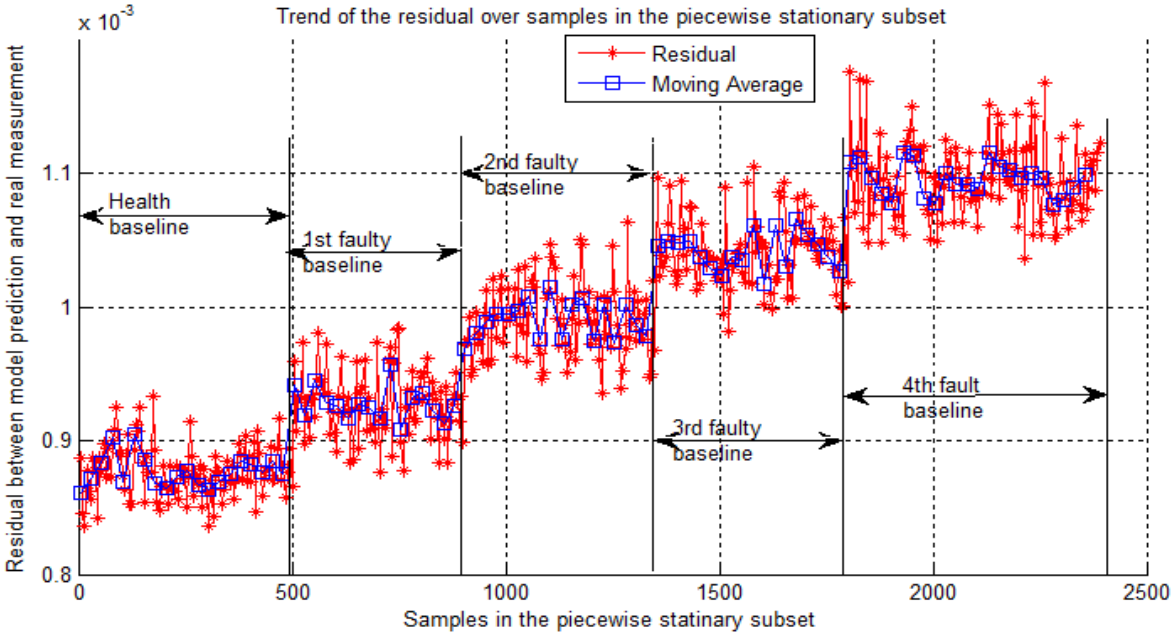

Fig.77 Trend of electrical indicator under full load

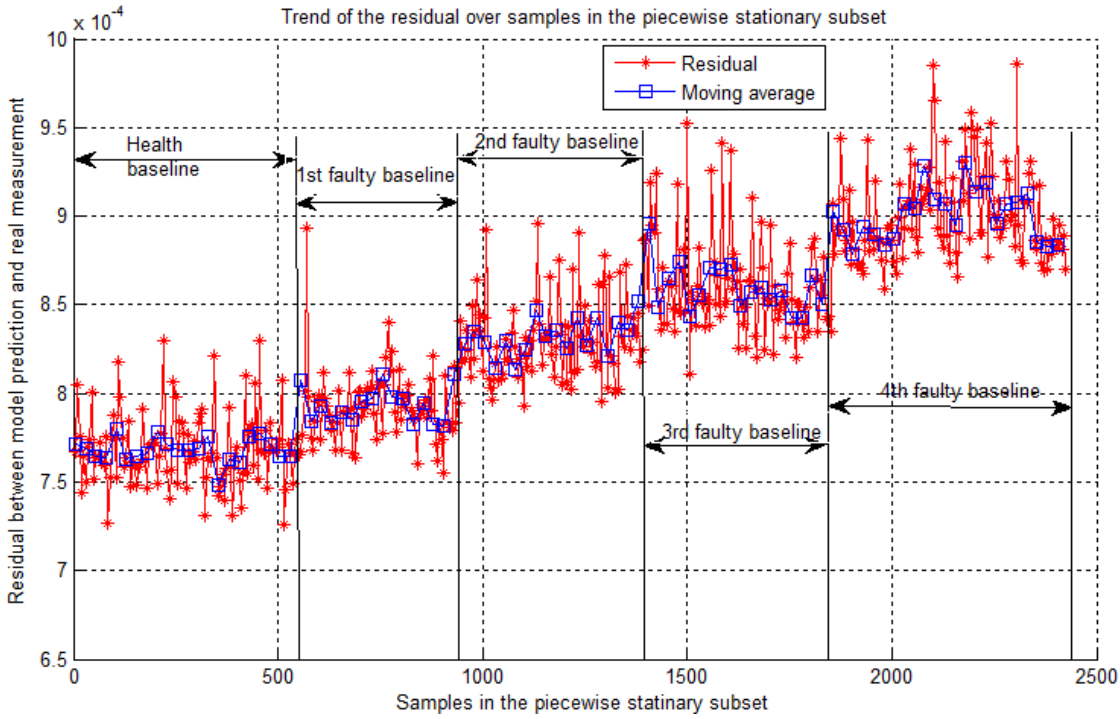

Fig.78 Trend of electrical indicator under half load

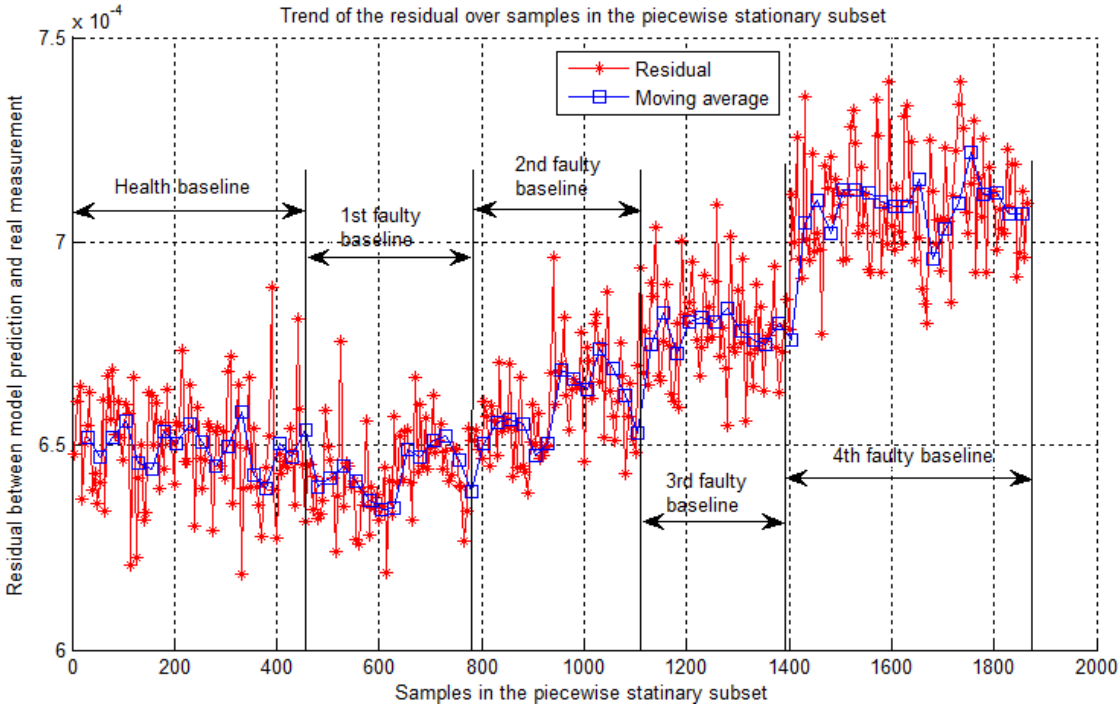

Fig.79 Trend of electrical indicator under no load

This experiment consists of a health baseline and four faulty baselines with increasing severity. The trend shows the electrical indicator rises up as the bearing deteriorates worse and worse. The moving average operation is applied to smooth the change of indicator, by observing the change of moving averaged trend, the residual changed around 26% at the final faulty baseline comparing with the healthy baseline.

In the previous subsection, electrical indicator was trended under full load condition. Two other experiments are also conducted under half load and no load conditions. Fig.78-Fig.79 present the trend of electrical indicator of them. The relative percentage of change between final faulty baseline and it healthy baseline are around 25.9%, 17.6% and 9% for full load, half load and no load conditions respectively.

The increment of electrical indicator between faulty baselines and healthy baseline are shown in Tab.7. The results show that the change electrical indicator will be sensitive as the load increase. The explanation is that the more load will produce more distortion in the current signature for the bearing with the same health condition, so the anomaly signature will be more significant than the case with less load. The Ratio of change between vibration and electrical indicator at full load is around 19, which shows that the electrical indicator can track the vibration indicator but less significant.

Tab.7 Increment of electrical indicator as health condition change

Change relative to healthy baseline	1st baseline	2nd baseline	3rd baseline	4th baseline
No Load Condition	0%	1.8%	4.3%	8.6%
Half Load Condition	3.5%	8.2%	12.4%	17.6%
Full Load Condition	6.3%	13.2%	19.0%	25.9%
Ratio of change between vibration and electrical indicator at full load	19.8	17.3	19.7	19.2

CHAPTER VII

SUMMARY AND CONCLUSIONS

In this chapter, the work of this research is briefed. The conclusions from this research are summarized. Finally some suggestions for future work are given.

A. Summary of Research

The main objective of this dissertation was to analyze the mechanical anomalies such as generalized roughness bearing defect and torsional vibration by using ESA. The developed approach for generalized roughness bearing defect analysis could isolate the influence of power quality variation by employing signal segmentation technique, which improved the reliability of ESA of bearing defect. The improved experimental procedure also isolates the impact of shaft current on the reliability of ESA of bearing defect. For the torsional vibration, the

In Chapter I of the dissertation, a brief introduction to the generalized roughness bearing defect and torsional vibration, and the techniques to analyze both of them is discussed. The research objectives and a roadmap of the proposed method are also outlined. Finally the anticipated contributions of this work are listed.

In Chapter II, The lateral and torsional vibrations of synchronous motor were illustrated to show how the mechanical anomalies affect the interface variable --- air-gap eccentricity and rotor speed, which interface the electromechanical dynamics. Then electromechanical fundamental of synchronous machine, amplitude and phase

modulation mechanism was discussed to explain the transmission of mechanical anomalies to electric signature.

In chapter III, the nature of the generalized roughness bearing defect and its physical link to current signature were investigated. The signal segmentation technique was applied to isolate the influence of nonstationary power input on the subtle current signature of generalized roughness bearing defect.

In Chapter IV, the thermal effects induced by shaft current was shown to be a critical factor affect the electromagnetic field along the air-gap and rotordynamics of shaft assembly. This lead to an improved experimental procedure is to closely resemble the practical bearing degradation process in the field.

In Chapter V, the free and forced responses of the torsional dynamics of rotor were discussed. Coupled equivalent circuit method was introduced to investigate the intercoupling between the electromagnetic and rotor dynamics of the whole system.

In Chapter VI, a practical case study – submersible electric pump was employed to show the significance of ESA to analyze the torsional vibration of shaft assembly.

B. Conclusions

The conclusions drawn from this research are summarized as follows:

(1) The bearing deterioration experiment showed the influence of shaft current on the vibration and current signature of bearing defect. The improved experimental procedure was proved effective to isolate that influence from the shaft current.

(2) The experiment showed the effective of signal segmentation approach to assist the analysis of mechanical anomalies with just subtle current signature under the influence of nonstationary power input. The isolation of load change was also verified.

(3) The coupled equivalent circuit method was proved effective to investigate the intercoupling between the electromagnetic and rotor dynamics of the whole system, which usually was ignored by just considered as a one-way interaction. The steady state analysis can be applied to prevent the torsional resonance.

(4) The coupled field analysis during transient showed how the transient harmonics in electromagnetic torque excite the torsional vibration of shaft assembly, and how the excited torsional vibration amplifies the electromagnetic toque in return. This coupling was illustrated by the spectrogram in the time-frequency domain.

C. Suggestions for Future Works

The proposed ESA approach of mechanical anomalies in this research has proven to be effective to analyze the generalized roughness bearing defect and torsional vibration of rotor. There are still some important issues suggested for future research to make this approach more reliable and extendable to more general conditions.

(1) Integration with the variable frequency drive – Synchronous motor is usually driven by variable frequency drive, which could introduce rich harmonics and inter-harmonics. These harmonic components will bring about hard challenging to the ESA of generalized roughness because its current signature is usually subtle during incipient anomaly.

(2) Speed dependence – The experiments also studied how load change could affect the sensitivity of ESA, but did not investigate the influence of rotating speed change on electrical signature of bearing anomaly. An ideal method should be load independent so that it will be more applicable for practical analysis. To justify the load effects of the bearing fault detection method is one of the topics for future research.

(3) Experiment on torsional vibration of synchronous motor – This experiment can be implemented by using strain gauge and vibrometer, and strongly encouraged to verify the effectiveness of ESA. Due to the limitation of resource, this costly experiment cannot be implemented in lab.

(4) Fatigue life prediction of rotor shaft – The allowable startup cycles can be estimated by cumulative fatigue stress analysis

REFERENCES

[1] M.M.Al-Hamrani, A.V. Jouanne and A.Wallace, “Power factor correction in industrial facilities using adaptive excitation control of synchronous machines”, Pulp and paper industry technical conference, June 2002, pp. 148-154

[2] A.H. Isfahani and S. Sadeghi, “Design of a permanent magnet synchronous machine for the hybrid electric vehicle”, World academy of science, engineering and technology, 21, 2008, pp. 566-570

[3] R.M. Tallam, S.B Lee, G.C. Stone, G.B. Kliman, J. Yoo, T.G. Habetler and R.G. Harley, “A survey of methods for detection of stator-related faults in induction machines”, IEEE transactions of industry applications, Vol.43, No.4, Jul./Aug., 2007, pp 920-933

[4] F.C. Trutt, J. Sottile, and J.L. Kohler, “Detection of AC machine winding deterioration using electrically excited vibrations”, IEEE transaction on industrial applications, Vol.37, No.1, Jan./Feb. 2001, pp. 10-14

[5] H.D. Haynes, “Electrical signature analysis (ESA) developments at the Oak Ridge diagnostics applied research center”, Proceedings of COMADEM '95, the 8th international congress on condition monitoring and diagnostic engineering management, Kingston, Ontario, Canada, Vol. 2, June 26-28, 1995, pp. 511-518

[6] T. Feese and C. Hill, “Prevention of torsional vibration problems in reciprocating machinery”, Proceedings of the 38th turbomachinery symposium, Houston, 2009, pp. 213-238

[7] J.R. Stack, T.G. Habetler and R.G. Harley, “Fault classification and fault signature production for rolling element bearings in electric machiens”, IEEE transactions on industrial applications, Vol.40, No.3, May/Jun. 2004, pp. 735-739

[8] J.R. Stack, R.G. Harley and T.G. Habetler, “An amplitude modulation detector for fault diagnosis in rolling element bearings”, IEEE transactions on industrial electronics, Vol. 51, No. 5, October 2004, pp. 1097-1102

[9] M. Blödt, P. Granjon, B. Raison and G. Rostaing, “Models for bearing damage detection in induction motors using stator current monitoring”, IEEE transactions on industrial electronics, Vol. 55, No. 4, April 2008, pp. 1813-1822

[10] H.A. Toliyat, N.A. Al-Nuaim, “Simulation and detection of dynamic air-gap eccentricity in salient-pole synchronous machines”, IEEE transactions on industry applications. Vol.35, No.1, Jan/Feb, 1999, pp. 86-93

[11] J. Sottile, F.C. Trutt and A.W. Leedy, “Condition monitoring of brushless three-phase synchronous generators with stator winding or rotor circuit deterioration”, IEEE transactions on industry application, vol.42, No.5, Sep/Oct 2006, pp. 1209-1215

[12] N.A.Al-Nuaim, H.A. Toliyat, “A novel method for modeling dynamic air-gap eccentricity in synchronous machines based on modified winding function theory”, IEEE transactions on energy conversion, Vol.13, No.2, June 1998, pp. 156-162

[13] X. Tu a, L.-A. Dessaint, M. El Kahel and A. Barry, “Modeling and experimental validation of internal faults in salient pole synchronous machines including space harmonics”, mathematics and computers in simulation Vol.71, 2006, pp. 425-439

[14] B.M. Ebrahimi, J. Faiz, M.J. Roshtkhari, “Static-, dynamic, and mix-eccentricity fault diagnoses in permanent-magnet synchronous motors”, IEEE transactions on industrial electronics. Vol.56, No.11, Nov. 2009, pp. 4727-4739

[15] C. Bruzzese, A.Rossi, E. Santini, V. Benucci, and A. Millerani, “Ship brushless-generator shaft misalignment simulation by using a complete mesh-model for machine voltage signature analysis”, IEEE electric ship technologies symposium, 2009, pp.113-118

[16] C.B. Mayer, “Torsional vibration problem and analysis of cement industry drives”, IEEE transactions on industry application, vol.IA-17, No.1, Jan/Feb 1981, pp. 81-89

[17] T. Feese and R. Maxfield, “Torsional vibration problems with Motor/Id fan system due to PWM variable frequency drive”, Proceedings of the thirty-seventh turbomachinery symposium, Houston, 2008, pp. 45-56

[18] F.R. Szenasi and W.W. Von Nimitz, “Transient analysis of synchronous motor trains”, Proceedings of the eleventh turbomachinery symposium, Houston, 1978, pp. 111-117

[19] J.O. Ojo, V.Ostovic, T.A. Lipo and J.C. White, “Measurement and computation of starting torque pulsations of salient pole synchronous motors”, IEEE transactions oil energy conversion, Vol. 5, No.1, March 1990, pp. 176-182

[20] L. Parsa and T. Kim, “Reducing torque pulsation of multi-phase interior permanent magnet machines”, IEEE industry applications conference, 2006, pp. 1978-1983

[21] H. Kim, “On-line mechanical unbalance estimation for permanent magnet synchronous machine drives”, IET Electr. Power Appl., Vol. 3, Iss. 3, 2009, pp. 178-186

[22] X.J. Shi, J.P. Shao, J.S. Si and B.N. Li, “Experimental and simulation of rotor’s torsional vibration based on sensorless detection technology”, Proceeding of the IEEE ICAL, 2008, pp. 2673-2678

[23] S.H. Kia, H. Henao, and G.A Capolino, “A modeling approach for gearbox monitoring using stator current signature in induction machines”, IEEE Industry Applications Society Annual Meeting, 2008, pp. 1-6

[24] N.W. Duncan, *Torsional vibration of turbomachinery*, McG-Hill, New York, 2004, pp.126-135

[25] K. Gatzwiller, Bruel&Kjar, “Measuring torsional operational defection shapes of rotating shafts”, B&K application note

[26] J.W. Choi, “Analysis of electrical signatures in synchronous generators characterized by bearing faults”, Master Thesis, Dept. Mechanical Engineering, Texas A&M University, Dec 2006.

[27] F. Immovilli, A. Bellini, R. Rubini and C. Tassoni, “Diagnosis of bearing faults in induction machines by vibration or current signals: a critical comparision”, IEEE transaction on industrial applications,Vol.46, No.4, Jul./Aug., 2010, pp. 1350-1359

[28] J.R. Stack, T.G. Habetler and R.G. Harley, “Bearing fault detection via autoregressive stator current modeling ”, IEEE transaction on industrial applications, Vol. 40, No.3, May/Jun. 2004, pp. 740-747

[29] W. Zhou, T. G. Habetler and R.G. Harley, “Bearing fault detection via stator current noise cancellation and statistical control”, Industrial Electronics, IEEE Transactions on, Vol. 55, Iss. 12, 2008, pp. 4260-4269

[30] B. Lu, M. NowakAn, S. Grubic and T.G. Habetler, “Adaptive noise-cancellation method for detecting generalized roughness bearing faults under dynamic load conditions” IEEE energy conversion congress and exposition, Milwaukee, WI, USA, 2009, pp. 1091-1097

[31] R.R. Schoen, T.G. Habetler, and R.G. Bartheld, “Experimentally generating faults in rolling element bearings via shaft current”, IEEE Transaction on industrial application, Vol. 41, pp.25-29, Jan./Feb. 2005, pp. 25-29

[32] F. Zare, “EMI in modern AC motor drive systems”, IEEE EMC Society Newsletters, summer(222), pp. 53-58.

[33] S. Adak, “Time-dependent spectral analysis of nonstatioanry time series”, Journal of American statistical association. Vol.93, No.444, December 1998, pp. 1488-1501

[34] A. Abbate, C. DeCusatis, P.K. Das, *Wavelets and subbands: fundamentals and applications*, Birkhäuser, Boston, 2002

[35] D.E. Bently, *Fundamental of rotating machinery diagnostics*, Bently Pressurized Bearing Press, Minden, NV, 2002

[36] M Sarangi, B.C. Majumdar, “Stiffness and damping characteristics of lubricated ball bearings considering the surface roughness effect. Part 1: theoretical formulation”, Journal of engineering tribology, Vol. 218, No. 6, 2004, pp. 529-538

[37] M Sarangi, B.C. Majumdar, “Stiffness and damping characteristics of lubricated ball bearings considering the surface roughness effect. Part 2: numerical results and application”, Journal of engineering tribology, Vol. 218, No. 6, 2004, pp. 539-548

[38] S.H.Upadhyay, “Dynamic analysis of ball bearings due to clearance effect”, Proceeding of the ASME 2009 IDETC/CIE, Aug.30-Sept.2, 2009, San Diego, pp. 1179-1186

[39] P. Vicente J. Rodríguez and A. Belahcen, “Air-gap force distribution and vibration pattern of induction motors under dynamic eccentricity”, Electrical engineering, Vol.90 No.3, 2008, pp.209–218

[40] P. Pennacchi and L. Frosini, “Dynamical behaviour of a three-phase generator due to unbalanced magnetic pull”, IEE Proceeding of electrical power application, Vol. 152, No. 6, November 2005, pp. 1389-1400

[41] E. D. Goodman, “Steady-state and transient torque of a synchronous motor”, Phd. Dissertation, McGill University, 1975

[42] R.L. Hyde and Thomas, R.Brinner, “Starting characteristic of electric submersible oil well pumps”, IEEE transactions on industrial applications, Vol.IA-22, No.1, Jan./Feb., 1986, pp. 133-144

[43] P. Girdhar and C. Scheffer, *Practical machinery vibration analysis and predictive maintenance*, Elsevier, Boston, 2004

[44] A. Muszynska, *Rotordynamics*, CRC Press, Taylor & Francis, New York, 2005

[45] P.C. Krause, O. Wasynczuk and S.D. Sudhoff, *Analysis of electric machinery and Drive System*, Wiley-IEEE press, New York, 2002

[46] D. G. Dorrell, “Calculation of unbalanced magnetic pull in small cage induction motors with skewed rotors and dynamic rotor eccentricity”, IEEE transactions on energy conversion Vol.11, Iss. 3, 1996, pp. 483-488.

[47] M.H.J. Bollen, I.Y.H. Gu, “Bridging the gap between signal and power”, IEEE signal processing magazine, Vol.26, Iss. 4, July, 2009, pp. 12-31

[48] P. Prandoni, *Optimal segmentation techniques for piecewise stationary signals*, thesis, Ecole polytechnique federale de lausanne, 1999

[49] R.C. Dugan and M. F. McGranaghan, *Electrical power systems quality*, McGraw-Hill, New York, 2002

[50] J. Antoni, “The spectral kurtosis: a useful tool for characterizing non-stationary signals”, Mechanical systems and signal processing, Vol.20, Iss. 2, 2006, pp. 282-307

[51] S. Adak, “Time-dependent spectrum analysis of nonstationary time series”, Journal of the American statistical association, Vol.93, No.444, 1998, pp. 1488-1501

[52] T.S. Rao, “A cumulative sum test for detecting change in time series”, International journal of control, Vol. 34, Iss. 2, 1981, pp. 285-293

[53] L. Brieman, J. Friedman, R. Olshen, and C. Stone, *Classification and regression trees*, Chapman and Hal, Wadsworth, CA, 1984

[54] J.M. Erdman, R.J. Kerkman, D.W. Schlegel, G.L. Skibinski, “Effect of PWM inverters on AC motor bearing currents and shaft voltages”, IEEE transactions on industry applications, Vol. 32, No.2, Mar/Apr 1996, pp. 250-259

[55] P. Dietl, J. Wensing and G C van Nijen, “Rolling bearing damping for dynamic analysis of multi-body systems—experimental and theoretical results”, Journal of multi-body dynamics, March 1, 2000, vol. 214, No.1, pp. 33-43

[56] R. Serrato, M.M. Maru and L.R. Padovese, “Effect of lubricant viscosity grade on mechanical vibration of roller bearings”, Tribology International, Vol.40, Iss. 8, 2007, pp.1270-1275

[57] N. Baxter, “Forty-eight case histories of intriguing machinery problems”, Sound & vibration magazine, January 2012, pp. 36-50

[58] P.E. Duncan and R. E. Taylor, (1979), “A note on the dynamic analysis of non-proportionally damped systems”, Earthquake engineering and structural dynamics, Vol.7, Iss. 1, Jan/Feb 1979, pp. 99–105.

[59] A.S. Rangwala, *Reciprocating machinery dynamics: design and analysis*, Marcell Dekker, New York, 2001

[60] J.C. Wachel and Fred R. Szenasi, “Analysis of torsional vibration in rotating machinery”. Proceeding of the 22nd turbomachinery symposium, Houston, 1993, pp. 127-151

[61] ESP model and specificiations,

http://www.cnpc.com.cn/cptdc/en/productsservices/cysb/part4/

APPENDIX A

Coupled Equivalent Circuit of Torsional Vibration Model

Simulink block of equivalent circuit of torsional vibration

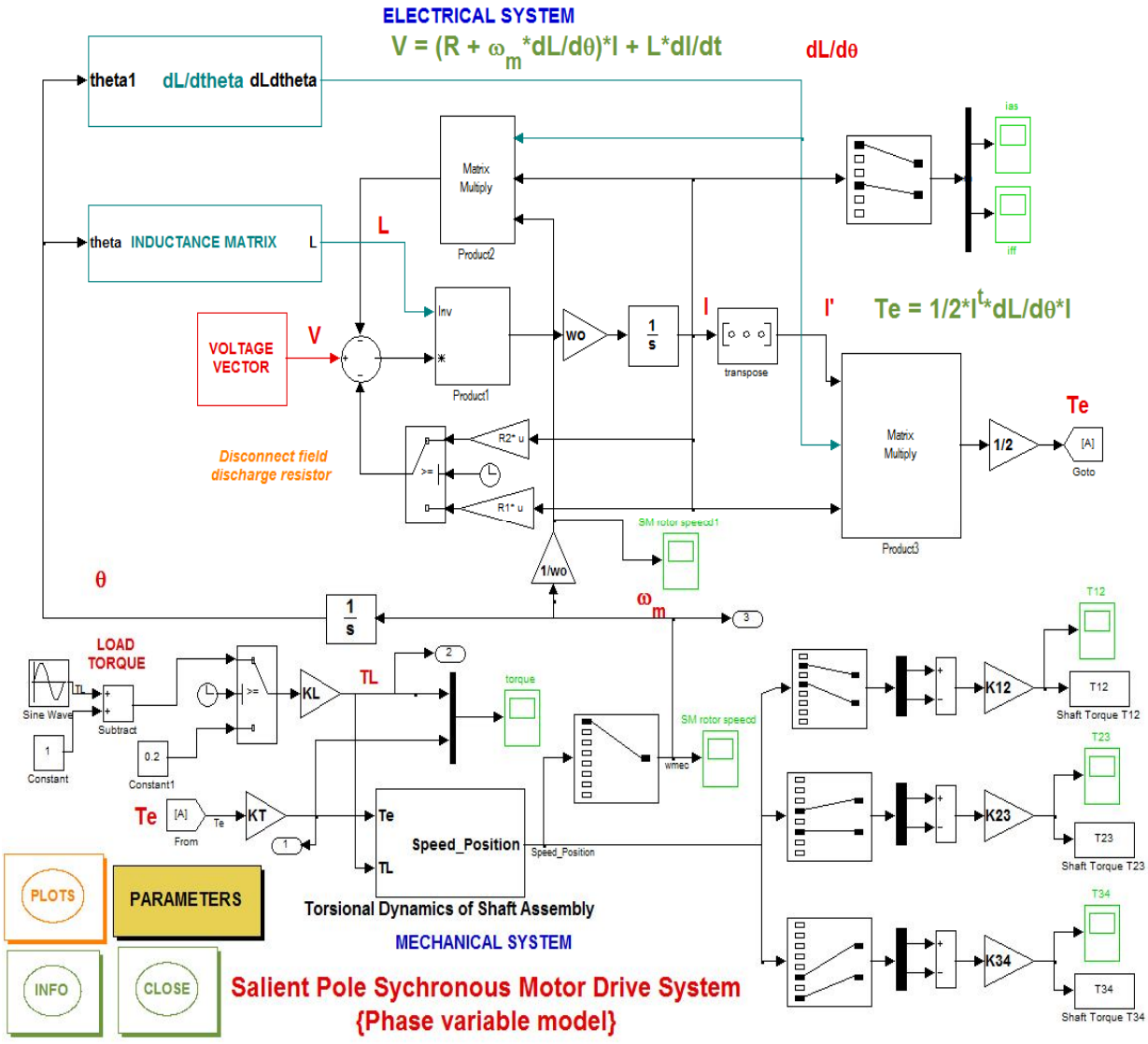

Subsystem block of torsional dynamics of shaft assembly

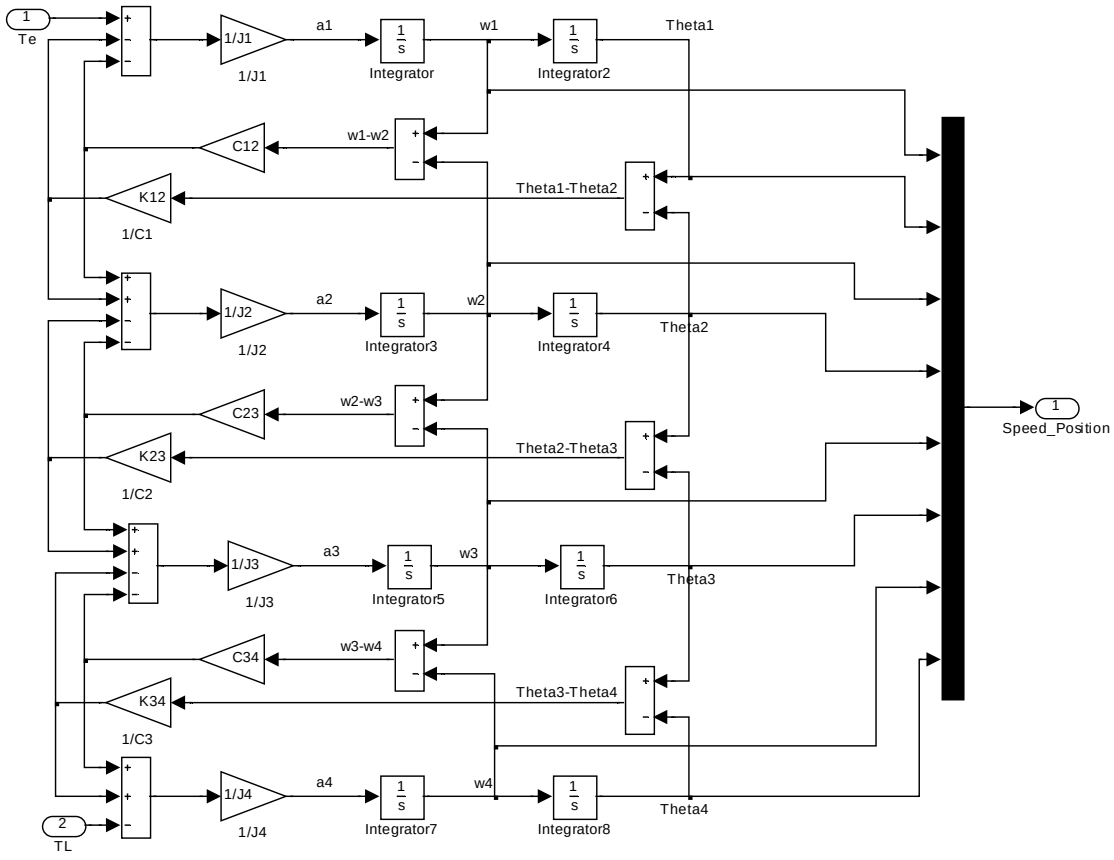

APPENDIX B

Symmetrical Component Analysis for 3-phase Unbalanced Voltage Supply

The method of symmetrical components is widely used to simplify analysis of unbalanced three phase power systems under both normal and abnormal conditions. In a three-phase machine, three unbalanced phasors could be expressed as the sum of three symmetrical sets of balanced phasors. Essentially, this method converts three unbalanced phases into three independent sources, which makes asymmetric fault analysis more tractable.

Physically, in a three phase winding of electric machines, a positive sequence set of currents produces a normal rotating field, a negative sequence set produces a field with the opposite rotation, and the zero sequence set produces a field that oscillates but does not rotate between phase windings.

If the phase quantities are expressed in phasor notation using complex numbers, a vector can be formed for the three phase quantities. For example, a vector for three phase voltages could be written as

$$V_{abc} = \begin{bmatrix} V_a \\ V_b \\ V_c \end{bmatrix} = \begin{bmatrix} V_{an} \\ V_{bn} \\ V_{cn} \end{bmatrix} + \begin{bmatrix} V_{ap} \\ V_{bp} \\ V_{cz} \end{bmatrix} + \begin{bmatrix} V_{az} \\ V_{bz} \\ V_{cz} \end{bmatrix}$$

where the subscripts p, n, and z refer respectively to the positive, negative and zero sequence components. The sequence components differ only by their phase angles,

which are symmetrical and so are $2\pi/3$ radians or 120°. Define the operator α phasor vector forward by that angle.

$\alpha = e^{\frac{2}{3}\pi i}$, note that α^3=1, the zero sequence components are in phase, denote them as:

$$V_n \equiv V_{an} = V_{bn} = V_{cn}$$

and the other phase sequences as:

$$V_p \equiv V_{ap} = V_{bp} = V_{cp}, \quad V_n \equiv V_{an} = V_{bn} = V_{cn}$$

Thus,

$$V_{abc} = \begin{bmatrix} V_z \\ V_z \\ V_z \end{bmatrix} + \begin{bmatrix} V_p \\ \alpha^2 V_p \\ \alpha V_p \end{bmatrix} + \begin{bmatrix} V_n \\ \alpha V_n \\ \alpha^2 V_n \end{bmatrix} = \begin{bmatrix} 1 & 1 & 1 \\ 1 & \alpha^2 & \alpha \\ 1 & \alpha & \alpha^2 \end{bmatrix} \begin{bmatrix} V_z \\ V_p \\ V_n \end{bmatrix} = TV_{npz}$$

Where

$$V_{npz} = \begin{bmatrix} V_z \\ V_p \\ V_n \end{bmatrix}, \quad T = \begin{bmatrix} 1 & 1 & 1 \\ 1 & \alpha^2 & \alpha \\ 1 & \alpha & \alpha^2 \end{bmatrix}$$